DYNAMIC TWO PHASE MODELLING AND ANFIS-BASED CONTROL OF ETHYLENE COPOLYMERIZATION IN CATALYTIC FLUIDIZED BED REACTOR

MOHAMMAD REZA ABBASI

FACULTY OF ENGINEERING
UNIVERSITY OF MALAYA
KUALA LUMPUR

2019

DYNAMIC TWO PHASE MODELLING AND ANFIS-BASED CONTROL OF ETHYLENE COPOLYMERIZATION IN CATALYTIC FLUIDIZED BED REACTOR

MOHAMMAD REZA ABBASI

THESIS SUBMITTED IN FULFILMENT OF THE REQUIREMENTS FOR THE DEGREE OF DOCTOR OF PHILOSOPHY

FACULTY OF ENGINEERING
UNIVERSITY OF MALAYA
KUALA LUMPUR

2019

UNIVERSITI MALAYA

ORIGINAL LITERARY WORK DECLARATION

Name of Candidate: **Mohammad Reza Abbasi**

Registration/Matric No.: **KHA130062**

Name of Degree: **Doctor of Philosophy**

Title of Project Paper/Research Report/Dissertation/Thesis ("this Work"): **DYNAMIC TWO PHASE MODELLING AND ANFIS-BASED CONTROL OF ETHYLENE COPOLYMERIZATION IN CATALYTIC FLUIDIZED BED REACTOR**

Field of Study:

I do solemnly and sincerely declare that:

(1) I am the sole author/writer of this Work;
(2) This work is original;
(3) Any use of any work in which copyright exists was done by way of fair dealing and for permitted purposes and any excerpt or extract from, or reference to or reproduction of any copyright work has been disclosed expressly and sufficiently and the title of the Work and its authorship have been acknowledged in this Work;
(4) I do not have any actual knowledge nor do I ought reasonably to know that the making of this work constitutes an infringement of any copyright work;
(5) I hereby assign all and every rights in the copyright to this Work to the University of Malaya ("UM"), who henceforth shall be owner of the copyright in this Work and that any reproduction or use in any form or by any means whatsoever is prohibited without the written consent of UM having been first had and obtained;
(6) I am fully aware that if in the course of making this Work I have infringed any copyright whether intentionally or otherwise, I may be subject to legal action or any other action as may be determined by UM.

Candidate's Signature Date:

Subscribed and solemnly declared before,

Witness's Signature Date:

Name:
Designation:

DYNAMIC TWO PHASE MODELLING AND ANFIS-BASED CONTROL OF ETHYLENE COPOLYMERIZATION IN CATALYTIC FLUIDIZED BED REACTOR

ABSTRACT

The worldwide demand for polyolefins has reached more than 140 million tons per year and low-pressure processes using different catalytic systems are utilized to produce more than 80 *wt*% of the total production. Polyethylene (PE) is the most extensively consumed plastic in the world and gas-phase processes are widely used for its production due to their flexibility. The sole type of reactor that can produce PE in gas phase is Fluidized Bed Reactor (FBR). This is due to their ability to dissipate heat of reaction in quantities that make reliable production rates possible. Given the scale of production of polyolefins produced via catalytic polymerization, the development of reliable process models to simulate the behavior of the related process units in general and the commercial reactor units in particular is becoming more and more important. In this study, a modified dynamic model for ethylene co-polymerization in an industrial fluidized-bed reactor (FBR) is developed to describe its behavior and calculate the polymer properties. The model considers particle entrainment and polymerization reaction in two phases. Two-site kinetics and hydrodynamics in combination, provide a comprehensive model for the gas phase fluidized-bed polyethylene production reactor. The governing moment and mass and energy balance differential equations have been solved simultaneously and the results were compared with literature as well as industrial data. Nonetheless, since the model is dynamic, it can be used in control studies as well and it was utilized as a base to control two of the most important process variables namely polymer Melt Flow Index (MFI) and the temperature. The results showed that the dynamic model predicts more accurate

results for Polydispersity Index (PDI), Molecular Weight Distribution (MWD), reactor temperature and polymer production rate. The open loop simulation analysis revealed that the behavior of the polyethylene fluidized bed reactor is strongly dependent on the superficial gas velocity and feed concentrations and that the process is highly sensitive and nonlinear, thus justifying the use of an advanced control algorithm for efficient control of the process variables. To test the model and control the polymer MFI and temperature, inlet hydrogen concentration and cool water flow rate have been manipulated respectively. Firstly, conventional Proportional-Integral-Differential (PID) controller was used to control the variables in both servo and regulatory scenarios. The results confirm the disadvantages of the conventional controllers for applications to this nonlinear system. Intelligent and expert system-based controllers have proven to have the capability to control these systems. As a result, Adaptive Neuro-Fuzzy Inference System (ANFIS) is utilized in this study. The findings have shown the superiority of this Artificial Intelligence (AI) based controller in set-point tracking and disturbance rejection profiles; solely or in hybrid architectures with conventional controllers. This process model can equip the user-engineer with the essential tools required for the process design, optimization, and control which could ultimately lead to significant savings in time and cost during the process development and operation.

Keywords: *polyethylene, fluidized-bed reactors, olefin polymerization, process control, process modeling.*

PEMODELAN DINAMIK DUA FASA BERASASKAN KAWALAN ANFIS KE ATAS KOPOLIMERISASI ETILENA DALAM REAKTOR KATIL BERMANGKIN CATALYTIK

ABSTRAK

Permintaan sedunia untuk poliolefin telah mencapai lebih daripada 140 juta tan setahun dan proses tekanan rendah yang menggunakan pelbagai sistem pemangkin digunakan untuk menghasilkan lebih daripada 80% berat daripada jumlah pengeluaran. Polietilena (PE) adalah plastik yang paling banyak digunakan di dunia dan proses-proses fasa gas digunakan secara meluas untuk pengeluarannya disebabkan ciri keanjalannya. Hanya sejenis reaktor yang mampu menghasilkan PE dalam fasa gas adalah Reaktor Katil Perbendaliran atau Fluidized Bed Reactor (FBR). Ini disebabkan oleh keupayaan FBR untuk menghilangkan haba reaksi dalam kuantiti yang membolehkan penghasilan kadar pengeluaran yang boleh dipercayai. Memandangkan skala pengeluaran poliolefin yang dihasilkan melalui pempolimeran catalytik, pembinaan model proses yang boleh dipercayai untuk mensimulasikan tingkah laku unit proses berkaitan secara umum dan unit reaktor komersial khususnya menjadi semakin penting. Dalam kajian ini, satu model dinamik yang diubahsuai khas untuk pempolimeran etilena dalam FBR bertahap industri dibina untuk menggambarkan perilaku dan mengira sifat polimer. Model ini mempertimbangkan tindak balas zarah dan tindak balas pempolimeran dalam dua fasa. Penggabungan kinetik dua tapak dan hidrodinamika membolehkan pembinaan model komprehensif untuk reaktor pengeluaran polyethylene FBR berfasa gas. Momen, dengan persamaan kebezaan massa dan tenaga diselesaikan secara serentak dan hasilnya dibandingkan dengan sastera serta data perindustrian. Walau bagaimanapun, kerana model tersebut berciri dinamik, ia boleh digunakan dalam kajian kawalan dan juga digunakan sebagai dasar untuk mengawal

dua pemboleh ubah proses yang paling penting iaitu Indeks Melt Flow Index (MFI) dan suhu. Keputusannya ialah model dinamik meramalkan hasil yang lebih tepat untuk Indeks Polydispersity (PDI), Pengedaran Berat Molekul (MWD), suhu reaktor dan kadar pengeluaran polimer. Analisis simulasi gelung terbuka menunjukkan bahawa kelakuan FBR sangat bergantung kepada halaju gas superfisi, kepekatan bahan masuk dan juga prosesnya yang sangat sensitif dan tidak linear membenarkan penggunaan algoritma kawalan lebih maju untuk kawalan pembolehubah proses yang cekap. Untuk menguji model dan mengawal MFI polimer dan suhu, kepekatan hidrogen masuk dan kadar aliran air sejuk masing-masing telah dimanipulasikan. Pertamanya, pengawal PID konvensional digunakan untuk mengawal pemboleh ubah dalam kedua-dua senario servo dan regulasi. Keputusannya mengesahkan kelemahan pengawal konvensional untuk aplikasi ke sistem tidak linear ini. Pengawal berasaskan sistem pintar yang pakar terbukti mempunyai keupayaan untuk mengawal sistem-sistem ini. Akibatnya, pengawal hibrid Sistem Kesimpulan Neuro-Fuzzy Adaptive (ANFIS) digunakan dalam kajian ini. Penemuan menunjukkan keunggulan Artificial Intelligence (AI) ini dalam pengesanan set-point dan profil penolakan gangguan; secara sendiri atau dalam senibina hibrid dengan pengawal konvensional. Model proses ini boleh melengkapkan jurutera-pengguna dengan peralatan penting yang diperlukan untuk reka bentuk proses, pengoptimuman dan kawalan, yang akhirnya akan menjimatkan masa dan kos yang cukup signifikan sewaktu pembinaan dan operasi proses.

kata kunci: *polietilena, reaktor katil dibendalir, Pempolimeran olefin, kawalan proses, pemodelan proses.*

ACKNOWLEDGEMENTS

I would like to express my sincere gratitude and sincere thanks to my advisors Prof. Ir. Dr. Mohamed Azlan Hussain and Dr. Ahmad Shamiri for the continuous support of my Ph.D study and related research, for their patience, motivation, and immense knowledge. Their encouragement and guidance helped me in all the time of research and writing of this thesis. It is with their supervision that this work came into existence and I take full responsibility for any faults.

I thank all who in one way or another contributed in the completion of this thesis. I am so grateful to the University of Malaya High Impact Center (HIR) and Institute of Research Management & Monitoring (IPPP) for financially supporting the project. I am also deeply thankful to all the staffs of University of Malaya who helped me in completing this project.

I am also so appreciative of my fellow lab mates whose challenges, stimulating discussions and productive critics have provided new ideas to the work. I will always remember the sleepless nights we were working together before deadlines, and for all the fun we have had in the last few years.

Nobody has been more important to me in the pursuit of this project than the members of my family. I thank them for their endless love, guidance, encouragement, and full support throughout my life. This thesis is wholeheartedly dedicated to them.

TABLE OF CONTENTS

LIST OF FIGURES

LIST OF TABLES

LIST OF SYMBOLS AND ABBREVIATIONS

A	cross sectional area of the reactor (m^2)
AI	artificial intelligence
$ALDMC$	Adaptive linear DMC
$AlEt3$	triethyl aluminum co-catalyst
$APMBC$	Adaptive Predictive Model-Based Control
Ar	Archimedes number
B_i	moles of reacted monomer bound in the polymer in the reactor
CFD	computational fluid dynamics
Cp_{pol}	specific heat capacity of solid product ($J/kg.K$)
Cp_g	specific heat capacity of gaseous stream ($J/kg.K$)
Cp_i	specific heat capacity of component i ($J/kg.K$)
$CSTR$	continuous stirred tank reactor
d_b	bubble diameter (m)
d_{b_0}	initiate bubble diameter (m)
D_g	gas diffusion coefficient (m^2/s)
DMC	dynamic matrix control
d_p	particle diameter (m)
D_t	reactor diameter (m)
FBR	fluidized bed reactor (kg/s)
F_{cat}	catalyst feed rate (kg/s)
FDM	Fuzzy decision making
f_i	fraction of total monomer in the reactant gas

FH	Fuzzy Hammerstein
g	gravitational acceleration (m/s^2)
GPC	gel permeation chromatography
H	height of the reactor, (m)
H_2	hydrogen
H_{bc}	bubble to cloud heat transfer coefficient, $(W/m^3.K)$
H_{be}	bubble to emulsion heat transfer coefficient, $(W/m^3.K)$
H_{ce}	cloud to emulsion heat transfer coefficient, $(W/m^3.K)$
$HDPE$	high density polyethylene
ICA	induced condensing agent
i	monomer type
I_m	impurity such as carbon monoxide $(kmol/m^3)$
J	active site type
K_b	elutriation constant in bubble phase $(kg.m^2/s)$
K_{b_c}	bubble to cloud mass transfer coefficient $(1/s)$
K_{b_e}	bubble to emulsion mass transfer coefficient $(1/s)$
K_{c_e}	cloud to emulsion mass transfer coefficient $(1/s)$
$k_{dI}(j)$	deactivation by impurities rate constant for a site of type j
$k_{ds}(j)$	spontaneous deactivation rate constant for a site of type j
K_e	elutriation constant in emulsion phase $(kg.m^2/s)$
$k_f(j)$	formation rate constant for a site of type j
$k_{fh_i}(j)$	transfer rate constant for a site of type j with terminal monomer M_i reacting with hydrogen
$k_{fm_i}(j)$	transfer rate constant for a site of type j with terminal monomer M_i reacting with monomer M_k

$k_{fr_i}(j)$	transfer rate constant for a site of type j with terminal monomer M_i reacting with $AlEt3$
$k_{fs_i}(j)$	spontaneous transfer rate constant for a site of type j with terminal monomer M_i
k_g	gas thermal conductivity $(W/m.K)$
$k_{h_i}(j)$	rate constant for reinitiating of a site of type j by monomer M_i
$k_{h_r}(j)$	rate constant for reinitiating of a site of type j by cocatalyst
$k_{i_i}(j)$	rate constant for initiation of a site of type j by monomer M_i
$k_{p_{ik}}(j)$	propagation rate constant for a site of type j with terminal monomer Mi reacting with monomer M_k
k_{pT_i}	propagation rate constant $(m^3/kmol.s)$
$LDMC$	Linear DMC
$LDPE$	low density polyethylene
$LLDPE$	linear low-density polyethylene
MFI	melt flow index $(g/10min)$
$[M_i]$	concentration of component i in the reactor $(kmol/m^3)$
$[M_i]_{in}$	concentration of component i in the inlet gaseous stream
$MIMO$	multi input-multi output
Mn	number average molecular weight of polymer $(kg/kmol)$
MPC	model predictive controller
Mw	weight average molecular weight of polymer $(kg/kmol)$
MWD	molecular weight distribution
mw_i	molecular weight of monomer i (g/mol)
$N(0, j)$	uninitiated site of type j produced by formation reaction

$N(j)$	potential active site of type j
$N_d(j)$	spontaneously deactivated site of type j
$N_{dIH}(0, j)$	impurity killed sites of type j
N_H	uninitiated site of type j produced by transfer to hydrogen reaction
$N_j(r, j)$	living polymer molecule of length r, growing at an active site of type j, with terminal monomer
P	pressure (Pa)
PDI	polydispersity index
$Q(r, j)$	dead polymer molecule of length r produced at a site of type j
r	number of units in polymer chain
Re_{mf}	Reynolds number of particles at minimum fluidization condition
R_i	instantaneous consumption rate of monomer $(kmol/s)$
R_p	production rate (kg/s)
R_v	volumetric polymer phase outflow rate from the reactor (m^3/s)
$SISO$	single input-single output
T	temperature (K)
t	time (s)
T_{in}	temperature of the inlet gaseous stream, (K)
TS	Takagi-Sugeno fuzzy inference system
T_{ref}	reference temperature (K)
U_t^*	dimensionless terminal falling velocity coefficient

U_0 superficial gas velocity (m/s)

U_b bubble velocity (m/s)

U_{br} bubble rise velocity (m/s)

U_{mf} minimum fluidization velocity (m/s)

U_t terminal velocity of falling particles (m/s)

V reactor volume (m^3)

V_p volume of polymer phase in the reactor (m^3)

W_b weight of solids in the bubble phase (kg)

W_e weight of solids in the emulsion phase (kg)

$X(n, j)$ nth moment of chain length distribution for dead polymer produced at a site of type j

$Y(n, j)$ nth moment of chain length distribution for living polymer produced at a site of type j

$Z - N$ Ziegler-Natta catalyst

Greek letters

ΔH_R heat of reaction (J/kg)

δ volume fraction of bubbles in the bed

ε_b void fraction of bubble for Geldart B particles

ε_e void fraction of emulsion for Geldart B particles

ε_{mf} void fraction of the bed at minimum fluidization

μ gas viscosity $(Pa.s)$

ρ_g gas density (kg/m^3)

ρ_{pol} polymer density (kg/m^3)

φ_s sphericity for sphere particles

Subscripts and superscripts

1	ethylene
2	1-butene
b	bubble phase
e	emulsion phase
i	component type number
j	active site type number
mf	minimum fluidization
pol	polymer
ref	reference condition
T, TT	Pseudo kinetic rate constants

LIST OF APPENDICES

CHAPTER 1: INTRODUCTION

1.1 Background

Polyethylene (PE), with a projected production capacity of more than 100 million tons in 2020, will continue to be the most widely used plastic resin in the world for some time to come, and low-pressure catalytic processes are expected to account for more than three-quarters of this production. The global demand for polyolefins has reached more than 140 million tons per year worldwide, and low-pressure processes using different catalytic systems account for the production of more than 80 *wt*% of this global demand (The Freedonia Group, 2014). Given the scale of polyolefins produced via catalytic polymerization, the development of reliable process models to simulate the behavior of the related process units in general and the commercial reactor units in particular is gaining in importance. These process models can equip the user or engineer with the essential tools required for the process design, optimization, and control which could ultimately lead to significant savings in time and cost during the process development and operation.

Industrial processes for the production of polyethylene (PE) can be divided into different categories according to the phase in which the polymerization takes place: solution, slurry, and gas-phase processes, with the latter two being more significant in terms of production volumes. While slurry phase processes are commercially important for a number of reasons, gas-phase processes are even more widely used due to their versatility, easy processability, low cost, and the ability to being recycled. Gas-phase can be used to produce resins with a full range of densities, from linear low density polyethylene (LLDPE) to high density polyethylene (HDPE) in the same process. The most widely type of reactor used for production of gas-phase PE are Fluidized–Bed Reactors (FBR), since this is the only reactor type that can be used to remove enough heat from the reactor to achieve

commercially pertinent rates of polymerization (Soares & McKenna, 2012).

The reactor is essentially an empty cylinder with an expansion zone at the top (to reduce the gas velocity and help prevent any fine particles from flowing out of the reactor and into the recycle compressor), and a distributor plate at the bottom. Catalyst (or prepolymerized catalyst) is fed into the reactor at a point slightly above the distributor plate, and the fluids are typically fed through the bottom of the reactor, usually (but not always) below the distributor plate. The polymer is removed through a product discharge valve, following into a series of degassing tanks to separate the unreacted monomer. The gaseous recycle stream is compressed, cooled and afterwards mixed with fresh monomer, hydrogen and eventually other compounds, then fed back into the reactor (Figure 2.1).

In contrast to ethylene polymerizations in slurry phase, only few studies have been published related to gas phase polymerization. The most widely established industrial gas phase technology is polymerization in Fluidized–bed Reactors (FBRs) and experimental investigation studies of gas phase ethylene polymerization in FBRs are rare. The study reported in this thesis includes the modeling and control of industrial FBRs. To study the polymerization in such a reactor an industrially validated model is required.

1.2 Problem statement

The complicated reaction, heat and mass transfer mechanisms as well as the complex gas and solid flow characteristics in the FBR introduce extreme nonlinearities in the dynamics of the reactor. As such, the modeling and control of such a process is a huge challenge.

The fundamental modeling and control problem in the ethylene polymerization FBR is further complicated by the existence of strong interactions between reactor variables, of which conventional process modeling and control strategies are incapable of coping with these difficulties. Although there are studies reported in the literature on the modeling and control of polymerization process in FBRs, there are still numerous gaps in this research

field to be filled.

The conventional models assume that the emulsion is at minimum fluidization ($\varepsilon_e = \varepsilon_{mf}$) and bubbles are solid-free ($\varepsilon_b = 1$). By this assumption, it is not possible to predict the effect of the dynamic gas–solid distribution on the apparent reaction and heat/mass transfer rates in the fluidized–beds properly at velocities higher than minimum fluidization. However, the presence of solids in the bubbles has been shown experimentally (Aoyagi & Kunii, 1974) and theoretically (Gilbertson & Yates, 1996). The emulsion phase also does not remain at minimum fluidization conditions and it may contain more gas at higher gas velocities (Abrahamsen & Geldart, 1980). An increase of superficial gas velocity entering the FBR improves phase mixing which results in more solid particles entering the bubbles and more gas entering the emulsion phase. Furthermore, the effect of particle elutriation which is the gas-borne particles that leave the reactor with the gas stream and to the cyclone is neglected in the available models. This important stage can not be neglected as it highly affects the hydrodynamics and transport phenomena. Therefore, a comprehensive model is needed to provide a more realistic understanding of the phenomena encountered in the bed hydrodynamics and improve the quantitative understanding of the actual process. In addition, an efficient advanced process control scheme is required to cope with dynamic nonlinearities and difficulties involved in the control of the gas phase ethylene polymerization process in FBRs since conventional controllers generally lack these capabilities. One subcategory of advanced controllers are Artificial Intelligence (AI) based controllers. These controllers may utilize fuzzy logic, neural networks, machine learning, neuro-fuzzy etc. or a hybrid of them with conventional controllers to be intelligent and self learning. Studies have shown that combination of these intelligent controllers with the adaptiveness is a promising research area for practical implementation and control of industrial processes.

1.3 Objectives

The objective of this work is to develop a comprehensive model for a gas-phase ethylene polymerization in a catalytic FBR encompassing all aspects of the polymerization of ethylene with a heterogeneous Ziegler–Natta catalyst for describing the molecular weight distribution, polydispersity index and melt flow index of the produced polymer and dynamic behavior of a FBR. The application of efficient advanced process control of this system based on artificial intelligence and its hybridization schemes is the other objective of this study. To summarize, the objectives of this study are:

1. To dynamically model the transport phenomena, hydrodynamics and kinetics of the system considering particle elutriation and validate the model with real world industrial data as well as literature.
2. To design various advanced controllers based on AI to optimally regulate necessary reactor and polymer operating variables and compare them with conventional controllers.

1.4 Scope of work

The objectives of this study are accomplished by considering the following work scopes:
The kinetics, hydrodynamics and transport phenomena equations are gathered and coded in MATLAB®.
The model is then linked to SIMULINK® to solve the equations with respect to time (dynamically).
The results are compared with the industrial data and literature for validation.
PID controllers are designed to check how they perform in controlling the Melt Flow Index (MFI) and temperature.

An Adaptive Neuro-Fuzzy Inference System (ANFIS) controller is designed to cover the drawbacks of the PID and optimally control the MFI.

An ANFIS controller is designed to check how it performs in controlling the temperature.

A hybrid PID–ANFIS controller is designed to cover the drawbacks of the PID and ANFIS controllers and optimally control the temperature.

1.5 Contributions

Based on the objectives and results of this study, contributions of the current work are as follows:

- An improved fully dynamic two–phase ethylene and 1-butene copolymerization model with two–site kinetics is developed to predict the behavior of industrial polyethylene production reactors and polymer properties.
- Particle elutriation is considered in order to take the losses of entrained catalyst and polymer particles from the fluidized–bed into account.
- Artificial Intelligence (AI) based controllers are applied in this system to control the parameters. An ANFIS controller for MFI and a hybrid ANFIS-PID controller for the reactor temperature were designed which could control these variables optimally.

1.6 Thesis organization

This thesis dealing with different aspects relevant to the topic of the study as follows:

Chapter 1: Introduction

This chapter includes a brief introduction to the research and objectives of the study.

Chapter 2: Literature Review

This chapter gives a comprehensive literature survey for the classification of olefin polymerization processes and the kinetic, mathematical modeling and control of ethylene polymerization in FBRs.

Chapter 3: Dynamic two–phase modeling of catalytic ethylene copolymerization in fluidized–bed reactors

This chapter describes how and why the system is dynamically modelled in two phases and by considering heterogeneous ethylene copolymerization reactions to take place at two sites within the Ziegler–Natta (Z–N) catalyst. The results of the developed model is presented and is then validated with industrial and compared to the literature data.

Chapter 4: Advanced control of reactor temperature and polymer melt flow index

The model developed in the third chapter is used to study control structures on polymer MFI and reactor temperature. Hybrid AI-based controllers are used for this goal.

Chapter 5: Conclusions and future works In the last chapter, results and findings of the study were summarized followed by ideas and gaps that may be used as objectives for future works.

CHAPTER 2: LITERATURE REVIEW

2.1 Introduction

Olefin polymerization in gas-phase fluidized–bed reactors is known to be one of the most economic methods of manufacturing commodity polymers including polyethylene (PE), polypropylene (PP) and ethylene-propylene rubber (EPR). Some chemical processes are catalyzed by solids and fluidized–bed reactors are extensively used within these operations. The act of producing polyolefins by using heterogeneous Ziegler–Natta catalysts is a common instance. Not like other processes to produce polyethylene, the polymerizing of monomers in a gas-phase fluidized–bed reactor is shown to have better heat removal, working at much lower temperatures and pressures, and not needing solvents, all contributing to its very broad use in industries (M. Alizadeh, Mostoufi, Pourmahdian, & Sotudeh-Gharebagh, 2004). Figure 2.1 sheds light on a typical fluidized–bed polyethylene reactor process flow diagram.

Under normal circumstances, fluidized–bed reactors for polyethylene production are available in the industry at temperatures between $75°C$ to $110°C$ and pressures ranging from 20 to 40 *bar* (Xie, McAuley, Hsu, & Bacon, 1994).

2.2 Background

Various models have been recommended so that one can understand how a gas-phase ethylene polymerization works in real-life applications. Researchers have modeled these fluidized–bed reactors in the form of single, two or three phase reactors (Choi & Ray, 1985; McAuley, Talbot, & Harris, 1994; Fernandes & Lona Batista, 1999).

Several researchers have reviewed modeling or control of fluidized–bed reactors. Kiparissides (1996) classified the various polymers according to their molecular structure and briefly reviewed the various polymerization mechanisms, main mathematical

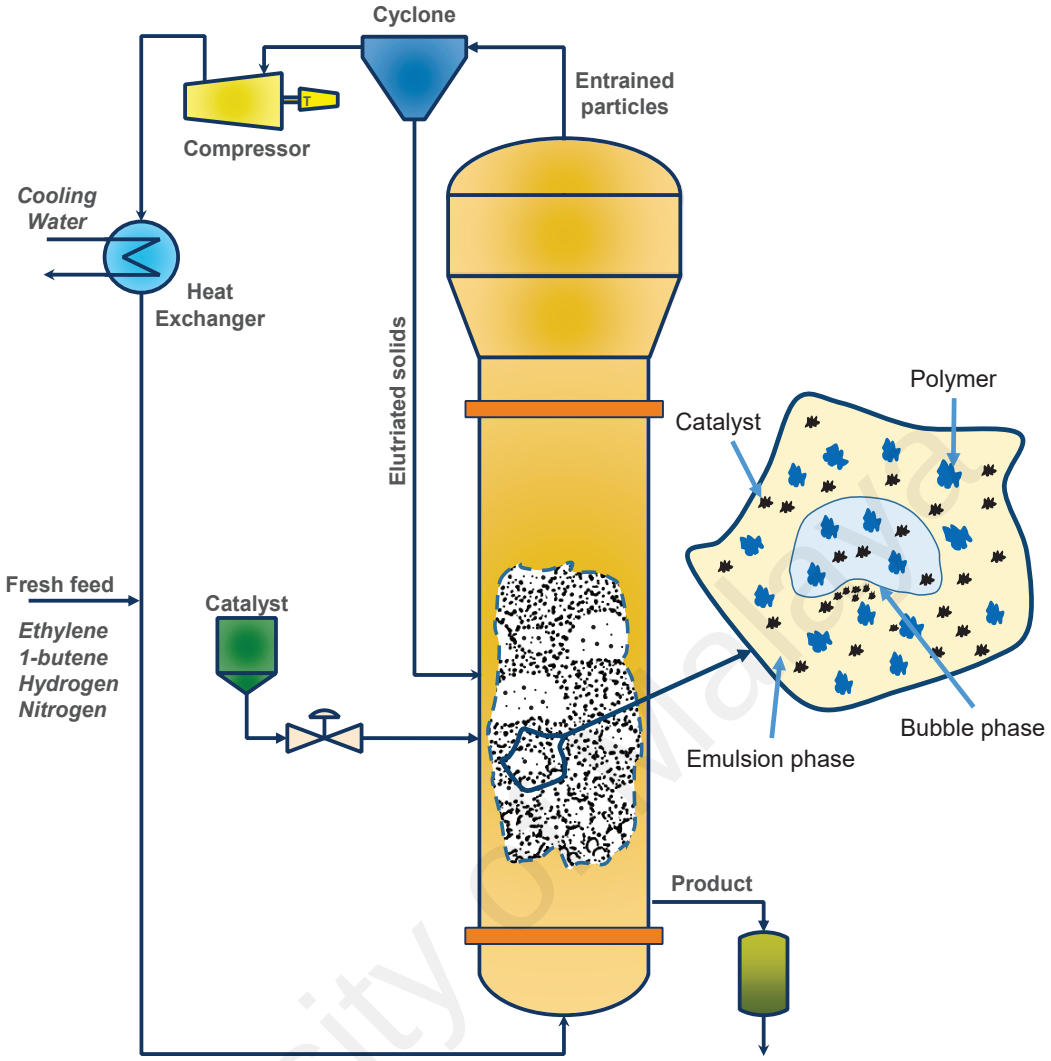

Figure 2.1: Schematic diagram of an industrial fluidized–bed polyethylene reactor and the existing phases

approaches available at the time and presented a method for developing polymer reactor models. They also discussed the benefits of optimization and control of polymer reactors and future directions related to the development of computer-aided design, monitoring, optimization, and control for polymerization processes. Harmon Ray and Villa (2000) examined the key reaction parameters for a variety of polymers produced using several types of reactors and illustrated the nonlinearity which can arise in industrial reactors. Some of the effects of imperfect mixing were also shown. McKenna and Soares (2001) have reviewed some single particle models for olefin polymerization that can be used

to describe particle growth, polymerization rates, concentration and temperature radial profiles, polymer micro-structure, and particle morphology. Mahecha-Botero, Grace, Elnashaie, and Lim (2009) presented a comprehensive review of fluidized–bed catalytic reactor models. The authors analyzed and categorized forty models depending on the characteristics of the conservation equations and their underlying assumptions. Since some approaches consider the reactor as a black box and try to model it using artificial intelligence, Noor, Ahmad, Don, and Uzir (2010) reviewed the use of neural networks in modeling and control of polymerization processes. Computational fluid dynamics (CFD) has also been used extensively in modeling polymerization in fluidized–bed reactors. Khan et al. (2014) reviewed the applications of these approaches and analyzed their capabilities and shortcomings. Recently, Philippsen, Vilela, and Zen (2015) presented a general summary of the mathematical models used in modeling fluidized–bed reactors in all its process applications.

Process modeling and control are two fields that are fast-changing, proving that they are useful towards achieving sustainability and green processing. They help forecast the system performance without having to build pilot plants that can be expensive and tedious. Furthermore, judging the strict environmental constraints we have today, advanced controllers are vital to guarantee that the operation is safe.

2.3 Polymer classification and processes for olefin polymerization

2.3.1 Classification of polymers

Polymers are made up from many monomers which are connected. These monomers connect in a series of kinetic reactions called polymerization reactions. One way to classify polymers is by their kinetic mechanism and molecular structure. Polymers can be classified into several types by categorizing them based on the number of different structural entities present in a polymer chain:

- Homo-polymers which are the polymer chains that are made of many single repeating units linked together.
- copolymers are those polymers which are made from two or more types of monomers.

Bi-polymers, ter-polymers, multi-polymers are the varying types of copolymers made from two, three or more types of monomers. Polymerizations can be classified into varying categories based on their chain growth mechanism:

- Step-growth polymerizations: Typically, step-growth polymerization advances by the reactions among two functional groups that are dissimilar to one another.
- Chain polymerizations: Chain polymerization or addition polymerization occurs when monomer molecules continue to be added to an active chain center in a very brief period until the polymer chains grow to the largest size. Chain polymerization can make its way through free-radical, anionic, cationic, coordination polymerization and group transfer mechanisms, which need a chain initiator that creates the main active sites centers (Kiparissides, 1996).

2.3.2 Processes for olefin polymerization

Polymerization processes can be broken down into homogeneous and heterogeneous. While the reactions of the former occur in one phase only, that of the latter occurs when a different phase is present. In the latter case, chemical reactions, heat transfer, and inter-phase mass transfers are impending. Two scenarios prevail in the heterogeneous system. One is that polymerization may deal with several phases (e.g. dispersion polymerizations, solid catalytic polymerizations) and other is that polymer be insoluble in the monomer phase (e.g. bulk precipitation polymerization of acrilonitrile). In fact, polymerization processes can be distinguished as: bulk, solution, precipitation, suspension, emulsion,

solid state, inter-facial polycondensation and solid catalyzed polymerization (Kiparissides, 1996).

In heterogeneous systems either the polymer is insoluble in the monomer phase (e.g. bulk precipitation polymerization of acrilonitrile) or the polymerization involves the presence of different phases (e.g. dispersion polymerizations, solid catalytic polymerizations). More specifically one can distinguish the following polymerization processes: (i) Bulk, (ii) Solution, (iii) Precipitation, (iv) Suspension, (v) Emulsion, (vi) Solid catalyzed polymerization, (vii) Interracial polycondensation, (viii) Solid state.

Heterogeneous catalysts are normally used for olefin polymerization processes, but some processes also make use of soluble catalysts. There are three major types of catalysts used for olefin polymerization processes: Ziegler–Natta, Phillips, and Metallocene. Most Ziegler–Natta polymerization reactions depend on titanium catalyst systems. Ziegler–Natta catalysts consisting of a transition metal compound and an activator are in general, variations that have the same theme, integrated with a wide range of electron donors and co-catalysts. The most popular catalysts are the Ziegler–Natta catalysts, used for polyethylene and polypropylene production. Phillips catalysts are made up of a chromium oxide support-ed on an amorphous material such as silica or silica/alumina (Soares, 2001) while Metallocene catalysts are based on the metallocene of group 4 transition metals with methylalumin oxane.

In solid catalyzed polymerization, the main processes adopted to produce polyolefins are: slurry-phase process, solution process and gas-phase process. Continuous-stirred tank and loop reactors are the main reactors for slurry-phase olefin polymerization, and fluidized–beds or vertical or horizontal stirred bed reactors are chosen for gas-phase processes. The existing processes for olefins polymerizations are normally different in the reactor media's physical state and the process unit's operating condition. The catalyst,

desired range of products to be produced, economics and feed stock availability are the main parameters or loosely speaking, determinants to the olefin polymerization process method. Olefin monomers can be polymerized to make up polyolefin. Ethylene or propylene may be homo-polymerized to create polyethylene and polypropylene, or copolymerized together or with higher 1-olefins such as 1-butene, 1-pentene, 4-methyl-1-pentene, 1-hexene and others using one or more catalytic metal compounds, usually transition metals, together with a co-catalyst and/or a support for example, with alumina or silica. Olefin polymerization processes and their characteristics that are most common are summarized in Table 2.1 (Ray, 1991).

Table 2.1: Most common olefin polymerization processes

Process	Solution	Slurry	Gas Phase
Particle Size (μm)	—-	$10 - 10^4$	$10 - 10^4$
Commercial Reactor Types	CSTR	Batch,CSTR,Loop	Fluidized Bed, Stirred Bed
Kinetic Mechanism	Coordination	Coordination	Coordination
Examples (including co-polymers)	LDPE	HDPE, PP, EP	HDPE, LLDPE, PP, EP

2.3.2.1 Slurry and solution phase processes

The two primary reactors for slurry-phase olefin polymerization are the loop reactor and continuous-stirred tanks. In a typical way, slurry polymerization processes are carried out in a high-pressure continuous reactor. In the process, components such as one or more monomers, a diluent, and a catalyst system and other reactants are introduced to the polymerization reactor to create a reaction mixture, the solid olefin polymer particles and catalyst particles are suspended and mixed well in a liquid diluent. On the other hand, for solution polymerization processes, a monomer is dissolved in a non-reactive solvent having a catalyst where the solvent temperature is high enough for the dissolution of the polymer material. The heat released by the reaction is absorbed by the solvent, and thereby

reducing the reaction rate. In both processes, concentrations of the monomers are high, and the liquid can well remove the polymerization heat from the polymer particles which is the most attractive feature about these processes. However, separation of the polymer from the solution is often an expensive operation (Zacca, Debling, & Ray, 1996).

2.3.2.2 Gas-phase processes

Gas-phase olefin polymerization processes prepare an environment that is conducive for olefin polymerization. The remarkable characteristics of gas-phase olefin polymerization lie in the fact that as the system does not involve any liquid phase in the polymerization zone, the gas phase plays a role in the provision of monomers, the integration of polymer particles and removal of the heat of reaction. In this system, polymerization reaction occurs at the interface between the solid catalyst and the polymer matrix. This process includes the vertical stirred bed reactor (VSBR), horizontal stirred bed reactor (HSBR) and fluidized–bed reactor (FBR). In the gas-phase polymerization process, reactors must work closely to the dew point of the monomer mixture to achieve high monomer concentrations and high yields and the catalyst morphology must be very tightly controlled so that particle melting and agglomeration due to the heat transfer limitation of the gas can be prevented.

2.4 Modeling of fluidized–bed polymerization reactors

The ability to justify how the reaction mechanism, the transport phenomena, the reactor type and reactor operating conditions affect the polymer quality of the final product is an important aim of polymerization processes (Kiparissides, 1996). The polymer quality concerns with all the molecular structure properties and the polymer product's macroscopic morphological properties. Thus, it is only practical to classify these various phenomena that take place into the following:

- Chemical Reaction engineering

- Hydrodynamics
- Transport phenomena
- Particle population balance

Chemical reaction engineering is concerned with the reaction chemistry and reaction mechanisms and rate laws. The particle size and trajectory depends on the specific hydrodynamic correlations that are applied. Transport phenomena defines the transient mass and energy balance equations, while the population balances offer the steady state particle population balance. All the chemical and physical phenomena seen in polymerization can be classified into these modeling levels (Ray, 1991; Kiparissides, 1996; McKenna & Soares, 2001):

- **Microscale:** Modelling of polymerization kinetics, the nature of active sites, diffusion of monomer in the polymer and crystallization of polymer molecules.
- **Mesoscale:** Modelling of inter-particle, intra-particle, and particle–wall interactions, especially in terms of heat and mass transfer.
- **Macroscale:** Detailed description of reactor hydrodynamics in order to model mixing and reactor stability, reactor and particle size distributions, particle entrainment, etc.

In fact, multi scale models are needed to fully discuss the nature of this process.

2.4.1 Review of fluidization basics

In such reactors, gas or liquid is passed through solid particles at some velocities considered high enough to suspend the solid and makes it act like fluid. Fluidization has an extensive use in industries and the applications of fluidization can be divided into physical and chemical operations. The fluidized–bed reactor functions in diverse industrial applications because of the high contacting methods, uniform particle mixing, uniform

temperature gradients and the ability to run reactor continuously. Various processes have been able to adopt this technology, successfully. This includes olefin polymerization, reforming and cracking of hydrocarbons, coal gasification and carbonization, and many others.

2.4.1.1 Flow regimes in fluidization

There are different behaviors noted for the fluidized–beds in which the solid particles are fluidized because of the variety in the gas, solid and velocity properties. With a growth in the gas velocity in the minimum fluidization regime, the bed voidage will escalate marginally and the drag force conveyed by the rising gas equals the weight of the particles. Next, the bed will go into the gas fluidization state. Higher levels of gas velocity mean that bubbles will set in and a bubbling fluidized–bed would be seen. The bubbles in a bubbling fluidized–bed will propagate and coalesce when it rises while the velocity intensifies. In the slugging bed, the height to diameter ratio (H/D) of the bed is high enough and the bubble size may become the same as the bed's diameter. The fluidization of particles will occur at a high enough gas flow rate in a turbulent bed, where the velocity will exceed the particles' terminal velocity. Instead of the bubbles, the upper surface of the bed vanishes and a turbulent motion of solid masses and voids of gas with different dimensions are seen. Pneumatic transport of solids occurs with higher amount of gas velocity, and the fluidized–bed becomes an entrained bed in which dispersed, lean or dilute phase fluidized–bed would be found.

2.4.1.2 Bubbling fluidized–beds

Gas fluidized–beds are differentiated by the bubbles formed at superficial gas velocities larger than minimum fluidization velocity. In this state, it appears that the bed is distributed into the emulsion phase and the bubble phase. The bubbles are very analogous to gas

bubbles in liquid form, and they act similarly, and merge while rising through the bed. The movement of particles in fluidized–beds receives most influence from the rising bubbles passing through the bed. The bubbles formation, the way particles are transported and their path through the bed should not to be taken lightly. As the result, extreme consideration is given to these bubbles and their properties.

2.4.2 Modeling approaches

Mixing conditions and the number of phases existing in the bed are the focal point of the literature in terms of modeling the operation of a catalytic olefin polymerization in fluidized–bed reactors. The many phases that carry their own chemical reactions and inter-phase heat and mass transfer exist in various heterogeneous polymerization system, resulting in a comprehensive and realistic model that will account for all these complex gas and solid flows, mechanisms of mass and heat transfers and polymerization kinetics. Regarding the hydrodynamics, several methods were recommended in the literature to explain in detail the fluidized–bed polyolefin reactors.

McAuley et al. (1994) and Xie et al. (1994) introduced a well-mixed reactor as their attempt to describe fluidized–bed polyolefin reactors. They drew a comparison between this approach and simple two–phase models in steady state and conclusively said that the latter shows very little error when it predicts the reactor temperature and monomer concentration. Choi and Ray (1985) considered the reactor to come in two phases of emulsion and bubble and they recommended the simple two–phase model. They rested their conclusion on the solid-free bubbles which shows that polymerization only takes place in the emulsion phase.

Fernandes and Lona (2001) pitched the idea of a three-phase heterogeneous model which considered emulsion, bubble and solid phases and believed that they work as a plug flow. Hatzantonis, Yiannoulakis, Yiagopoulos, and Kiparissides (2000) broke the

reactor further into several solid-free well-mixed compartments in series and considered that the emulsion and bubble phases are altogether mixed. M. Alizadeh et al. (2004) also embodied the reactor hydrodynamics using a tanks-in-series model. Harshe, Utikar, and Ranade (2004) further created an inclusive mathematical model based on the mixing cell framework to study the fluidized–bed polypropylene reactors' momentary behavior. The authors also combined this model with a population balance model in steady state.

Ibrehem, Hussain, and Ghasem (2009) put forth a four-phase model and suggested that a fluidized–bed reactor can involve emulsion, bubble, solid and cloud phases, but the authors assumed that the polymerization reactions only happen in the emulsion and solid phases. They also accounted for the effect of catalyst particles type and porosity on the reaction rate. Kiashemshaki, Mostoufi, Sotudeh-Gharebagh, and Pourmahdian (2004) had reserved four parallel sections for the reactor. Each section has its emulsion phase and the mixed and the bubble phase as plug flow. The authors assumed that the polymerization would occur in both phases. Khare et al. (2004) and Luo, Su, Shi, and Zheng (2009) used software like Aspen Dynamic and Polymer Plus together with major basics of chemical engineering for the development of their model. Consideration was given to key issues such as selecting thermodynamic model and physical property, catalyst characterization, to name but a few. Khare et al. (2004) introduced a model for gas phase polypropylene polymerization in stirred-bed reactors applicable to both steady-state and dynamic gas phase while Luo et al. (2009) built a model for commercial bulk polypropylene polymerization with Hypo Technology. An assumption is made by Khare et al. (2004) with respect to the existence of multiple catalyst active sites in Ziegler–Natta catalyst. Their model that has a set of thermodynamic and kinetic parameters predicts the polymer production rate, polydispersity index, and molecular weight. The authors highlighted measures for the development and validation of the polymerization model by focusing on

the thermodynamic and physical model selections, reactor model, catalyst characterization, and Ziegler–Natta polymerization kinetics.

The very intention of the reactor modeling and control is to reach acceptable heat removal and production rate from the reactor. The reactor model behavior is subjected to several process variables like monomer concentration, catalyst feed rate, feed gas temperature, superficial gas velocity and catalyst activity.

2.4.2.1 Hydrodynamics

Fluidized–bed reactors carry with them several issues. They are non-ideal and challenging to elaborate due to complicated transport phenomena, flow patterns, and polymerization reactions. Myriad studies have centered on several mixing models to model such non-ideality to characterize fluidized–bed reactors' behavior. Non-ideal fluidized–bed reactor modeling would need the integration of transport phenomena, kinetics, and hydrodynamics equations. Choi and Ray (1985) put forth a two–phase model with constant bubble. The authors placed it on a plug-flow bubble phase and a fully mixed emulsion phase to find traits of the FBR dynamic behavior. McAuley et al. (1990) further guessed that there is an unlimited heat and mass transfer between the emulsion and bubble phases and recommended a much simpler well-mixed model.

The traditional well mixed and constant bubble size models assumes solid-free bubbles ($\varepsilon_b = 1$) and that the fluidization of the emulsion phase is at the minimum ($\varepsilon_e = \varepsilon_{mf}$). This concept does not gauge the impact of the dynamic gas–solid distribution on the heat/mass transfer and reaction rate in the fluidized–beds and has its restrictions when it comes to describing the low-velocity bubbling fluidization. Cui, Mostoufi, and Chaouki (2000) nonetheless, have been able to prove theoretically and experimentally the presence of solid particles in the bubbles. They also proved that the emulsion phase may have more gas at higher gas velocities and it does not stay at minimum conditions of fluidization. Increasing

the superficial gas velocity contributes towards the better mixture of the two phases to better mix together, making more amounts of gas to be able to enter the emulsion phase and further leading to higher solid particles entering the bubbles.

2.4.2.2 The well-mixed model

McAuley et al. (1990, 1994) made a proper introduction of the fluidized–bed approximated by a single phase continuous stirred tank reactor in the well-mixed model. This assumption is believed valid for very high mass and heat transfer rates between phases (uniform monomer concentration and temperature throughout the bed) or small size bubbles. Bubble phase does not function in the model and the bed voidage (ε_{bed}) contemplates on the entire gas volume fraction in the bed. The following is a set of assumptions that would work for the well mixed model:

- Polymerization reactor is a single phase (emulsion phase) well mixed reactor because of high heat and mass transfer rates between phases or possibly because bubbles are sufficiently small.
- Composition and temperature are the same throughout the bed.
- The emulsion phase stays at minimum fluidization state.

Dynamic mass and energy balances are obtainable for the system based on the above assumptions, for hydrogen and monomers.

The mole balance is given by:

$$(V\varepsilon_{mf})\frac{d[M_i]}{dt} = U_0 A\,([M_i]_{in} - [M_i]) - R_v\varepsilon_{mf}[M_i] - (1-\varepsilon_{mf})R_i \qquad (2.1)$$

The energy balance is expressed by:

$$\left[\sum_{i=1}^{m}[M_i]C_{pi}V\varepsilon_{mf} + V(1-\varepsilon_{mf})\rho_{pol}C_{p,po1}\right]\frac{dT}{dt} = U_0A\sum_{i=1}^{m}[M_i]C_{pi}(T_{in}-T_{ref})$$
$$-R_v\left[\sum_{i=1}^{m}[M_i]C_{pi}\varepsilon_{mf} + (1-\varepsilon_{mf})\rho_{po1}C_{p,po1}\right](T-T_{ref}) + (1-\varepsilon_{mf})\Delta H_R R_p \qquad (2.2)$$
$$-U_0A\sum_{i=1}^{m}[M_i]C_{pi}(T-T_{ref})$$

In the energy balance equation, the monomer internal energy is deemed insignificant. The conditions needed to address the model equation are as follows:

$$[M_i]_{t=o} = [M_i]_{in} \qquad (2.3)$$

$$T(t=0) = T_{in} \qquad (2.4)$$

For kinetics and hydrodynamics equations, one can take guidance from the literature for additional information (McAuley et al., 1994, 1990; Hatzantonis et al., 2000).

2.4.2.3 The constant bubble size model

In this model, we consider the assumption made by (Choi & Ray, 1985) that the fluidized–bed comes in two phases: the phase where polymerization happens (emulsion or bubble phase). In the constant bubble size model, it is safe to assume that the bubbles, at constant velocity, travel through the bed in plug flow where the spherical size is characterized as fixed and consistent. We also need to consider the fact that the emulsion phase is interchanging heat and mass with the bubble phase and the mixture comes in full mixture. To add, the mass and heat transfer coefficients are constant throughout the bed, and we are led to believe that the heat and mass transfer resistances between the solid polymer particles and the monomer gas in the emulsion phase are trivial (Floyd, Choi, Taylor, & Ray, 1986). The constant bubble size model however, consider these

assumptions:

1. The fluidized–bed is made of the emulsion and bubble phases. The former is where the reactions would occur.
2. The bubbles are in plug flow and the spherical size is the same among each other. Their velocity is also constant.
3. It is believed that the emulsion phase is fixed at the minimum stage of fluidization, and that it the mixture is perfect, exchanging mass and heat with the bubble phase at constant rates over the bed height.
4. The gas and the solid polymer particles in the emulsion phase possess negligible inter-phase heat and mass transfer resistances (Floyd et al., 1986).

It is through these assumptions that the steady-state mass and energy balances are derived. The mole balance for monomer and hydrogen can be expresses as such:

$$\begin{aligned}[\bar{M}_i]_b &= \tfrac{1}{H}\int_0^H [M_i]_b\, dh \\ &= [M_i]_e + \left([M_i]_{e,(in)} - [M_i]_e\right)\tfrac{U_b}{K_{be}H}\left(1-\exp\left(-\tfrac{K_{be}H}{U_b}\right)\right)\end{aligned} \tag{2.5}$$

The bubble phase energy balance can be written as in the following:

$$\sum_{i=1}^{m}[M_i]_b C_{pi}\frac{dT_b}{dz} = \frac{H_{be}}{U_b}(T_b - T_e) \tag{2.6}$$

The dynamic molar balance for the i-th monomer in the emulsion phase is expressed by:

$$\begin{aligned}&(V_e\varepsilon_{mf})\tfrac{d[M_i]_e}{dt} = U_e A_e \varepsilon_{mf}\left([M_i]_{e,(in)} - [M_i]_e\right) + \tfrac{V_e\delta K_{be}}{(1-\delta)}\left(\left[\bar{M}_i\right]_b - [M_i]_e\right) \\ &-R_v\varepsilon_{mf}[M_i]_e - (1-\varepsilon_{mf})R_i\end{aligned} \tag{2.7}$$

The dynamic energy balance for emulsion phase can be written below:

$$\begin{aligned}
&\left[\sum_{i=1}^{m} V_e \varepsilon_{mf} [M_i]_e C_{pi} + V_e(1-\varepsilon_{mf})\rho_{Po1} C_{p,po1}\right] \frac{dT_e}{dt} = \\
&-\sum_{i=1}^{m} V_e \varepsilon_{mf} C_{pi} \frac{d[M_i]_e}{dt}(T_e - T_{ref}) + U_e A_e \varepsilon_{mf} \sum_{i=1}^{m} [M_i]_{e,(in)} C_{pi}(T_{e,(in)} - T_{ref}) \\
&-U_e A_e \varepsilon_{mf} \sum_{i=1}^{m} [M_i]_e C_{pi}(T_e - T_{ref}) - \frac{V_e \delta H_{be}}{(1-\delta)}(T_e - \bar{T}_b) \\
&+R_v \left((1-\varepsilon_{mf})\rho_{po1} C_{p,po1} + \varepsilon_{mf} \sum_{i=1}^{m} [M_i]_e C_{pi}\right)(T_e - T_{ref}) + (1-\varepsilon_{mf})\Delta H_R R_p
\end{aligned} \tag{2.8}$$

The boundary and initial conditions for solving the model equations are as follows:

$$[M_i]_{b,z=0} = [M_i]_{in} \tag{2.9}$$

$$T_b(z=0) = T_{in} \tag{2.10}$$

$$[M_i]_{e,t=0} = [M_i]_{in} \tag{2.11}$$

$$T_e(t=0) T_{in} \tag{2.12}$$

To estimate the gas velocities for bubble phase and emulsion phases, the bubble phase and emulsion phases voidage, the bed bubble volume fraction, and heat and mass transfer coefficients for the constant bubble size mode, the correlations needed for that purpose can be found from diverse sources in the literature (Shamiri, Wei, Fauzi, Hussain, & Mostoufi, 2015; Shamiri, Hussain, Mjalli, & Mostoufi, 2012).

2.4.2.4 The bubble-growth model

As we base it on the two–phase fluidization theory, In the bubble-growth model, based on the two–phase fluidization theory, the constant bubble size model was extended to account for the varying bubble size with respect to that must depend on the bed's height (Hatzantonis et al., 2000). Spurred by the developments of Kato and Wen (1969), in this

model, an assumption is that the bubble phase is divided into "N" well-mixed sections in series and the emulsion phase is mixed perfectly and at developing fluidization conditions ($\varepsilon_{bed} = \varepsilon_{mf}$). The bubble phase sections' size is fixed to be equal to the bubble diameter at the equivalent bed height. The local mass and heat transfer coefficients between the emulsion and bubble phases, the bubble rise velocity, and the local bubble volume fraction are ascertained by the bubble diameter and, thus, the equivalent bed height. This is owing to the fact that the bubble size has its minimum value at the gas distributor and it enlarges to its maximum constant size while it moves through the bed.

This model does not weigh the heat and mass transfer restrictions between the solid particles and the surrounding gas in the emulsion phase. Nevertheless, these limitations can become something that should not be taken lightly for high rates of polymerization.

If the bubbles are solid-free (no reaction), we can write the molar balance for the i monomer in the n compartment:

$$\begin{aligned}[M_i]_{b,n} &= [1 + (K_{be,n} d_{b,n}/u_{b,n})]^{-1} \\ &\times \left\{ \frac{\delta_{b,n-1} u_{b,n-1}}{\delta_{b,n} u_{b,n}} [M_i]_{b,n-1} + \frac{K_{be,n} d_{b,n}}{u_{b,n}} [M_i]_e \right\}\end{aligned} \tag{2.13}$$

where $d_{b,n}$ is the bubble size corresponding to the n compartment.

In effect, the energy balance for the n compartment can be written as follows:

$$\begin{aligned}T_{b,n} &= \left(\sum_{i=1}^{N_m} [M_i]_{b,n} C_{pM_i} + \frac{H_{be,n} d_{b,n}}{u_{b,n}} \right)^{-1} \\ &\times \left\{ \begin{array}{ll} \frac{\delta_{b,n-1} u_{b,n-1}}{\delta_{b,n} u_{b,n}} \sum_{i=1}^{N_m} & [M_i]_{b,n-1} C_{pM_i} (T_{b,n-1} - T_{ref}) \\ & + \sum_{i=1}^{N_m} [M_i]_{b,n} C_{pM_i} T_{ref} + \frac{H_{be,n} d_{b,n}}{u_{b,n}} T_e \end{array} \right\}\end{aligned} \tag{2.14}$$

The dynamic mass and energy equations can also be derived as follows, and this had been discussed by Hatzantonis et al. (2000).

2.4.2.5 Other mathematical approaches

Fernandes and Ferrareso Lona (2001) had contemplated on gas in bubble and emulsion phases plus solid polymer particles, all as plug flow phases, to suggest on their three-phase heterogeneous model. Jafari, Sotudeh-Gharebagh, and Mostoufi (2004) brought to comparison the performance of some available models of the time such as simple two phase model and generalized bubbling/turbulent model. They summed up that the later model gives the most fitted results to experimental data. Luo et al. (2009) had worked further on a methodology to model the polypropylene process based on Hypol Technology. The authors adopted the Polymer Plus and Aspen Dynamics to foresee process behavior and physical properties in the steady-state and dynamic modes. In something similar, Zheng, Shi, Su, Luo, and Li (2011) developed a steady- state and dynamic methodology to model the propylene process with the aid of the Spheripol Technology. Their kinetic model leaned on both single and multi-site catalyst and their molecular weight distribution results were fitted with the help of the actual gel permeation chromatography (GPC) data.

In the meantime, some researchers focused on particle size distribution studies in fluidized–beds rather than kinetic or property estimation (Ashrafi, Nazari-pouya, & Mostoufi, 2008; Khang & Lee, 1997; Immanuel et al., 2002). That said, fluidization regimes have also been studied in vast literature. Different methods that can ascertain the fluidization regimes in gas-solid fluidized–bed reactors have been applied on these reactors to study a number of hydrodynamic aspects (Tamadondar, Azizpour, Zarghami, Mostoufi, & Chaouki, 2012; Makkawi & Wright, 2002; Sederman, Gladden, & Mantle, 2007).

M. Alizadeh et al. (2004) put forth a pseudo-homogeneous tanks-in-series model to guess on the behavior of industrial-scale gas-phase polyethylene production reactor. Kiashemshaki, Mostoufi, and Sotudeh-Gharebagh (2006) were inspired by this model and they suggested a two–phase model to describe the fluidized–bed ethylene polymerization

reactor. Their model was a dynamic model except in terms of the computation of the temperature and comonomer concentrations.

Shamiri et al. (2015); Shamiri, Chakrabarti, et al. (2014); Shamiri, Hussain, Mjalli, Shafeeyan, and Mostoufi (2014); Shamiri, Hussain, sabri Mjalli, Mostoufi, and Hajimolana (2013); Shamiri et al. (2012); Shamiri, Hussain, Sabri Mjalli, Mostoufi, and Saleh Shafeeyan (2011); Shamiri, Hussain, Mjalli, and Mostoufi (2010) also analyzed different dynamic and non-dynamic modeling and control approaches for gas phase homopolymerization or copolymerization of olefin in fluidized–bed reactors.

2.4.2.6 Condensed mode cooling modeling

Injection of a quench liquid into the reactor is an accepted heat removal method in olefin polymerization FBRs. Although in polyethylene the "quench" liquid is usually an inert alkane (often referred to as an induced condensing agent, ICA), but it is the liquefied monomer in the case of polypropylene. Introduction of propylene copolymers and heavier monomers such as hexene or butene, provide the possibility of condensing these monomers and inserting them in liquid form in a gas phase process. To find out the effect of liquefied comonomer injection on the reaction rate, the influence of these components on solubility, transport, and other "physical" processes on one hand and their impact on the reaction on other hand need to be identified. As an example, instantaneous rate of ethylene polymerization increased in the presence of an ICA in the study which was done by Namkajorn, Alizadeh, Somsook, and McKenna (2014). The authors related this to the enhancement of the local concentration of ethylene due to the heavier hydrocarbon at the catalyst active sites. They also examined different isomers of pentane and hexane. A. Alizadeh, Namkajorn, Somsook, and McKenna (2015) concluded that the complex effects were the result of the alkane replacement with an similar alkene. Although based on thermodynamics both the alkanes and alkenes increase the rate of ethylene polymerization

via the cosolubility effect, but considering that the alkenes are also comonomers, they have a direct influence on the reaction rate. Moreover, they boost the polymerization rate (called comonomer effect) at low concentrations, nonetheless they decrease the reaction rate at higher concentrations in spite of the cosolubility effect. Nevertheless, the ethylene's concentration is higher in the existence of a heavier compound rather than ethylene alone.

Although, condensed mode cooling is common in industries, few studies have focused on modeling this approach to analyze its effect on the hydrodynamics, transport phenomena and polymerization reactions and there is still a need for models that can accurately account for the whole process considering the condensed mode cooling practice (Pan, Liang, Zhu, & Luo, 2017; A. Alizadeh et al., 2017; Zhou, Wang, Yang, & Wu, 2013; Mirzaei, Kiashemshaki, & Emami, 2007; Yang, Yang, Chen, & Rong, 2002; Jiang, McAuley, & Hsu, 1997).

2.4.2.7 Computational fluid dynamics (CFD) approaches

Computational fluid dynamics (CFD) is a category of fluid mechanics that uses numerical analysis and data structures to solve and analyze problems that involve flow of fluids (Schneiderbauer, Puttinger, Pirker, Aguayo, & Kanellopoulos, 2015). Researchers use computers to do the essential calculations to simulate the fluid and surface interactions defined by boundary conditions. With high performance computations, better solutions can be completed in less time.

CFD model development is a progressive research area for picturing fundamental phenomena without executing real-time experiments. It can be used to solve momentum and conservation equations in multiphase flows. For polymerization reactors, an added benefit of CFD is that it can offer information on turbulent zoneswhich is very important because the reactants are mostly inserted within these areas where the reaction yield is superior (Dompazis, Kanellopoulos, Touloupides, & Kiparissides, 2008).

Two methods of CFD models, i.e., Eulerian and Lagrangian, are generally used to define gas–solid fluidized–bed reactors. Both phases (gas and solid) are counted as continuum (fluid) in the Eulerian model, and momentum and continuity equations are dealt with for both phases. The Lagrangian model on the other hand, solves Newton's equations of motion for each particle and particle–particle collisions and applied forces on the particle are considered. The Eulerian–Lagrangian method, which is also known as discrete element method (DEM) or discrete particle model (DPM), studies the fluid as a continuum and considers solids to be dispersed phase (Schneiderbauer, Haider, Hauzenberger, & Pirker, 2016). The DEM models the continuous phase and particle trajectories using uses the Eulerian and Lagrangian frameworks respectively. The continuous phase can be modeled by averaging its properties over a extensive varieties of these paths or trajectories. However, to obtain an average of all quantities in a moment, it is advised that a plentiful of particle trajectories be simulated. Gas and emulsion phases are presumed to be continuous in the Eulerian–Eulerian approach while they are considered completely interpenetrating in all control volumes.

Particle size distribution is a key factor in CFD studies of this system. To define the particle size distribution in a multiphase flow, the population balance equation (PBE), continuity, momentum, and energy equations need to be solved simultaneously. Researchers have used a combination of PBE solving methods with CFD in order to address particle size distributions and flow patterns within polymerization FBRs (Akbari, Borhani, et al., 2015; Akbari, Nejad Ghaffar Borhani, Shamiri, & Kamaruddin Abd. Hamid, 2015; Che et al., 2015a, 2016; Yan, Luo, Lu, & Chen, 2012).

Several researchers also performed advanced investigations on the influence of operating conditions and geometry of the reactor, like type of distributor, size of solid particles, gas velocity and operating pressure on the hydrodynamics of the reactor, for accurate scale-up

and design of reactors (Akbari, Nejad Ghaffar Borhani, Aramesh, et al., 2015; Akbari, Borhani, Godini, & Hamid, 2014; Che et al., 2015b).

2.5 Control of olefin polymerization in fluidized–bed reactors

Modeling and controlling polyolefins polymerization in fluidized–bed reactors are difficult to perform because of its highly non-linear behavior. This is the direct impact of having complex flow characteristics of gas and solids, various mass and heat transfer mechanisms, very complex reaction mechanisms and the interaction that takes place between process control loops. Bequette (1991) reviewed the nonlinear control system techniques extensively. He regarded the techniques promising since they can address common problems associated with chemical processes. While the progress in nonlinear control is encouraging, several goals for future research in nonlinear control of chemical processes were explained thoroughly. Several research articles were published in the past years surrounding the modeling and control of olefin polymerization processes. This literature using various algorithm types as control strategy is shown in a summary in Table 2.2.

Table 2.2: Summary of control studies in olefin polymerization

Reactor type	Model	Controller	Control variables	Reference
CSTR–PP	well mixed	PID	temperature, bed level, pressure	(Choi & Ray, 1988)
FBR–PE	two phase	PID	temperature, bed level, feed concentration, pressure	(Vahidi et al., 2008)
FBR–PE	well mixed	LMPC, NMPC, PI	bleed flow and pressure, feed flow rates , temperature	(E. Ali et al., 2003)

Table2.2: Summary of control studies in olefin polymerization, cont.

Reactor type	Model	Controller	Control variables	Reference
FBR–PE	well mixed	ETC	temperature	(Dadebo et al., 1997)
FBR–PE	well mixed	PID	melt index and density	(McAuley & MacGregor, 1992)
FBR–PE&PP	two phase	PI	temperature	(Choi & Ray, 1985)
HSR–PP	well mixed	GMC	melt index, monomer conversion	(M. A. Ali et al., 2007)
FBR–PE	well mixed	IMC	melt index, density	(Mcauley & Macgregor, 1993)
FBR–PE	two phase	MPC	temperature, melt index, production rate and density	(Brempt et al., 2001)
FBR–PE	four phase	NNMPC	molecular weight, temperature	(Ibrehem et al., 2008)
FBR–PE	two phase & well mixed	PID	temperature, pressure, bed level	(Sarvaramini et al., 2008)
CSTR–PE	well mixed	NMPC	production rate, partial pressures of the gas phase compositions	(Seki et al., 2001)
FBR–PE	two phase	PI	temperature, monomer concentration	(E. M. Ali & Abasaeed, 1999)
FBR–PE	two phase	PI, NMPC	temperature, monomer concentration	(E. M. Ali & Abasaeed, 1998)
FBR–PE	well mixed	NMPC	molecular weight distribution	(E. M. Ali & Ali, 2010)

Table2.2: Summary of control studies in olefin polymerization, cont.

Reactor type	Model	Controller	Control variables	Reference
FBR–PE	two phase	PID	bed level	(Hassimi et al., 2009)
FBR–PE	well mixed	PI	bed level, production rate, temperature, melt flow index, pressure, density	(Chatzidoukas et al., 2003)
FBR–PE	well mixed	PID, optimal servo system	density and melt flow index	(Sato et al., 2000)
FBR–PE	well mixed	PID	temperature	(Salau et al., 2008)
FBR–PE	two phase	PI	temperature	(Ghasem, 2000)
FBR–PE	well mixed	fuzzy logic	temperature	(Ghasem, 2006)
slurry–PE	well mixed	NMPC	amount of unreacted monomer, melt flow index	(Bolsoni et al., 2000)
jCSTR–PS	well mixed	adaptive back stepping	Temperature, monomer concentration	(Biswas & Samanta, 2013)
FBR–PP	Two phase	MPC	Temperature, production rate	(Shamiri, Hussain, sabri Mjalli, et al., 2013)
FBR–PP	Two phase	APMBC	Temperature, production rate	(Ho et al., 2012)
Batch–PS	Kinetics based NN	NN-MPC	temperature	(Anwar et al., 2011)

2.5.1 Conventional control

Despite many sophisticated control theories and techniques that have been devised in the last decades, conventional controllers especially proportional integral (PI) controllers are still the most implemented in real-world cases. In fact, due to their simple structure, PI controllers are easy to tune, and their use is well understood by a clear majority of industrial practitioners and automatic control designers.

Choi and Ray (1985) used PI controller to control the reactor temperature in an olefin homopolymerization FBR by manipulating feed gas temperature. The authors concluded that reactor temperature can be controlled if there is sufficient heat removal capacity in the system. The authors later studied the PID control of temperature, bed level, and pressure in a solid catalyzed gas phase CSTR.

The closed-loop simulations by E. M. Ali and Abasaeed (1998) using a PI controller on an industrial model of gas-phase ethylene polymerization reactor showed that a single control loop with the feed temperature as the manipulated variable is not sufficient to stabilize the reactor temperature against external disturbances. Another met disadvantage of the PI controller was the need to re-tune the controller parameters from case to case. The authors found that a multi-loop control scheme must be used to improve the feedback response and they did so using an NLMPC controller. The authors later in another study, tried to overcome the PI shortcomings in SISO and MIMO cases by on-line adaptive tuning and finding proper control structures. Ghasem (2000) also studied the dynamics of a UNIPOL® process using their model an PI controller. In the same ear, Sato et al. (2000) developed a model based on the work of McAuley et al. (1990) and applied a two by two MIMO PI control structure to control MFI and density by changing feed hydrogen and butene flow rates.

Salau et al. (2008) studied dynamic behavior of this process using their proposed model and utilized PID controller designed via optimization in the frequency domain to control the reactor temperature by manipulating the cold-water valve position.

2.5.2 AI-based control

Conventional controllers such as PID controllers are popular in industrial applications since their design is easy, the structure is straightforward, and the cost is reasonable. However, their performance is abysmal when they are vulnerable to unknown disturbances. An effective way of handling such non-linearity is to adopt fuzzy logic, characterizing an enhancement in the transient characteristic of the control performance. By contrast, setting up a systematic design method for fuzzy controls is not an easy task to do, since it is non-linear in nature and as a result, has no mathematical design method as its support. The excellent performance of fuzzy control in transient state combined with the high accuracy of PI control in the steady state, would give us a solution that be very workable.

Alexandridis, Siettos, Sarimveis, Boudouvis, and Bafas (2002), based on fuzzy systems, had set up a systematic method to the nonlinear system identification problem. This fresh method had led to a linguistic and an analytic system model. The method was tested in a Continuous Stirred Tank Reactor (CSTR) to diagnose fixed operating states. The model could display several types of nonlinear manners successfully.

Mollov, van den Boom, Cuesta, Ollero, and Babuska (2002), offered the synthesis of a TS fuzzy based predictive controller for a nonlinear process which led to a robust control system. The successfulness of this method was proven via both simulation and laboratory setups for on-line control of a cascaded-tanks setup. A predictive control technique which takes its guidance from the dynamic TS fuzzy model was put forth by Sarimveis and Bafas (2003). This model was employed to forecast the upcoming performance of the control variable in a SISO control loop. Aided by a genetic algorithm, the controller's objective function was solved on line. The suggested method was put on an arbitrary process in a non-isothermal CSTR and the authors claimed that it can be applied to all types of fuzzy models, being primarily beneficial in cases where a fuzzy controller cannot be constructed directly as the system is found to be a complicated one.

Habbi, Zelmat, and Ould Bouamama (2003) studied a natural circulation drum-boiler-turbine and suggested a nonlinear dynamic fuzzy model. The authors showed that the dynamic fuzzy model brings proper and precise universal nonlinear estimates, and at the same time, the proposed local models are near estimates to the local linearization of the

non-linear dynamic system.

Cerrada, Aguilar, Colina, and Titli (2005) introduced a method for adaptive dynamic fuzzy modeling. Their method combines the historical performance of the system variables with membership functions of fuzzy systems. The authors illustrated tolerable identification errors by giving some descriptive examples of system identification which can unravel the effectiveness of the fuzzy models suggested. Despite the abrupt fluctuations in the input variables, these models adhere to the real output which is vital in an acceptable identification model in experimental practices. The focus of this tactic rests on cases that cause an identification model.

The usage of fuzzy logic in modeling of the systems and their control studies needs to be stressed, as they may propel a more straightforward execution of algorithms for integration. They are interesting since they boast off execution simplicity, time, ability to swiftly model complex systems, and its moderately low cost.

Ghasem (2006) used the fuzzy logic controllers based on the TS inference method to regulate the reaction temperature of the industrial ethylene polymerization fluidized–bed reactors. The simulation results suggest that the conventional fuzzy logic controller will oscillate in the process response. For a better performance of the conventional scheme, the authors proposed that a hybrid control scheme needs to be adopted. Some striking improvements in the controller performance could be achieved by bringing together these approaches. The hybrid control scheme mitigates the severe oscillations of the common method and contributes towards better control precision. The comparison between Mamdani fuzzy logic and Takagi-Sugeno type fuzzy controller has been investigated. Results have shown that Mamdani fuzzy logic is not difficult to build, that it is too simple to control the process quickly and that it only works with the long delay system. Takagi-Sugeno controller is ideal to play its role as multiple linear controllers to run dynamic non-linear systems. This says that it can control the process that changes swiftly and has high frequent input signals.

2.5.3 Model-based control

2.5.3.1 Model predictive control

Polymerization plants must function under different grade transition scenarios. This is to fully cater for the many types of product qualities needed for various applications. The best answer for this situation depends on a suitable objective function defined for a minimization problem. This optimization problem depends on time needed to change product quality specifications, process safety limitations and the quantity of off-spec polymer. Since choosing the best control scheme has significant impacts on process quality and process operability optimization, the time optimal transition problem needs to be considered together with this control strategy simultaneously.

It should be said that many conventional control algorithms are not enough in dealing with the strict limitations enforced in a few industrial processes, specifically once a first-rate commodity is needed. This is particularly valid for polymerization processes wherein definite properties like MFI or average molecular weight with the effect on plastic quality should be fulfilled. At this point, a proper way is to adopt an MPC (Model Predictive Control), that makes use of a process tailored dynamic model as an essential part for the process control structure.

The Model Predictive Control (MPC) is an optimization-based control strategy which is very suitable for constrained, multi-variable processes. The model predictive controller predicts the actual system's future behavior over a time interval defined by the prediction horizon. The implication made by the simpler diagram of the MPC algorithm shown in Figure 2.2 is that a parallel process model to the controller is used in MPC to predict the controlled variable.

MPC works by minimizing a cost function given by Seborg, Edgar, Mellichamp, and Doyle (2016):

$$V(k) = \sum_{i=1}^{P} \sum_{j=1}^{n_y} \left\{ w_j^y [y_i(k+1) - r_j(k+1)] \right\}^2 + \sum_{i=1}^{M} \sum_{j=1}^{n_{mv}} \left\{ w_j^{\Delta u} [\Delta u_j(k+i-1) \right\}^2 \quad (2.15)$$

where P is the prediction horizon, n_y is the number of plant outputs, w_j^y is the weight for output j, k is the current sampling interval, $k+i$ is a future sampling interval (within the

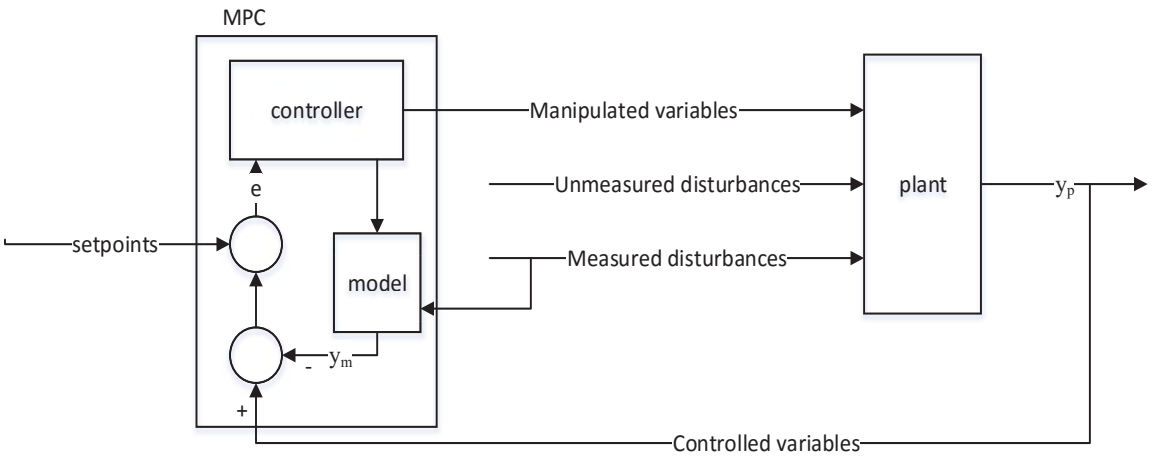

Figure 2.2: Model predictive control system

prediction horizon), $[y_i(k+i) - r_j(k+i)]$ is the predicted deviation at future instant $k+i$, n_{mv} is the number of manipulated variables (inputs), M is the control horizon, $w_j^{\Delta u}$ is the weight for input j and $\Delta u_j(k+i-1)$ is the predicted adjustment (*i.e.*, move) in manipulated variable j at future (or current) sampling interval $k+i$.

The cost function is also restricted by the unequal constraints of the manipulated and control variables as follows:

Manipulated variable constraint:

$$u_{max}(k) \geq u(k+i-1) \geq u_{min}(k) \tag{2.16}$$

Manipulated variable rate constraint:

$$\Delta u_{max}(k) \geq u(k+i-1) \geq \Delta u_{min}(k) \tag{2.17}$$

Output variable constraint:

$$y_{max}(k) \geq u(k+i-1) \geq y_{min}(k) \tag{2.18}$$

The problem formulation would decide if several parameters such as the control horizon, prediction horizon and weighting matrices in the optimization formulation should be finalized so that the predicted output can perform better.

As mentioned by Campello, Von Zuben, Amaral, Meleiro, and Maciel Filho (2003),

MPC algorithms have been used for chemical process control for their us-age simplicity and capability to deal with limitations that involve the input and output variables in procedures. Schnelle and Rollins (1997) adopted a continuous polymerization (CP) process design and applied a model predictive control. They illustrated that MPC technology proved to be a promising substitute for this type of process.

Santos, Afonso, Castro, Oliveira, and Biegler (2001) made the effort to control the temperature and liquid level in a pilot plant CSTR reactor and they implemented an on-line nonlinear model predictive control algorithm. The authors also established several sources of unmeasured disturbances and model mismatch. They leave an impact on the model quality in representing the reactor dynamics. While there are mismatches and disturbances, the closed loop system performed credibly in terms of disturbance rejection and set-point tracking. The application of a nonlinear MPC based on extended Kalman filter to control polymer properties had been analyzed by Park and Rhee (2003), for a semi batch Methyl MethAcrylate/MethAcrylate copolymerization reactor. The authors drew a comparison between the experimental results and other techniques to show the superior performance of this control strategy.

Ramaswamy, Cutright, and Qammar (2005) had sought to control an unsteady state CSTR bioreactor with the help of an MPC. A vital MPC parameter for its tuning is prediction horizon which was analyzed in this work by concentrating on the variation effects.

Within chemical industries, MPC has stood out to become the principal method of advanced multi-variable. In another approach, Dougherty and Cooper (2003) had given a multiple model adaptive control approach for multi-variable DMC. The DMC (dynamic matrix control) strategy has the utmost applications in industry between MPC control techniques. It is because of its design and application straightforwardness together with its ability to soundly handle cases where manipulated variable is restricted within a range. This technique blends the output of multiple linear DMCs without adding extra computational intricacy contrasting to the non-adaptive DMC.

Adaptive Linear DMC (ALDMC) algorithm was developed and employed by Guiamba and Mulholland (2004) in a Multi Input Multi Output (MIMO) pump-tank setup. Where the

plant/model mismatch is concerned, ALDMC presented better performance in comparison to the non-adaptive Linear DMC (LDMC). Haeri and Beik (2005) considered the handling of MIMO systems within specified circumstances and recommended an approach which extended the nonlinear DMC procedure. The authors have illustrated that the method usefulness is clear by presenting the simulated control results of a MIMO stirred reactor nonlinear model and another MIMO power unit nonlinear model.

Carlos E., David M., and Manfred (1989) highlighted critical issues whereby any control system should discuss and review MPC techniques in the light of those issues to highlight their advantages in terms of the design and implementation. Several design techniques such as Internal Model Control and Inferential Control emanate from MPC; they were put in perspective with respect to one another and the similarity with more traditional methods like Linear Quadratic Control were investigated. The malleable constraint management capabilities of MPC were a prominent asset in the framework of the global operating goals of the process industries and the 1–; 2–; and $\infty - norm$ formulations of the performance goal. The application of MPC to non-linear systems was examined and its attractions were also studied. The authors also suggested that, although the MPC is not any stronger than classical feedback, its robustness can be adjusted more easily.

The nonlinear model based control was applied by Özkan, Özen, Erdoğan, Hapoğlu, and Alpbaz (2001) to the styrene solution polymerization in a jacketed batch reactor and checked its effectiveness to reach the required molecular weight and monomer conversion. The authors used Hamiltonian optimization to assess the optimal temperature profiles for the properties of polymer quality. Analytical and experimental nonlinear model based control were analyzed to keep tab of the temperature at the trajectory which was believed to be optimal. Two types of parametric and nonparametric models were assessed to control temperature optimally. Nonlinear auto regressive moving average exogenous (NARMAX) gives an association among reactor temperature and heat input to depict the system dynamics. It should also be added that this model served to define the control system as a parametric model. Simulation results were brought to comparison with experimental control data. Authors summed up that the control simulation program is the representative of the behavior of the con-trolled reactor temperature with some

good prediction capabilities. Moreover, nonlinear model based control keeps the reactor temperature stable within the optimal trajectory.

Qin and Badgwell (2003) did a survey on commercially available model predictive control (MPC) technology, both linear and nonlinear, based primarily on data provided by MPC vendors and described approaches taken by each vendor for the various aspects of the calculation. A review of the identification technology was needed to enable a list of similarities and differences to be found between the approaches. MPC applications performed by each vendor were summarized following the application area. Ibrehem et al. (2008) implemented Adaptive Predictive Model-Based Control to control the system and compared with the conventional PID controller, giving acceptable results.

Ho et al. (2012) had concentrated on the control of a gas phase propylene polymerization model in a fluidized–bed reactor, where a two–phase dynamic model was used, and since the process is nonlinear, an advanced control scheme was adopted to ensure an efficient regulation of the process variables. Adaptive Predictive Model-Based Control (AP-MBC) strategy (an integration of the Recursive Least Squares algorithm, RLS and the Generalized Predictive Control algorithm, GPC) have the function to control the emulsion phase temperature and polypropylene production rate by manipulating the reactor cooling water flow rate and catalyst feed rate again. The APMBC in set point tracking was reported to be superior, as compared to the conventional PI controller and the ability of APMBC to capture the effects of monomer concentration, hydrogen concentration and superficial gas velocity on the process variables as efficiently as possible. It is common for the polymerization processes to have a highly nonlinear dynamic behavior leading to an abysmal performance of controllers based on conventional internal models to be poor or for it to need a considerable amount of effort in controller tuning.

Shamiri, Hussain, sabri Mjalli, et al. (2013) took advantage of a two–phase model to delve into the dynamic behavior and process control of a fluidized–bed polypropylene production reactor production rate and temperature. To control the reactor temperature and the polypropylene production rate , a centralized model predictive controller (MPC) technique was used by making use of the catalyst feed rate and cooling water flow rate respectively. They reached a conclusion that the MPC could yield some controller moves

which not only were subjected to the specified input constraints for both control variables, but also that they are characteristically non-aggressive and sufficiently smooth for practical use.

Broadly speaking, the challenge is to organize the sophisticated chemical processes due to their volatile nature of parameters and structural mismatch. Adaptive linear or non-linear algorithm is a very important tool to control these kinds of processes. In normal circumstances, the stability of Lyapunov functions serves to design nonlinear adaptive controllers. This algorithm can also deal with other parametric uncertainties throughout the input saturation. Biswas and Samanta (2013) considered the controlling polymerization process with input saturation and parametric uncertainty and worked on an adaptive back stepping methodology. The controller is showed to be robust in modeling uncertainties in a polymerization process and it also showed a powerful disturbance rejection ability. The adaptive controller could take both matched and unmatched uncertainties. In addition, to get better results, the authors made use of several parameters in which the controller gave a sturdy performance even around high parametric uncertainty.

2.5.3.2 Fuzzy based model predictive control

Nascimento Lima, Manenti, Filho, Embiruçu, and Wolf Maciel (2009) built a predictive control system based on type Takagi-Sugeno fuzzy models for polymerization, where they had a close look into the copolymerization of methyl methacrylate with vinyl acetate to test the ability of the recommended control system. They adopted a nonlinear mathematical model to justify the reaction plant that can generate data and probe deeper into the controller performance. The fuzzy approach adopted in their work suggested that it can predict outputs as a function of dynamic data input. The authors drew a comparison with this fuzzy approach with conventional predictive control in regulatory and servo issues, and as the result, the fuzzy controller was easy to implement, and its response is much more reliable.

Bringing together the capability of fuzzy logic predictive approaches and system characterization is appealing for designing controllers. Roubos, Mollov, Babuška, and Verbruggen (1999) integrated the MPC algorithms with Takagi-Sugeno fuzzy models.

In this approach, what happens first is that the model identification using fuzzy logic is given for MIMO architectures. With the establishment of the fuzzy model, it was brought together with MPC. The authors ran a test on this method for a two input-four output MIMO liquid level control case. With the help of Fuzzy Hammerstein (FH) models, the nonlinear system was identified and controlled and this was described by Abonyi, Madar, and Szeifert (2002). This model carries a static fuzzy model linked with a series of a linear dynamic model. This model was integrated in a MPC control structure and a new method was introduced to handle constraints. To elaborate further, a simulated water-heater process was adopted. Simulation results have shown not only good dynamic modeling performance but also a well captured steady-state behavior of the system. The application of fuzzy decision making (FDM) in MPC was studied by da Costa Sousa and Kaymak (2001), and there is a conformity of the results with those obtained from the usual MPC. Experiments with nonlinear dynamics were run on three states namely: an air conditioning system, unstable linear system, and a non-minimum phase. Results have suggested that the MPC performance can be made better using fuzzy criteria in the framework of fuzzy decision making.

To address the many optimization problems that are non-convex which come from the application of MPCs to non-linear processes, Mendonça, Sousa, and Sá da Costa (2004) gave the simplified version of fuzzy predictive filters to multi-variable processes. The introduced structure was implemented on a portal crane control. The benefits of the method were presented following the simulation results. The TS fuzzy design for a hybrid fuzzy modeling methodology was an idea proposed by Karer, Mušič, Škrjanc, and Zupančič (2007). The authors analyzed an MPC algorithm which was fit for systems with discrete inputs and the results have given a clue on the advantages of the MPC algorithm using the proposed fusion fuzzy model on a batch-reactor simulation example. The hybrid fuzzy predictive control design that is leaning on a genetic algorithm was suggested by Causa et al. (2008). Using two on/off input valves and a discrete-position mixing valve, the batch reactor temperature was controlled. The strategy revealed to be a proper technique to control hybrid systems, delivering the same performance in comparison with conventional hybrid predictive controllers plus large reductions in computation time. To add, the authors

also formulated a problem with hybrid predictive adaptive control structure, and the results were believed highly potential.

2.5.3.3 Generic model controller

Generic Model Control (GMC) is a type of control scheme which directly uses the non-linear process model. The dynamic mass, momentum, and energy balances are used to get first-principle models. If the process was still ambiguous, black-box models can be used to represent the unknown parts. Being a process model based control algorithm, the Generic Model Control (GMC) incorporates a process model within the control structure directly. It has been illustrated to show excellent control, despite reasonable modeling errors. Abonyi et al. (2002) looked into these hybrid GMC models. They concluded that the first principles part of these models focuses on the main structure of the controller, while the black-box section plays its role as state/disturbance estimators.

Signal and Lee (1992) built an algorithm within a GMC framework which seeks to mitigate larger modeling errors by updating the model parameters occasionally. Authors made a strong claim that this adaptive algorithm had the capability of adapting model parameters in a nonlinear model, where the parameters manifest themselves nonlinearly. Several examples were presented to highlight the technique principles.

M. A. Ali et al. (2007) had worked on a modified generic model controller and simulated it to analyze the results. It entails a model-based control of a propylene polymerization reactor in which the melt index and monomer conversion of the polymer are controlled by manipulating the inlet hydrogen concentration and the reactor cooling water flow. Non-linear control is made, using a simplified non-linear model, to show the strength of the control strategy. Two model variables are updated on-line to make sure that the outputs of the controlled process and their estimated values are followed carefully. The controller is the static inverse of the process model with set points of the measured process outputs changed to set points for several state variables. The simulation study illustrated that the suggested controller has good set point tracking and disturbance rejection properties and is the best, compared to the conventional generic model control and Smith predictor control approaches.

2.5.4 On-line monitoring of polymerization processes

As the need to produce polymers with pre-specified properties intensifies, a great emphasis is laid on the progress of precise, strong instruments developments that can be used for on-line monitoring of polymerization reactions. The viscous and complex nature of polymerization systems make on-line measurements difficult. Poor reliability and long measurement delays are two prevalent issues which leads to these difficulties. Even the off-line measurement of several polymer properties cannot be considered an easy task, as they need sophisticated and time-consuming analytical techniques. The manufacturing of on-line polymer sensors needs an interdisciplinary struggle, improved process knowledge and understanding, reactor design, and instrumentation engineering to name but a few.

Kammona, Chatzi, and Kiparissides (1999) reviewed the progress that has been made in developing on-line hardware sensors to over-see polymerization reactions, in addition to analyzing the accuracy and robustness of the on-line techniques used to gauge the molecular weight, monomer conversion, molecular weight distribution (MWD), copolymer composition, and particle size distribution (PSD) in a continuous manner in polymer reaction operations.

Automatic Continuous On-line Monitoring of Polymerization Reactions (ACOMP) is a name given to a technique that was developed at Tulane University by Reed (2004). The ACOMP technique oversees the polymerization reactions in real-time. In this method, small quantities of polymer are withdrawn from the reactor continuously and is diluted. After this step, the diluted polymer sample will undergo several detectors to calculate standard parameters such as intrinsic viscosity, light scattering, and refractive index. Subsequently, the polymer is continuously characterized as the reaction is running. ACOMP can be used for reaction optimization or feedback control of reactors. The method is independent from any model and it can perform an analysis on the polymer properties on-line. It is a direct measurement rather than a theoretical understanding of the reaction (Alb & Reed, 2008).

Different reaction parameters can be fine-tuned based on which ACOMP is used in real-time. This method would be helpful for the reaction efficiency and product consistency maximization and waste minimization (Alb & Reed, 2010).

2.6 Summary

Heterogeneous gas-phase olefin polymerization in fluidized–bed reactors using Ziegler–Natta catalyst is the most common process to produce polyolefins in chemical and petrochemical industries. This due to their advantageous characteristics of superior heat removal, low operating pressure and temperature, requiring no solvents, and easy product and catalyst removal among many others. However, the fact that different variables play vital roles in simulating such a process makes its mathematical modeling complex. There has been numerous efforts during the past few decades to develop comprehensive models that can predict the reactor behavior and product properties precisely. All of these modeling efforts are based on assumptions to simplify the mathematical model. Scientist have tried to reconsider these assumptions and too look at the process from different perspectives. Assumptions such as considering the phases withing reactor yielded models which are known as well-mixed, two–phase, three-phase or even four phase (considering cloud phase). Several attempts imagined the reactor to work in different interconnected sections and each section work as an ideal CSTR or PFR reactor to resemble bubble or emulsion phase. Others have worked on the chemistry side of the process (reaction mechanism) or inclusion of different number of active sites with different reaction constants which has led to different explanations of the the mechanism and kinetics. Moreover, numerous theoretical or empirical equations have been proposed to explain the hydrodynamics.

This study is another attempt to develop a more accurate model and to be as comprehensive as possible. Those works that have been vouched for by many scientists during the past decades have been somehow incorporated in the model, including the reaction mechanism, mass and energy balances and hydrodynamics. They have been linked together and build upon, such as inclusion of particle entrainment, and been tested with industrial data to get the most accurate model. As a result a dynamic two–phase catalytic copolymerization of ethylene and 1-butene with a comprehensive mechanism considering two active sites on Z–N catalyst is developed is this work(Chapter 3). Furthermore, the model was used to study process control of the process which is discussed in (Chapter 4). To utilize the power of AI-based controllers, ANFIS is used to design controllers. Moreover, with the advancement in on-line measurement of properties such as rheometers, an ANFIS

controller is designed to do the task. Moreover, temperature which is the most important parameter in this exothermic reaction and needs to be regulated is controlled using hybrid architecture of conventional PID and AI-based ANFIS controllers.

CHAPTER 3: DYNAMIC TWO-PHASE MODELING OF CATALYTIC ETHYLENE COPOLYMERIZATION IN FLUIDIZED–BED REACTORS

3.1 Introduction

To describe the kinetic scheme of heterogeneous Ziegler–Natta catalyst, single, as well as multiple, catalyst active sites models have been proposed by Hutchinson, Chen, and Ray (1992); McAuley and MacGregor (1992); Ray (1991). In this kinetic scheme the key elementary reactions was established, which include formation of active centers, insertion of monomer into the growing polymer chains, chain-transfer reactions, and catalyst deactivation. Most of the proposed mechanisms put the basis on the information about polymerization rate, molecular weight distribution and active center concentrations. In this study, a fully dynamic dual active site model is presented to describe the kinetic behavior, production rate and MWD of ethylene copolymerization in an industrial-scale gas-phase FBR. The present model focuses on characterizing the copolymerization kinetics occurring at the multiple active sites of the catalyst, determining the MWDs, density, monomer concentrations, hydrodynamics and polymer properties such as MFI and PDI. Moreover, the developed model considers the solids elutriation from the reactor which turns out to be very important since the amount of the solids in the reactor affects the whole process. The model is then verified using industrial and literature data. The proposed model is dynamic and is later used in Chapter 4 for process control studies.

3.2 Polymerization kinetics

The ability of the heterogeneous Ziegler–Natta catalysts to produce polymers with broad molecular-weight distributions has long being recognized. There are two factors responsible for exhibiting this distribution. One factor is mass and heat-transfer resistances that leads to a broadening of the molecular weight distribution. The other factor is the existence of multiple sites where each type has its own relative reactivity. However, it has been shown that under most polymerization conditions, the effect of multiple active site types is more important than that of transport resistances (Khare et al., 2004). The single-site kinetic model is not enough to describe the kinetic behavior, production rate and molecular weight distribution of ethylene copolymerization. Therefore, the present

study considers a two–type active site.

Using McAuley et al. (1990), Kissin (1985) and de Carvalho, Gloor, and Hamielec (1989) kinetic modelling methodology, the following kinetic model was developed using Ziegler–Natta catalysts containing multiple active sites to describe the homopolymer production rate, molecular weight and its distribution. Throughout this section, the index j refers to the type of active site. Each site type is associated with different rate constants for formation, initiation, propagation and chain transfer. Ziegler–Natta multi-site catalyst uses the following reactions:

3.2.1 Formation of active sites

For a typical Ziegler–Natta catalyst potential active sites of type j on the catalyst particle and the co-catalyst react to form active sites (Kissin, 1985) as follows:

$$N^*(j) + Cocatalyst \xrightarrow{k_f(j)} N(0, j) \tag{3.1}$$

3.2.2 Initiation of active sites

The active sites react with the monomer to form propagation sites given as:

$$N(0, j) + M \xrightarrow{k_i(j)} N(1, j) \tag{3.2}$$

3.2.3 Propagation

The propagation sites support the growth of living polymer chains. Addition of fresh monomer molecules to active sites increase the length of the chain by one unit as indicated below:

$$N(r, j) + M \xrightarrow{k_p(j)} N(r + 1, j) \tag{3.3}$$

3.2.4 Chain transfer reactions

Chain transfer reactions occur with monomers, hydrogen, co-catalyst and spontaneous transfer reactions (Kissin, 1985). The following sections describe these chain transfer reactions in more details.

3.2.4.1 Transfer to monomer

Chain transfer to monomer reactions are:

$$N(r, j) + M \xrightarrow{k_{f_m}(j)} N(1, j) + Q(r, j) \tag{3.4}$$

where $Q(r, j)$ is a dead polymer segment of length r which cannot undergo any further reactions. The living polymer chains of length one, $N(1, j)$, can propagate to form new polymer chains as follows.

3.2.4.2 Transfer to hydrogen

The main transfer step in industrial ethylene polymerization is the transfer to hydrogen. Varying hydrogen concentration in the reactor is the main technique to control molecular weight averages of industrial polyethylene resin, given as:

$$N(r, j) + H_2 \xrightarrow{k_{f_h}(j)} N_H(0, j) + Q(r, j) \tag{3.5}$$

$$N(0, j) + M \xrightarrow{k_h(j)} N(1, j) \tag{3.6}$$

Reacting with the co-catalyst reinitiates these sites quickly. If the co-catalyst is triethyl aluminum, Kissin (1985) gives the re-initiation reaction as:

$$N_H(0, j) + AlEt_3 \xrightarrow{k_{hr}(j)} N(1, j) \tag{3.7}$$

3.2.4.3 Transfer to co-catalyst

For particular reactor operation conditions, especially at elevated polymerization temperatures, transfer to co-catalyst may be considerable. It is, however, generally negligible at normal polymerization temperatures with Ziegler–Natta catalysts (McAuley et al., 1994), given as

$$N_H(r, j) + AlEt_3 \xrightarrow{k_{f_r}(j)} N(1, j) + Q(r, j) \tag{3.8}$$

3.2.4.4 Spontaneous transfer

Spontaneous transfer reactions is:

$$N(r,j) \xrightarrow{k_{fs}(j)} N_H(0,j) + Q(r,j) \tag{3.9}$$

This site can undergo initiation reactions with monomer as for transfer to hydrogen.

3.2.5 Deactivation reactions

Active sites may deactivate spontaneously to generate dead sites and dead polymer chains that are unable to catalyze polymerization, given as:

$$N(r,j) \xrightarrow{k_{ds}(j)} N_d(j) + Q(r,j) \tag{3.10}$$

$$N(0,j) \xrightarrow{k_{ds}(j)} N_d(j) \tag{3.11}$$

$$N_H(0,j) \xrightarrow{k_{ds}(j)} N_d(j) \tag{3.12}$$

3.2.6 Reactions with poisons

Industrial polymerization processes considers existence of catalyst poisons in the polymerization system an undesirable condition. One of the functions of alkyl aluminum co-catalysts is to passivate the system by removing most of the polar poisons in the reactor prior to catalyst injection and polymerization. Even low levels of some reactive impurities, such as carbon monoxide, can cause a nearly instantaneous drop in propagation rates. Adsorption of such an impurity onto a catalyst site can cause it inactive. These reactions are as follows:

$$N(r,j) + I_m \xrightarrow{k_{dI}(j)} N_{dIH}(0,j) + Q(r,j) \tag{3.13}$$

$$N_H(0,j) + I_m \xrightarrow{k_{dI}(j)} N_{dIH}(0,j) \tag{3.14}$$

$$N(0,j) + I_m \xrightarrow{k_{dI}(j)} N_{dI}(0,j) \tag{3.15}$$

The set of equations discussed in Section 3.2 are summarized in Table 3.1.

Table 3.1: Reactions occurring in a copolymerization reaction (McAuley et al., 1990)

Description	Reaction	
Formation reaction	$N^*(j) \xrightarrow{kf(j)} N(0,j)$	
Initiation reaction	$N(0,j) + M_i \xrightarrow{ki_i(j)} N_i(1,j)$	$i = 1,2,..$
Propagation	$N_i(r,j) + M_k \xrightarrow{kp_{ik}(j)} N_k(r+1,j)$	$i = k = 1,2,..$
Transfer to monomer	$N_i(r,j) + M_k \xrightarrow{kfm_{ik}(j)} N_k(1,j) + Q(r,j)$	$i = k = 1,2,..$
Transfer to hydrogen	$N_i(r,j) + H_2 \xrightarrow{kfh_i(j)} N_H(0,j) + Q(r,j)$	$i = 1,2,..$
	$N_H(0,j) + M_i \xrightarrow{kh_i(j)} N_i(1,j)$	$i = 1,2,..$
	$N_H(0,j) + AlEt_3 \xrightarrow{kh_r(j)} N_1(1,j)$	
Transfer to co-catalyst	$N_i(r,j) + AlEt_3 \xrightarrow{kfr_i(j)} N_1(1,j) + Q(r,j)$	$i = 1,2,..$
Spontaneous transfer	$N_i(r,j) \xrightarrow{kfs_i(j)} N_H(0,j) + Q(r,j)$	$i = 1,2,..$
Deactivation reactions	$N_i(r,j) \xrightarrow{kds_i(j)} N_d(0,j) + Q(r,j)$	$i = 1,2,..$
	$N(0,j) \xrightarrow{kds(j)} N_d(j)$	
	$N_H(0,j) \xrightarrow{kds(j)} N_d(j)$	
Reactions with poisons	$N_i(r,j) + I_m \xrightarrow{kdI(j)} N_{dIH}(0,j) + Q(r,j)$	$i = 1,2,..$
	$N_H(0,j) + I_m \xrightarrow{kdI(j)} N_{dIH}(0,j)$	
	$N(0,j) + I_m \xrightarrow{kdI(j)} N_{dI}(0,j)$	

3.3 Development of the modified model using the kinetic proposed in previous section

The present study derives a mathematical model based on the explained kinetic system. This model consists of mass balances on the species present in the reactor and a series of algebraic and differential equations presented in the next subsection. Characterization of polymer properties is modeled using the population balances and method of moments. Application of population balances and the method of moments allows for the prediction of the physiochemical characteristics of the polymer such as molecular weight, polydispersity index (PDI), melt flow index (MFI), density, polymer production rate, monomer conversion and active site information. In the method of moments, moments of the chain length

distribution are calculated for living and dead polymers. These moments are then used to calculate molecular weight or chain length averages of the polymer produced in the reactor.

Like any other modeling effort, some assumptions are needed to simplify the model. Some of the assumptions were chosen based on the recommendations by the literature and new assumptions were taken into account based on the objectives of the current study. The assumptions considered in developing the model are as follows:

1. The emulsion phase is considered to be completely mixed and not at the minimum fluidization condition.
2. Polymerization reactions are assumed to take place in both emulsion and bubble phases.
3. The bubbles are considered to be a sphere of constant dimensions and pass with unchanging velocity through the bed at plug flow condition.
4. Resistance of heat and mass transfer among gas and solid in emulsion and bubble phases are neglected.
5. Radial gradients for concentration and temperature in the reactor are neglected as a result of strict mixing brought about by the up-flowing gas.
6. Uniform particle size is considered all over the bed.
7. Solids entrainment is considered at the topmost part of the bed.

3.3.1 Mass balance equations for active sites and reacted monomers

The equation below gives the mass balance on the number of moles of potential active sites N*(j) in the reactor:

$$\frac{dN^*(j)}{dt} = F^*_{in}(j) - k_f(j)N^*(j) - N^*(j)\frac{R_v}{V_p} \tag{3.16}$$

The molar flow rate of potential active sites into the reactor $F^*_{in}(j)$ is proportional to the mass feed rate of the catalyst. The volumetric flow rate of polymer from the reactor is R_v and the volume of the polymer phase in the reactor isV_p. Similarly, the following equations

can be written for the number of moles of initiation sites $N(0, j)$ and $N_H(0, j)$ as:

$$\frac{dN(0,j)}{dt} = k_f(j)N^*(j) - N(0,j)\left\{k_i(j)[M_T] + k_{ds}(j) + k_{dI}(j)[I_m] + \frac{R_v}{V_p}\right\} \tag{3.17}$$

$$\frac{dN_H(0,j)}{dt} = Y(0,j)\left\{k_{fh_T}(j)[H_2] + k_{fs_T}(j)\right\} - N_H(0,j)\left\{k_h(j)[M_T] + k_{ds}(j) + k_{hr}(j)[AlEt_3] + k_{dI}(j)[I_m] + \frac{R_v}{V_p}\right\} \tag{3.18}$$

where $[M_T]$ is the total molar monomer concentration given by:

$$[M_T] = [M_1] + [M_2] + \cdots \tag{3.19}$$

where $[M_1]$, $[M_2]$ and $[H_2]$ are the concentrations of ethylene, 1-butene, and hydrogen, respectively. $Y(0, j)$ is the zeroth moment of the living polymer chain length distribution and is given by:

$$Y(0,j) = \sum_{r=1}^{\infty}\left\{N_1(r,j) + N_2(r,j) + \cdots\right\} \tag{3.20}$$

Rate constants with subscript $_T$ and $_{TT}$ are pseudo-kinetic rate constants. The full description and calculation method is given by McAuley et al. (1990). The following mass balance for initiated polymer chains of length $r = 1$ with ethylene as the terminal monomer is as follows:

$$\begin{aligned}\frac{dN_1(1,j)}{dt} =& k_{i1}(j)N(0,j)[M_1] + N_H(0,j)\left\{k_{h1}(j)[M_1] + k_{hr}(j)[AlEt_3]\right\} \\ &+ Y(0,j)\left\{k_{fm_{1T}}(j)[M_1] + k_{fr}(j)[AlEt_3]\right\} \\ &- N_1(1,j)\left\{k_{p_{1T}}(j)[M_T] + k_{fm_{1T}}(j)[M_T] + k_{fh_1}(j)[H_2]\right. \\ &\left. + k_{fr_1}(j)[AlEt_3] + k_{fs_1}(j) + k_{ds}(j) + k_{dI}(j)[I_m] + \frac{R_v}{V_p}\right\}\end{aligned} \tag{3.21}$$

Similarly, for any other terminal monomer, M_i:

$$\begin{aligned}\frac{dN_i(1,j)}{dt} =& k_{ii}(j)N(0,j)[M_i] + N_H(0,j)k_{hi}(j)[M_i] + Y(0,j)k_{fm_{iT}}(j)[M_i] \\ &- N_i(1,j)\left\{k_{p_{iT}}(j)[M_T] + k_{fm_{iT}}(j)[M_T] + k_{fh_i}(j)[H_2]\right. \\ &\left. + k_{fr_i}(j)[AlEt_3] + k_{fs_i}(j) + k_{ds}(j) + k_{dI}(j)[I_m] + \frac{R_v}{V_p}\right\} \qquad i = 2, 3, ..\end{aligned} \tag{3.22}$$

The number of moles of impurity-deactivated sites conform to the following mass balances:

$$\frac{dN_{dIH}(0,j)}{dt} = k_{dI}(j)[I_m]\{Y(0,j) + N_H(0,j)\} - N_{dIH}(0,j)\left\{k_a(j) + \frac{R_v}{V_p}\right\} \tag{3.23}$$

$$\frac{dN_{dI}(0,j)}{dt} = k_{dI}(j)[I_m]N(0,j) - N_{dIH}(0,j)\left\{k_a(j) + \frac{R_v}{V_p}\right\} \tag{3.24}$$

By deriving balances on living polymer of chain length r with terminal monomers M_i $(i = 1, 2, \cdots)$ using Equation (3.22) and substituting in Equation (3.20) and differentiating over time, the zeroth moment of the living polymer chain length distribution can be obtained as follows:

$$\begin{aligned}\frac{dY(0,j)}{dt} =& [M_T]\left\{k_{i_T}(j)N(0,j) + k_{h_T}(j)N_H(0,j)\right\} + k_{h_r}(j)N_H(0,j)[AlEt_3] \\ &- Y(0,j)\left\{k_{fh_T}(j)[H_2] + k_{fs_T}(j) + k_{ds}(j) + k_{dI}(j)[I_m] + \frac{R_v}{V_p}\right\}\end{aligned} \tag{3.25}$$

Mass balances on the first and second moments of the living polymer distribution can be determined as follows:

$$\begin{aligned}\frac{dY(1,j)}{dt} =& [M_T]\left\{k_{i_T}(j)N(0,j) + k_{h_T}(j)N_H(0,j)\right\} + k_{h_r}(j)N_H(0,j)[AlEt_3] \\ &+ [M_T]k_{pTT}(j)Y(0,j) \\ &+ \left\{Y(0,j) - Y(1,j)\right\}\left\{k_{fm_{TT}}(j)[M_T] + k_{fr_T}(j)[AlEt_3]\right\} \\ &- Y(1,j)\left\{k_{fh_T}(j)[H_2] + k_{fs_T}(j) + k_{ds}(j) + k_{dI}(j)[I_m] + \frac{R_v}{V_p}\right\}\end{aligned} \tag{3.26}$$

$$\begin{aligned}\frac{dY(2,j)}{dt} =& [M_T]\left\{k_{i_T}(j)N(0,j) + k_{h_T}(j)N_H(0,j)\right\} + k_{h_r}(j)N_H(0,j)[AlEt_3] \\ &+ [M_T]k_{pTT}(j)2Y(1,j - Y(0,j) \\ &+ \left\{Y(0,j) - Y(2,j)\right\}\left\{k_{fm_{TT}}(j)[M_T] + k_{fr_T}(j)[AlEt_3]\right\} \\ &- Y(2,j)\left\{k_{fh_T}(j)[H_2] + k_{fs_T}(j) + k_{ds}(j) + k_{dI}(j)[I_m] + \frac{R_v}{V_p}\right\}\end{aligned} \tag{3.27}$$

where $Y(n, j)$ which is the n^{th} moment of the living polymer chain length distribution is given by:

$$Y(n, j) = \sum_{r=1}^{\infty} r^n [N_1(r, j) + N_1(r, j) + \cdots] \qquad n = 1, 2, \cdots \tag{3.28}$$

The definition of moments of the dead polymer distribution is:

$$X(n, j) = \sum_{r=1}^{\infty} r^n Q(r, j) \tag{3.29}$$

The summation above starts at $r = 2$ because dead chains of length 1 are not considered polymer. By writing a mass balance on dead polymer segments of length r and substituting the result into Equation (3.29), the mass balances for the moments of the dead polymer chain length distribution can be obtained:

$$\begin{aligned} \frac{dX(n, j)}{dt} =& \Big\{Y(n, j) - N_T(1, j)\Big\} \\ &\times \left(\Big\{k_{fm_{TT}}(j)[M_T] + k_{fr_T}(j)[AlEt_3] + k_{fh_T}(j)[H_2] + k_{fs_T}(j)\Big\} \right. \\ &\left. + \Big\{k_d s(j) + k_d I(j)[I_m]\Big\} \right) - X(n, j)\frac{R_v}{V_p} \qquad n = 0, 1, 2 \end{aligned} \tag{3.30}$$

The set of moment equations discussed in Section 3.3 are summarized in Table 3.2.

If we assume that propagation reactions primarily consume monomers, we can obtain the equation for consumption rate of each component. Equation (3.31) shows this mathematical statement after solving the moment equations (McAuley et al., 1990):

$$R_k = \sum_{j}^{ns} \sum_{i}^{m} [M_k] Y(0, j) k_{p_i} k(j) \qquad k = 1, 2, \cdots \tag{3.31}$$

where m is the number of each type of monomer and ns is the number of each type of active site. Then, we can get the total polymer production from Equation Equation (3.32):

$$R_p = \sum_{k=1}^{m} m w_k R_k \tag{3.32}$$

Table 3.2: List of the moment equations

$$
\begin{aligned}
\frac{dY(0,j)}{dt} =& [M_T]\Big\{k_{i_T}(j)N(0,j) + k_{h_T}(j)N_H(0,j)\Big\} + k_{h_r}(j)N_H(0,j)[AlEt_3] \\
& - Y(0,j)\Big\{k_{fh_T}(j)[H_2] + k_{fs_T}(j) + k_{ds}(j) + k_{dI}(j)[I_m] + \frac{R_v}{V_p}\Big\} \\
\frac{dY(1,j)}{dt} =& [M_T]\Big\{k_{i_T}(j)N(0,j) + k_{h_T}(j)N_H(0,j)\Big\} + k_{h_r}(j)N_H(0,j)[AlEt_3] \\
& + [M_T]k_{p_{TT}}(j)Y(0,j) \\
& + \Big\{Y(0,j) - Y(1,j)\Big\}\Big\{k_{fm_{TT}}(j)[M_T] + k_{fr_T}(j)[AlEt_3]\Big\} \\
& - Y(1,j)\Big\{k_{fh_T}(j)[H_2] + k_{fs_T}(j) + k_{ds}(j) + k_{dI}(j)[I_m] + \frac{R_v}{V_p}\Big\} \\
\frac{dY(2,j)}{dt} =& [M_T]\Big\{k_{i_T}(j)N(0,j) + k_{h_T}(j)N_H(0,j)\Big\} + k_{h_r}(j)N_H(0,j)[AlEt_3] \\
& + [M_T]k_{p_{TT}}(j)2Y(1,j - Y(0,j) \\
& + \Big\{Y(0,j) - Y(2,j)\Big\}\Big\{k_{fm_{TT}}(j)[M_T] + k_{fr_T}(j)[AlEt_3]\Big\} \\
& - Y(2,j)\Big\{k_{fh_T}(j)[H_2] + k_{fs_T}(j) + k_{ds}(j) + k_{dI}(j)[I_m] + \frac{R_v}{V_p}\Big\} \\
\frac{dX(n,j)}{dt} =& \Big\{Y(n,j) - N_T(1,j)\Big\} \\
& \times \Bigg(\Big\{k_{fm_{TT}}(j)[M_T] + k_{fr_T}(j)[AlEt_3] + k_{fh_T}(j)[H_2] + k_{fs_T}(j)\Big) \\
& + \Big\{k_d s(j) + k_d I(j)[I_m]\Big\}\Bigg\} - X(n,j)\frac{R_v}{V_p} \qquad n = 0,1,2
\end{aligned}
$$

3.3.2 Reaction rate constants

It was shown that changes in the rate constants of formation, initiation, transfer to cocatalyst, spontaneous transfer and spontaneous catalyst deactivation reaction has marginal influence on the model predictions (McAuley et al., 1990). Hence, assuming similar values for these rate constants as the case of polyethylene is reasonable. In times when the catalyst particles are sufficiently small and the catalyst activity is not extremely high (low to moderate polymerization rates), we can make some simplifications. In these cases, mass and heat transfer resistances inside the polymer particle and between the gas and the solid polymer particles do not play an important role. This will not significantly affect the dynamic behavior of the reactor and the overall properties of the polyolefin. This theory is well established under various conditions in the literature (Luo et al., 2009; McAuley et al., 1990; Zacca et al., 1996). Therefore, the temperature inside the particles (where the reactions take pace) is practically the same as the bed temperature. Table 3.3 gives the rate constants of each reaction for both site types that were used in this work which is taken

from the work of McAuley et al. (1990).

Table 3.3: Reaction rate constants for polyethylene copolymerization (McAuley et al., 1990)

Reaction	Rate constant	Unit	Site type 1	Site type 2
Formation	$k_f(j)$	s^{-1}	1	1
Initiation	$k_{i_1}(j)$	$L/kmol.s$	1	1
	$k_{i_2}(j)$	$L/kmol.s$	0.14	0.14
	$k_{h_1}(j)$	$L/kmol.s$	1	1
	$k_{h_2}(j)$	$L/kmol.s$	0.1	0.1
	$k_{h_r}(j)$	$L/kmol.s$	20	20
Propagation	$k_{p_{11}}(j)$	$L/kmol.s$	85	85
	$k_{p_{12}}(j)$	$L/kmol.s$	2	15
	$k_{p_{21}}(j)$	$L/kmol.s$	64	64
	$k_{p_{22}}(j)$	$L/kmol.s$	1.5	6.2
Transfer	$k_{fm_{11}}(j)$	$L/kmol.s$	0.0021	0.0021
	$k_{fm_{12}}(j)$	$L/kmol.s$	0.006	0.11
	$k_{fm_{21}}(j)$	$L/kmol.s$	0.0021	0.001
	$k_{fm_{22}}(j)$	$L/kmol.s$	0.006	0.11
	$k_{fh_1}(j)$	$L/kmol.s$	0.088	0.37
	$k_{fh_2}(j)$	$L/kmol.s$	0.088	0.37
	$k_{fr_1}(j)$	$L/kmol.s$	0.024	0.12
	$k_{fr_2}(j)$	$L/kmol.s$	0.048	0.24
	$k_{fs_1}(j)$	$L/kmol.s$	0.0001	0.0001
	$k_{fs_2}(j)$	$L/kmol.s$	0.0001	0.0001
Deactivation	$k_{ds}(j)$	s^{-1}	0.0001	0.0001
	$k_{dI}(j)$	$L/kmol.s$	2000	2000
Impurity	$k_a(j)$	s^{-1}	0.0003	0.0003

3.3.3 Reactor hydrodynamics

The simple two–phase flow structure for the gas-phase olefin polymerization model has been used previously in the literature (Fernandes & Lona, 2001; Choi & Ray, 1985; Fernandes & Ferrareso Lona, 2001; Harshe et al., 2004; McAuley et al., 1994). This

model assumes the existence of solid-free bubbles in the fluidized–bed while the emulsion remains at minimum fluidization conditions. However, the voidage of the emulsion phase may differ far from that at the minimum fluidization. Moreover, the bubbles may contain different portions of solids (Cui et al., 2000). Based on this concept, Cui et al. (2000) proposed the dynamic two–phase structure (particle concentration in emulsion and bubbles varies with gas velocity) for the fluidized–bed hydrodynamics. Since the assumption of the minimum fluidization condition for the emulsion phase in the polyethylene reactor (simple two–phase model) is not realistic, this study uses the dynamic two–phase flow structure of fluidized–beds to calculate a better estimation of the average bed voidage.

In the present work, a modified dynamic two–phase model is developed by taking solid entrainment at the top of the reactor into account since there are many cases where we cannot ignore elutriation rates. Normally, most of the granular particles remain in the bed while the smaller ones will leave the reactor with the fluidizing gas. However, where velocities are several times greater than the terminal velocity, coarse particles can also be entrained from the bed (Rhodes, 2008). This phenomenon is called particle carry over or particle entrainment, and is very important in the design and operation of FBRs. Elutriation takes place in the cyclone outside the FBR, and it separates the solids from the gas reentering the reactor after some processing. This shows that it is vital to consider their effect on the process in cases were particle entrainment occurs. The amount of solids available in the reactor at the moment is vital for all the calculations since it affects the hydrodynamics, the surface area and as a result kinetics and the transport phenomena. As an example, assuming less solids in the reactor will lead to lower production rate rates.As a result, the present study considers solid entrainment in the model for mass and energy balances which makes the results more realistic. Equations that are needed to calculate the heat and mass transfer coefficients, velocities in bubble and emulsion phase, and other useful parameters in the two–phase model are listed in Table 3.4.

Based on Table 3.4 and assumptions of this model, the mass and energy balances for emulsion and bubble phases are obtained as follows:

Table 3.4: Hydrodynamic equations used in the model

Parameter	Formula	Reference
Minimum fluidization velocity	$Re_{mf} = (29.5^2 + 0.375Ar)^{0.5} - 29.5$	(Lucas et al., 1986)
Bubble velocity	$U_b = U_0 - U_{mf} + U_{br}$	(Kunii & Levenspiel, 1991)
Bubble rise velocity	$U_{br} = 0.711(g d_b)^{0.5}$	(Kunii & Levenspiel, 1991)
Emulsion velocity	$U_e = \frac{U_0 - U_b}{1-\delta}$	(Mostoufi et al., 2001)
Bubble diameter	$d_b = d_{b0}[1 + 27(U_0 - U_e)]^{0.33}(1 + 6.84H) d_{b0} = 0.0085$(for GeldartB)	(Hillegardt & Werther, 1986)
Mass transfer coefficient	$k_{be} = \left(\frac{1}{k_{bc}} + \frac{1}{k_{ce}}\right)^{-1}$	(Kunii & Levenspiel, 1991)
	$K_{bc} = 4.5\frac{U_e}{d_b} + 5.85\frac{{D_g}^{0.5} g^{0.25}}{{d_b}^{1.25}}$	(Kunii & Levenspiel, 1991)
	$K_{ce} = 6.77\frac{D_g \varepsilon_e U_b r}{d_b}$	(Kunii & Levenspiel, 1991)
Heat transfer coefficient	$H_{be} = \left(\frac{1}{H_{bc}} + \frac{1}{H_{ce}}\right)^{-1}$	(Kunii & Levenspiel, 1991)
	$H_{bc} = 4.5\frac{U_e \rho_g C_{pg}}{d_b} + 5.85\frac{(k_g \rho_g cpg)^{0.5} g^{0.25}}{d_b^{1.25}}$	(Kunii & Levenspiel, 1991)
	$H_{ce} = 6.77(\rho_g C_{pg} k_g)^{0.5}\left(\frac{\varepsilon_e U_{br}}{3}\right)^{0.5}$	(Kunii & Levenspiel, 1991)
Bubble phase fraction Emulsion	$\delta = 0.534[1 - \exp\left(\frac{U_0 - U_{mf}}{0.413}\right)]$	(Cui et al., 2000)
Emulsion phase porosity	$\varepsilon_e = \varepsilon_{mf} + 0.2 - 0.059\exp\left(-\frac{U_0 - U_{mf}}{0.429}\right)$	(Cui et al., 2000)
Bubble phase porosity	$\varepsilon_b = 1 - 0.146\exp\left(-\frac{U_0 - U_{mf}}{0.439}\right)$	(Cui et al., 2000)
Volume of polymer phase in the emulsion phase	$V_{Pe} = AH(1 - \varepsilon_e)(1 - \delta)$	(Shamiri et al., 2012)
Volume of polymer phase in the bubble phase	$V_{Pb} = AH(1 - \varepsilon_e)\delta$	(Shamiri et al., 2012)
Volume of the emulsion phase	$V_e = AH(1 - \delta)$	(Shamiri et al., 2012)
Volume of the bubble phase	$V_b = AH\delta$	(Shamiri et al., 2012)

Mass balance for emulsion phase:

$$\frac{d}{dt}(V_e\varepsilon_e[M_i]_e) = [M_i]_{e,(in)}U_eA_e - [M_i]_eU_eA_e - R_v\varepsilon_e[M_i]_e + K_{be}\Big([M_i]_b - [M_i]_e\Big)V_e\left(\frac{delta}{1-\delta}\right) - (1-\varepsilon_e)R_{ie} - \frac{K_eV_e\varepsilon_eA_e[M_i]_e}{W_e} \tag{3.33}$$

Mass balance for bubble phase:

$$\frac{d}{dt}(V_b\varepsilon_b[M_i]_b) = [M_i]_{b,(in)}U_bA_b - [M_i]_bU_bA_b - R_v\varepsilon_b[M_i]_b - K_{be}\Big([M_i]_b - [M_i]_e\Big)V_b - (1-\varepsilon_b)\frac{A_b}{V_{PFR}}\int R_{ib}dz - \frac{K_eV_e\varepsilon_eA_e[M_i]_e}{W_e} \tag{3.34}$$

Energy balance for emulsion phase:

$$\begin{aligned} &U_eA_e(T_{e.(in)}-T_{ref})\sum_{i=1}^{m}[M_i]_{e,(in)}C_{pi} - U_eA_e(T_e-T_{ref})\sum_{i=1}^{m}[M_i]_eC_{pi} \\ &- R_v(T_e-T_{ref})\left(\sum_{i=1}^{m}\varepsilon_eC_{pi}[M_i]_e + (1-\varepsilon_b)\rho_{pol}cppol\right) \\ &+ (1-\varepsilon_e)R_{pe}\Delta H_R - H_{be}V_e\left(\frac{\delta}{1-\delta}\right)(T_e-T_b) \\ &- V_e\varepsilon_e(T_e-T_{ref})\sum_{i=1}^{m}C_{pi}\frac{d}{dt}([M_i]_e) \\ &- \frac{K_eA_e}{W_e}(T_e-T_{ref})\left(\sum_{i=1}^{m}\varepsilon_eC_{pi}[M_i]_e + (1-\varepsilon_b)\rho_{pol}C_{p.pol}\right) \\ &= V_e\left(\varepsilon_e\sum_{i=1}^{m}C_{pi}[M_i]_e + (1-\varepsilon_e)\rho_{pol}C_{p.pol}\right)\frac{d}{dt}(T_e-T_{ref}) \end{aligned} \tag{3.35}$$

Energy balance for bubble phase:

$$U_b A_b (T_{b.(in)} - T_{ref}) \sum_{i=1}^{m} [M_i]_{b,(in)} C_{pi} - U_b A_b (T_b - T_{ref}) \sum_{i=1}^{m} [M_i]_b C_{pi} \tag{3.36}$$
$$- R_v (T_b - T_{ref}) (\sum_{i=1}^{m} \varepsilon_b C_{pi} [M_i]_b + (1-\varepsilon_e) \rho_{pol} C_{p.pol})$$
$$+ (1-\varepsilon_b) \frac{A_b \Delta H_R}{V_{PFR}} \int R_{pb} dz + H_{be} V_b (T_e - T_b)$$
$$- V_b \varepsilon_b (T_b - T_{ref}) \sum_{i=1}^{m} C_{pi} \frac{d}{dt} ([M_i]_b)$$
$$- \frac{K_b A_b}{W_b} (T_b - T_{ref}) (\sum_{i=1}^{m} \varepsilon_b C_{pi} [M_i]_b + (1-\varepsilon_b) \rho_{pol} C_{p.pol})$$
$$= (V_b (\varepsilon_b \sum_{i=1}^{m} C_{pi} [M_i]_b + (1-\varepsilon_b) \rho_{pol} C_{p.pol})) \frac{d}{dt} (T_b - T_{ref})$$

Solid elutriation constants are obtained from Rhodes (2008) and are as follows:

$$K_e = 23.7 \rho_g U_0 \frac{A}{W_e} exp\left(\frac{-5.4 U_t}{U_0}\right) \tag{3.37}$$

$$K_b = 23.7 \rho_g U_0 \frac{A}{W_b} exp\left(\frac{-5.4 U_t}{U_0}\right) \tag{3.38}$$

$$W_e = AH\,(1 - \varepsilon_e)\,\rho_{pol} \tag{3.39}$$

$$W_b = AH\,(1 - \varepsilon_b)\,\rho_{pol} \tag{3.40}$$

$$U_t = U_t^* \left[\mu \rho_g^{-2} \left(\rho_{pol} - \rho_g\right) g\right]^{0.33} \tag{3.41}$$

$$U_t^* = \left[18 \left(d_p^*\right)^{-2} + (2.335 - 1.7440 \emptyset_s) \left(d_p^*\right)^{-0.5}\right]^{-1} \tag{3.42}$$

$$d_p^* = d_p \left[\mu^{-2} \rho_g \left(\rho_{pol} - \rho_g\right) g\right]^{0.33} \qquad \text{for } 0.5 < \emptyset_s \leq 1 \tag{3.43}$$

One can solve these equations using the following initial conditions:

$$[M_i]_{b,t=0} = [M_i]_{in} \tag{3.44}$$

$$T_{b,t=0} = T_{in} \tag{3.45}$$

$$[M_i]_{e,t=0} = [M_i]_{in} \tag{3.46}$$

$$T_{e,t=0} = T_{in} \tag{3.47}$$

3.3.4 Polymer properties

Polymers are made of many repeated units (monomers) which attach together chemically and make very long chains. Having a perception of polymer chain length is obligatory to comprehend the physical properties of a polymer. Researchers frequently denote chain length as the molecular weight of the polymer chain, which correlates to the number of monomers connected in the chain and the relative molecular mass of the monomers. Nevertheless, all artificial polymers are polydisperse, which means that the length of polymer chains are unequal, and as a result, instead of being a single value, the polymer has a distribution of molecular weights and chain lengths. Consequently, one must calculate some average molecular weight from the molecular weights of all the chains in the polymer sample in order to define the molecular weight.

The number average molecular weight is the arithmetic mean of all the molecular weights of the polymer chains in the sample, given by:

$$\bar{M}_n = \frac{\sum N_i M_i}{\sum N_i} \tag{3.48}$$

where N_i is the number of chains of that molecular weight and M_i is the molecular weight of a chain. $\bar{M}_n$ is measured by approaches that define the number of molecules in a sample of a particular weight and can be predicted by means of polymerization mechanisms. If $\bar{M}_n$ is mentioned for a certain MWD, it means that identical numbers of molecules are present on both sides of the molecular weight in the distribution. On the other hand, the weight average molecular weight formula is:

$$\bar{M}_w = \frac{\sum N_i M_i^2}{\sum N_i M_i} \tag{3.49}$$

Compared to $\bar{M}_n$, $\bar{M}_w$ takes the molecular weight of a chain into consideration to decide how it contributes to the average molecular weight. The larger the chain gets, the effect of chain on the average molecular weight increases. Instead of the number of molecules, the procedures that measure the molecular size, such as through light scattering techniques

define weight average molecular weight. If $\bar{M}_w$ is mentioned for a certain MWD, it means that identical weight of molecules is present on both sides of the molecular weight in the distribution.

The PDI of a polymer is the weight average molecular weight to number average molecular weight proportion, and is used as a parameter to tell how broad a polymer MWD and is given by:

$$PDI = \frac{\bar{M}_w}{\bar{M}_n} \tag{3.50}$$

If a polymer has bigger PDI value, the polymer molecular weight is broader. A polymer with PDI = 1 in which all the chain lengths are equivalent (such as a protein) is called a monodisperse polymer. The narrowest artificial polymers built so far which are used for calibration, have PDI of 1.02–1.10. Chain reactions produce PDI values between 1.5 and 20 while step polymerization reactions usually result isn PDI values of around 2.0 (Braun, Cherdron, & Ritter, 2013). The PDI profile throughout the polymerization process is similar to the average molecular weight.

Another important property of a polymer is melt flow index (MFI). An analysis method controls how easily a plastic material flows and is a very important test for quality assurance. In order to measure MFI, we need to weigh the amount of a polymer that flows from a standard instrument over a timed interval.

The relationship between the molecular weight of polyethylene and its MFI is based on the type proposed by McAuley et al. (1990), whose constants have been modified to fit the actual data and is given by the following equation:

$$MFI = 3.346 \times 10^{17} \bar{M}_W^{-3.472} \tag{3.51}$$

The set of equations that have been discussed in this chapter are simultaneously solved using numerical methods using MATLAB® and SIMULINK® and the details are given in the Appendix A and Appendix B.

3.4 Results and discussions

Based on the proposed kinetics described in previous chapter, the set of mass balance equations for the active sites and reacted monomers, which are represented by a series of algebraic and differential equations, were used separately for the emulsion and bubble phase with a two–site type catalyst. Although the mechanism of polymerization in both phases is the same, the rates of reaction in the bubble and emulsion phases are different based on this dynamic two–phase model due to different amounts of solids in each phase and volume of polymer in the bubble phase and the emulsion phase.

In the bubbling FBR, the upward motion of the gas bubbles causes enough mixing of solid particles in the emulsion phase or dense phase. Consequently, the concentrations of various species and temperature are nearly uniform in the emulsion phase. Therefore, a pseudo-homogeneous well mixed model can be applied to this phase (McAuley et al., 1990). The bubbles travel up through the bed at a constant velocity and the particles present a downward flow, growing in size and weight as they flow downwards. These facts make the assumption of the plug flow valid for such a regime in the bubble phase.

In order to show how the model responds when tested with real data and to validate it, this study uses the operating conditions listed in Table 3.5 to perform the simulation study. The data of four different grades of polyethylene produced at a petrochemical company reported by Kiashemshaki et al. (2006) is used to both validate and compare the model. Unless mentioned otherwise, the results are based on the operating conditions for grade BP LL0209 as listed in Table 3.5. The conditions mentioned in this table are common to produce these grades of polyethylene in industrial reactors.

3.4.1 Polymer properties

Polymer properties such as molecular weight, PDI and Melt Flow Index (MFI), which are crucial to estimate the quality of a given polymer, were calculated based on the kinetic model used in this work. Figure 3.1 demonstrates how the simulation result, based on the presented model and industrial data of a LLDPE, predicts a narrow MWD for the polymer.

The number average molecular weight ($\bar{M}_n$) and weight average molecular weight ($\bar{M}_w$) values are illustrated in Figure 3.2. This figure shows that it takes less than an hour for

Table 3.5: Operating conditions for petrochemical complex 1

Parameter	BP LL0209	BP HD3840	BP HD5218	BP HD6070
D_t(m)	4.8	4.8	4.8	4.8
H(m)	14.5	14.5	14.5	14.5
$d_p(\mu$m)	1145	1049	1061	965
P(bar)	20	19.91	19.85	19.99
U_0(m/s)	0.57	0.56	0.54	0.55
Ethylene concentration (%)	40	40	40	34
1-Butene concentration (%)	17	6.43	2.36	0.34
Hydrogen concentration (%)	9	16	30	23.46
Nitrogen concentration (%)	34	37.57	27.64	42.2
Catalyst feed rate (g/s)	0.2	0.2	0.2	0.2

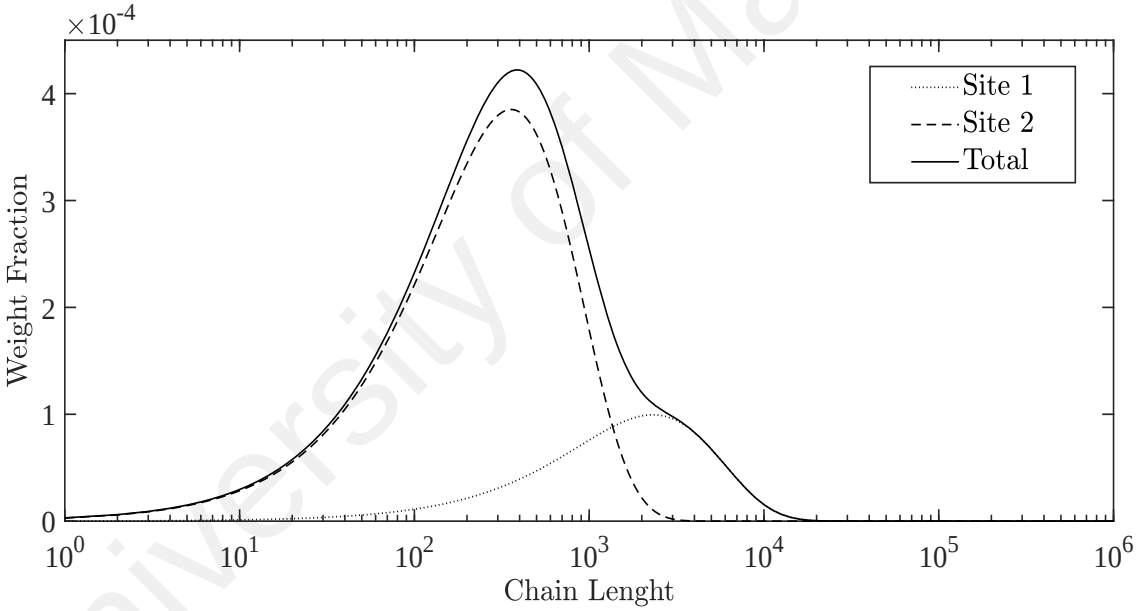

Figure 3.1: Molecular Weight Distribution of the produced LLDPE

the number average and weight average molecular weights of polymer to reach a constant value, since the molecular chain length grows rapidly during this time. As shown in this figure, the ultimate amount of weight average molecular weight reaches almost 99,000 kg/mole. This figure also shows the evolution of PDI and MFI with time in the reactor. The steady state value of PDI and MFI under the operating conditions given in Table 3.5 are 4.14 and 0.98 g/10 min respectively.

For model verification purposes, the results of the model presented in this work for

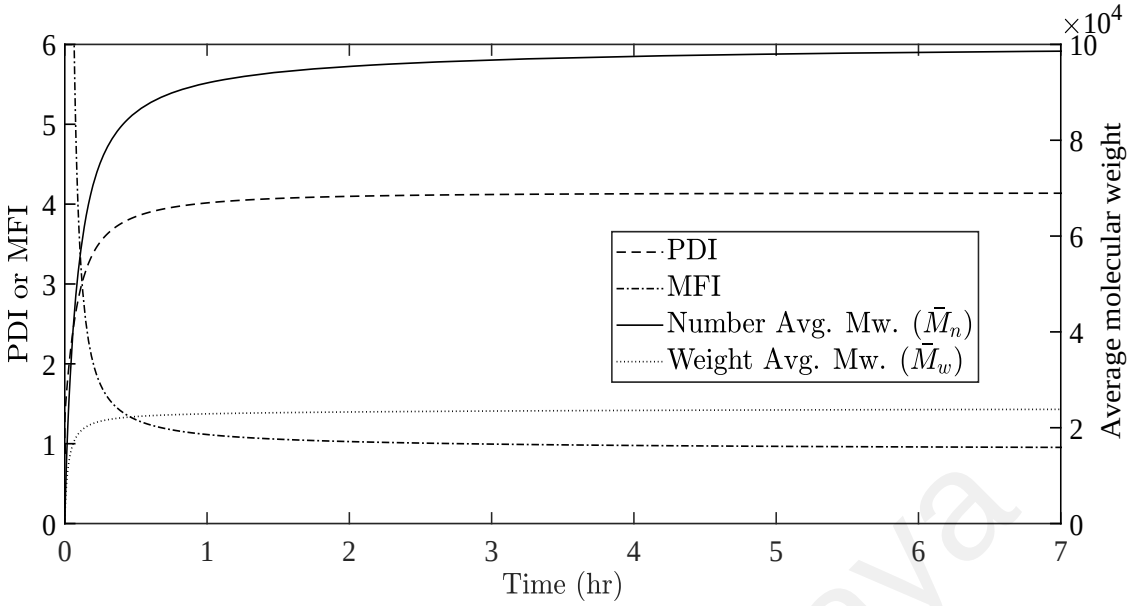

Figure 3.2: Evolution of the Melt Flow Index, Polydispersity Index, number and weight average molecular weights over time in the reactor

PDI and MWD have been compared with the actual plant data and results from the study done by Kiashemshaki et al. (2006). The parity plot of Figure 3.3 shows that the current dynamic model has been able to predict the PDI of LLDPE very accurately and very close to the work of Kiashemshaki et al. (2006). As mentioned by the authors, the difference in the calculated PDIs of HDPEs could be due to considering the same catalyst properties for all the grades. However, companies produce catalysts in different batches in this plant, could have slightly different properties and rate constants, and hence can result in the deviation from the actual PDIs.

Furthermore, the calculated steady state MWD has been compared with the literature (Kiashemshaki et al., 2006) and actual MWD data points for a LLDPE (BP LL0209) and a HDPE (BP HD5218) grade in Figure 3.4 for comparison. Gel permeation chromatography (GPC) data provided by the petrochemical complex is used to produce the actual data. This figure is produced by calculating and plotting the derivative of cumulative weight fraction against the logarithm of weight average molecular weight, which is a typical GPC output. As can be seen, aside from the slight differences, there is a very good agreement between all sets of data for both cases of LLDPE and HDPE grades. Although considering solids elutriation in the present model leads to predicting the polymer properties such as MFI, PDI and MWD accurately, its main advantages lie in calculating the process

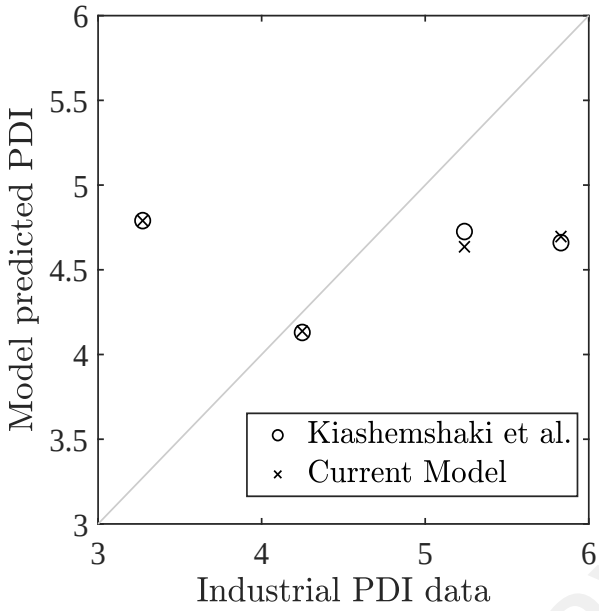

Figure 3.3: Polydispersity Index comparison of four grades of polyethylene with industrial and literature data

parameters such as production rate and reactor temperature more precisely. This is due to the improved dynamic mass and energy balance equations that consider solids entrainment and essentially improves the model to comply more with the real world process data. In addition, this model is able to predict the dynamic behavior of the FBR and can also be a basis for the control study and designing an efficient control system for this highly nonlinear process which is discussed later in Chapter 4.

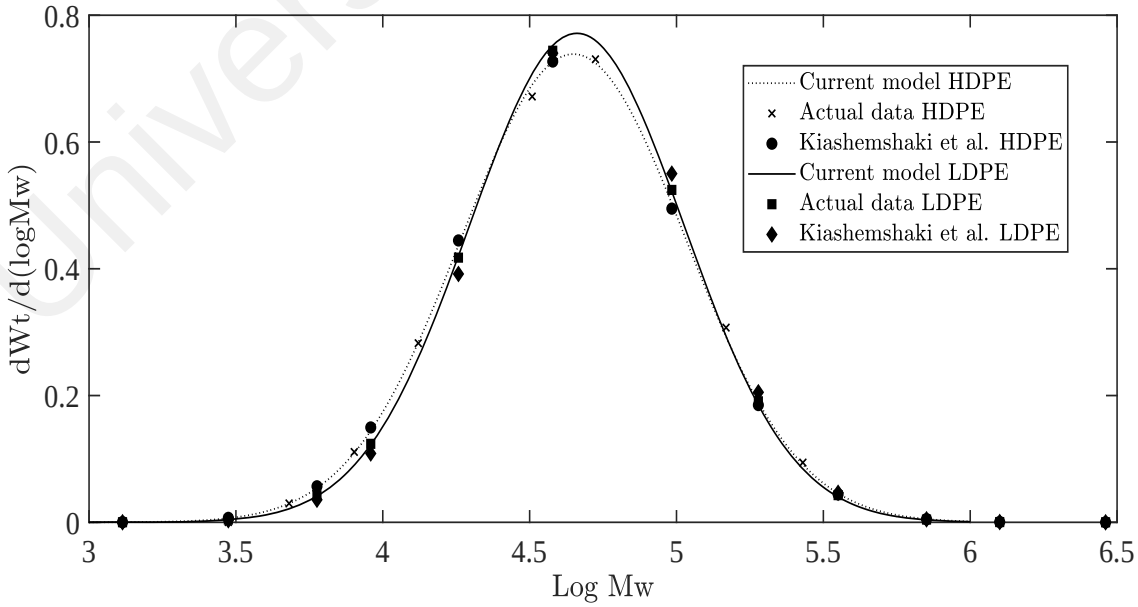

Figure 3.4: Molecular Weight Distribution comparison of LLDPE and HDPE with industrial and literature data

3.4.2 Reactor properties

Polymer production rate during residence time in the FBR is given by Equation (3.32) and is shown in Figure 3.5. This figure shows the evolution of production rate from the start-up moment when Z–N catalyst enters the reactor, and reaction starts until the time that solid particles settle in the FBR, and the fluidized–bed moves to the steady state condition and the production rate becomes steady.

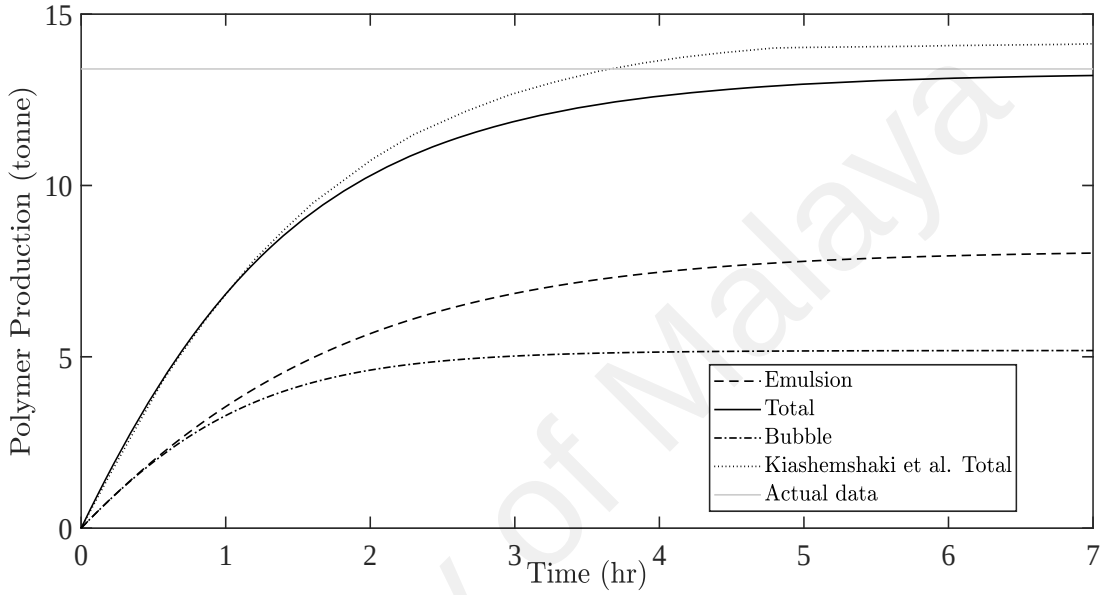

Figure 3.5: Evolution of polymer production with respect to time

This figure also shows polymer production rate in both the bubble and emulsion phases during the polymer residence time in the reactor. The calculated overall production rate soars from almost 7 t/hr in the first hour to almost 10 t/hr in the second hour, and becomes steady at 13.44 t/hr after nearly 5 hours of production. To show the model accuracy and validate the results, the production rate has been plotted against both the industrial data and the model of Kiashemshaki et al. (2006). The horizontal line showing actual data is the amount for the steady state production rate in the industrial FBR. As can be seen, the model was able to accurately predict the steady state production rate and stabilize very close to this data with a deviation of 0.4 tones. The figure also illustrates that nearly 60% of the polymer is produced within the emulsion phase and almost 40% of the total polymer production takes place within the bubble phase. The 20% increase in the production rate in bubble phase in comparison with Kiashemshaki et al. (2006) is due to the introduction

of recycled elutriated solids into the reactor. This predictably increases the amount of catalysts in the bubble phase and leads to higher production in this phase. Since most of the catalysts are within the emulsion phase, less reaction rate or polymer production in the bubble phase is inevitable.

The evolution of emulsion phase temperature during the polymer residence time in the reactor is shown in the Figure 3.6 for the four different grades of polymer.

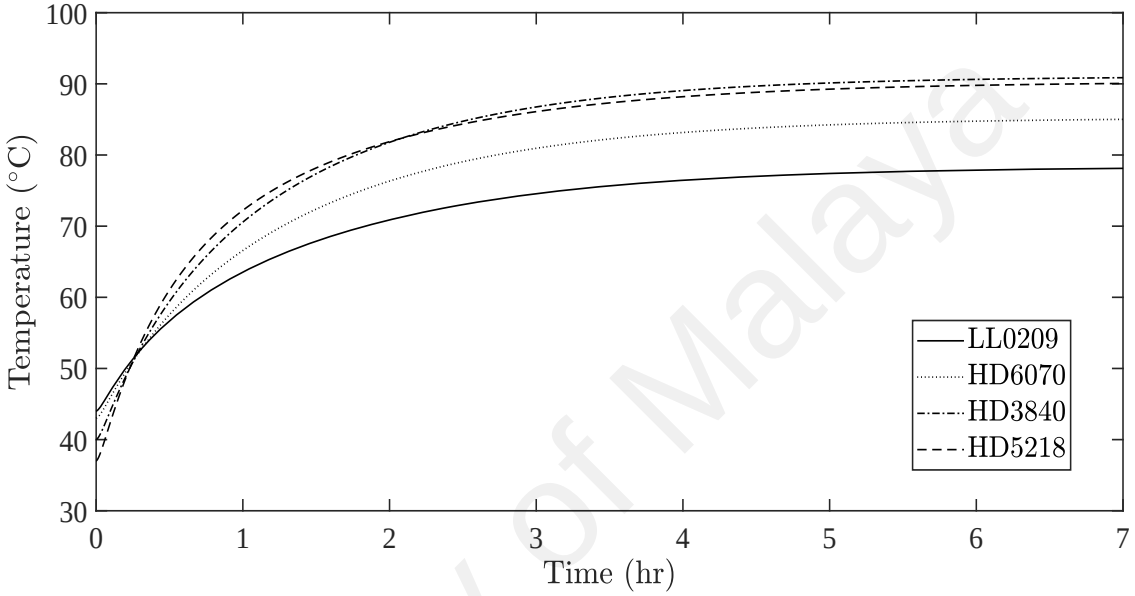

Figure 3.6: Evolution of temperature in the emulsion phase for the four different grades of polyethylene

All grades continue to increase with different slopes, and become steady after almost 5 hours. For example, the graph estimates that the temperature of the LLDPE reaches 78 °C after getting steady around the fifth hour and remains at that temperature. The temperature grows rapidly the first hour and reaches 58 °C after one hour from a temperature of 44 °C in the beginning, since the polymerization reaction is exothermic and this graph illustrates this clearly. The final steady state temperatures of these grades are compared with both industrial data and the work of Kiashemshaki et al. (2006) in the parity plot of Figure 3.7.

The lower LLDPE temperature compared with the HDPE temperatures and literature data is due to the higher superficial gas velocity of LLDPE grade compared to HDPE grade. There is a direct relation between superficial gas velocity and the monomer residence time in the reactor, heat removal rate from the reactor, particle mixing and fluidization conditions. In fact, by increasing the superficial gas velocity, gas passes faster through

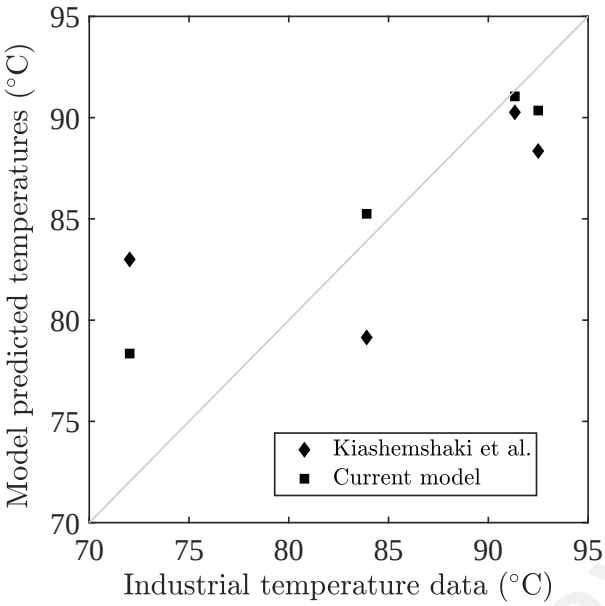

Figure 3.7: Emulsion phase temperature comparison with industrial and literature data for the four different grades of polyethylene after reaching steady state

the bed. As a result, more solid particles carry over, the amount of catalysts and polymer particles available in the reactor bed will be reduced, and some monomers may bypass the catalysts, and therefore, reaction extent will be reduced and lead to a reduction in the reaction rate. Less reactions in this exothermic reaction, means lower temperatures. Since particle entrainment is considered in this model, this will justify the lower temperature results of this model in LLDPE grade compared to those obtained by Kiashemshaki et al. (2006). Another advantage of the current model is calculating temperatures dynamically unlike the comparison work of Kiashemshaki et al. (2006) which calculates temperature and comonomer concentration in steady state. A dynamic model can have the advantage of being a basis in process control studies to test different approaches to control polymer properties and reactor parameters based on parameters like inlet gas compositions, catalyst input rate, gas superficial velocity, and reactor pressure. Moreover, solids elutriation is another phenomenon in FBRs, which cannot be neglected, and is included in this work to make the model be more realistic. Figure 3.7 shows that the temperatures calculated in this work acceptably close to the actual data and more accuare in compare with the work from literature.

Table 3.6 shows the operating conditions for another industrial polyethylene production reactor in a second petrochemical complex during one working shift. The operational

data and resulting temperature data were collected using the plant data acquisition and distributed control system. To validate the model further, it was tested using this dataset. The calculated reactor temperatures have been compared with real data in Figure 3.8.

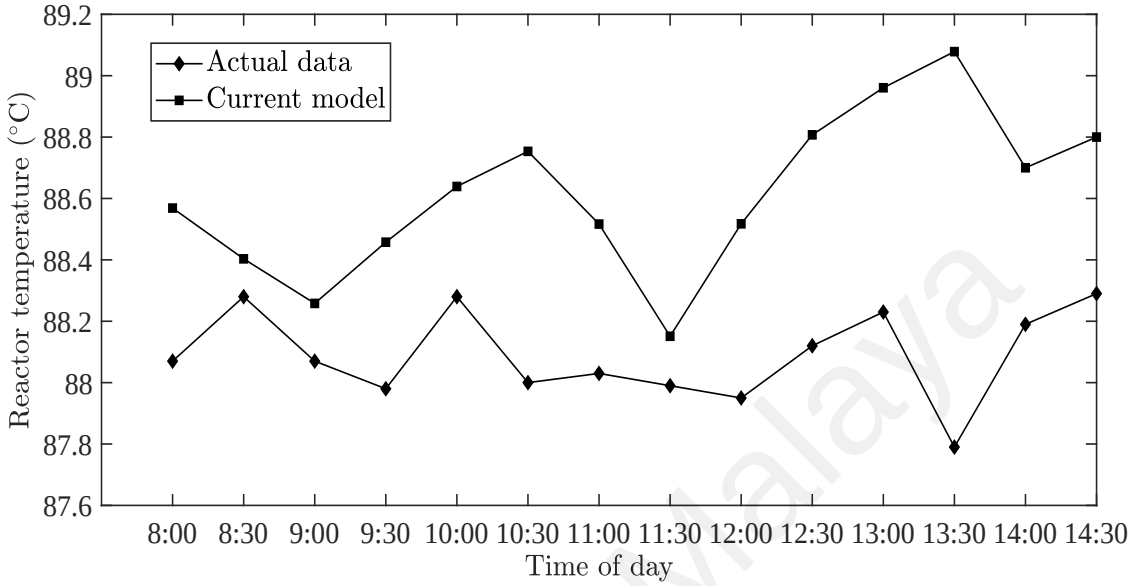

Figure 3.8: Reactor temperature comparison with industrial data during an operating shift

The model has again been capable of accurately predicting reactor temperature for this grade of polymer. The average error for this data set is 0.6 percent deviation from the industrial data, which is small in engineering context. Nevertheless, considering resistance of heat transfer among gas and solids in both phases, radial temperature gradients in the reactor and particle size distributions could further improve the model, which leads to better prediction of reactor parameters and polymer properties. However, this will increase model complexity and computational efforts.

The evolution of mean monomer concentrations throughout the bed during the residence time in the reactor are shown in Figure 3.9.

It is clear that the time of getting into a steady state is the same as production rate and temperature profile graphs. As can be seen, copolymerization reaction consumes ethylene as monomer and 1-butene as comonomer in order to produce the polymer. As a result, their concentrations decrease exponentially during the first 5 hours of the residence time before going flat in the steady zone.

Another imperative property of the polymer is its density. Several polymer grades

Table 3.6: Operating conditions for petrochemical complex 2

Parameter	BP LL0209													
Time	8:00	8:30	9:00	9:30	10:00	10:30	11:00	11:30	12:00	12:30	13:00	13:30	14:00	14:30
H(m)	19.76	19.77	19.74	19.79	19.87	19.87	19.83	19.6	19.91	20.12	20.13	20.04	20.11	20.12
$d_p(\mu\text{m})$	986	986	986	986	986	986	986	986	986	986	986	986	986	986
P(bar)	21.8	21.81	21.81	21.8	21.83	21.79	21.81	21.81	21.74	21.74	21.73	21.77	21.75	21.76
U_0(m/s)	0.634	0.635	0.636	0.635	0.635	0.633	0.634	0.633	0.634	0.634	0.631	0.629	0.631	0.632
Ethylene (%)	37.07	36.9	36.88	36.95	37.02	36.96	36.8	36.67	36.63	36.6	36.44	36.54	36.45	36.46
1-Butene (%)	13.73	13.75	13.73	13.71	13.69	13.67	13.63	13.64	13.55	13.55	13.57	13.54	13.56	13.57
Hydrogen (%)	4.57	4.58	4.62	4.62	4.6	4.6	4.65	4.65	4.63	4.65	4.69	4.66	4.69	4.68
Inert gas (%)	36.39	36.4	36.32	36.38	36.47	36.32	36.41	36.38	36.42	36.49	36.7	36.57	36.7	36.7
Catalyst feed rate (g/s)	0.661	0.661	0.661	0.661	0.661	0.661	0.661	0.661	0.661	0.661	0.661	0.661	0.661	0.661

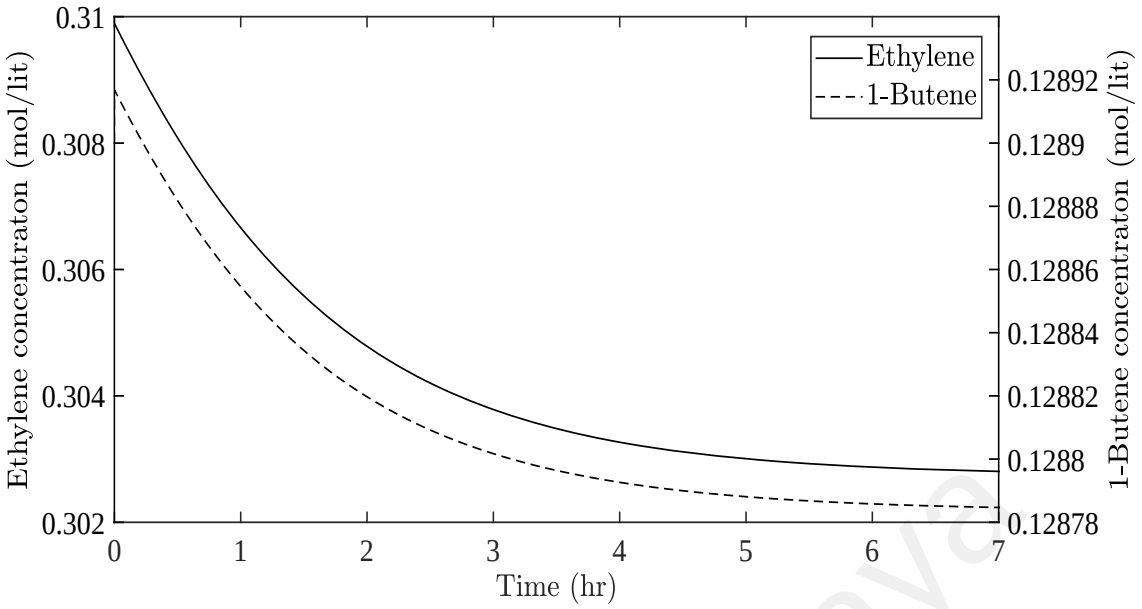

Figure 3.9: Evolution of mean ethylene and 1-butene concentration throughout the bed during residence time in the FBR

for different applications need to have specific densities. Since this model is dynamic, researchers can use it in future to study controlling polymer density. However, it is very complicated to find the correlation between density and polymer structure. Density could be altered by both the length and number of the short chain branches and to a small extent by the polymer molecular weight (Kunii & Levenspiel, 1991). McAuley et al. (1990) developed an experimental equation to relate the amount of comonomer in linear polyethylene to its density:

$$\rho = 0.966 - \alpha C_x^{\beta} \tag{3.52}$$

Where α and β are parameters which depend on comonomer, and C_x is the comonomer mole percent in the polymer. Variables α and β have been fitted at 0.02386 and 0.514 for butane grade polymers. Figure 3.10 shows the correlation between 1-butene concentration of the feed and the density calculated from Equation (3.52). Naturally, increasing 1-butene concentration leads to lower density values and it can be used as a manipulated variable in future process control studies to regulate the polymer density value.

3.5 Summary

In this chapter, the developed dynamic model of two-phase copolymerization of ethylene and 1-butene in industrial fluidized–bed reactors catalyzed by Z–N catalyst considering

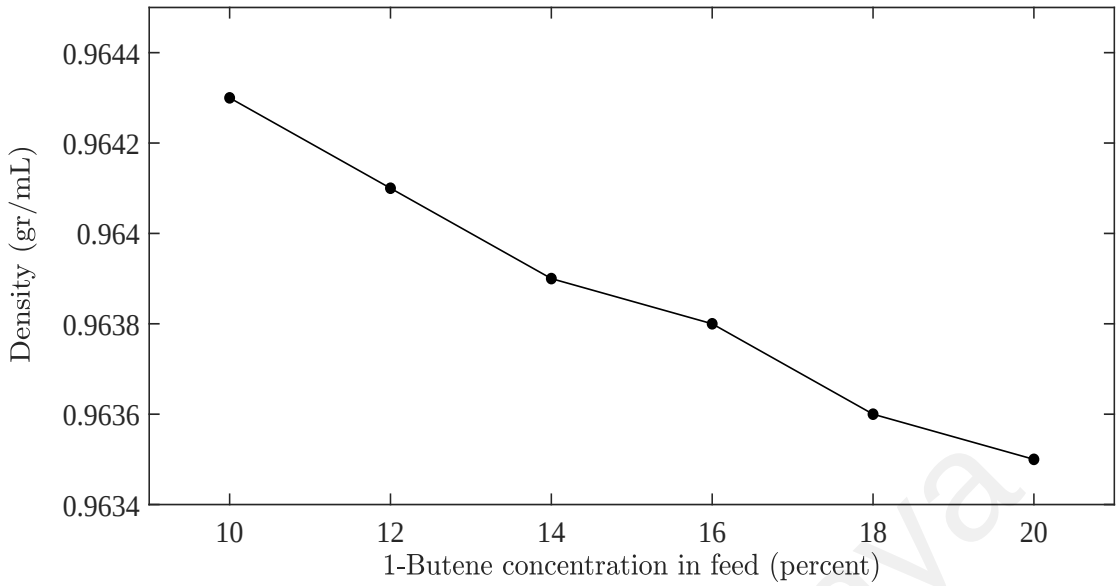

Figure 3.10: Relation between 1-butene concentration of the feed and polymer density

two–site kinetics was explained in detail and was utilized to predict the polymer properties and reactor behavior. The kinetics mechanism and rate laws are translated into differential moment equations. The governing hydrodynamics and mass and energy balances are solved simultaneously with moment equations to make it possible to predict the evolution of molecular weight distribution, melt flow index, polydispersity index, temperatures, production rate, density and concentration fractions with time. The model considers solid entrainment in the FBR modeling. The results were compared with industrial data as well as literature for validation purposes. This model provides a tool to study the operational, hydrodynamics and kinetic parameters on reactor performance in addition to polymer properties, and can be used as a base for control studies to regulate properties like PDI, MFI or density of a polymer beside reactor parameters such as temperature. The control studies are detailed in the next chapter.

CHAPTER 4: ADVANCED CONTROL OF REACTOR TEMPERATURE AND POLYMER MELT FLOW INDEX

4.1 Introduction

Modeling and control of the polymerization process in FBRs such as polyethylene production are challenging issues in process and control engineering. This is mainly because of the high non-linearity of the process dynamics due to complicated reaction mechanisms, complex flow characteristics of gas and solids, numerous heat and mass transfer mechanisms and the interaction between the process control loops. Many studies report the modeling and control of ethylene polymerization processes using various types of algorithms. However, there is very little work on control of gas phase ethylene polymerization in FBRs. In this work, AI-based control is utilized to control two of the main process variables namely Melt Flow Index (MFI) and reactor temperature. The developed model in Chapter 3 is used to simulate the system and the controllers are used to manipulate the input of the system in order to regulate chosen outputs. Adaptive Neuro Fuzzy Inference System (ANFIS) in different architectures is shown to be able to control these variables optimally. This chapter explains the details of this approach and the results are presented and discussed.

4.2 Control variables and process nonlinearity

A vital polymer property that should be carefully controlled is the polymer Melt Flow Index (MFI). Even though MFI is a quantity to measure polymer processability and its rheological behavior, it has been shown to correlate with the final product properties and one of the main bases to decide on the properties of a specific polymer grade is MFI. Two main standards are used to decide the polymer MFI. ASTM D1238 and ISO 1133 are the standards used throughout the industry which differ on the testing specifications. The basis is to put the polymer under a certain weight and temperature and measure the weight of melted polymer that passes an orifice with a certain size. For example, MFI of different linear low-density polyethylene (LLDPE) grades may range from 0.1 to 5 $g/10min$ or even higher for special uses. LLDPEs with high MFIs may be used in producing geomembrane, high strength film, food and industrial packaging, and shopping bags while applications

such as molded containers, chemical and water tanks and traffic cone need polymers with lower MFI. Although MFI was impossible to be measured on-line previously, recent modern technology with invention of new methods and instruments gave us the opportunity to control this vital polymer property online.

Another crucial aspect is the tight temperature control in gas phase polymerization reactors. The aim is to make sure that the reaction zone temperature stays higher than the reactants' dew point, but under the polymer's melting point; this is to avoid melting and subsequent particle agglomeration (Dadebo et al., 1997). Consequently, most of the commercial gas phase polyolefin fluidized–bed reactors work in such a small temperature range of 248 to 400 K (Xie et al., 1994). Even so, temperature excursions have to be prevented since they can cause some remarkable deviations in product properties and lead to low catalyst productivity (Shamiri et al., 2015).

Lacking temperature control, industrial polyolefin reactors have the tendency to be subjected to undesired situations such as unsteady states, or temperature trips toward undesirable high reaction zone temperature which is above the polymer softening point (Choi & Ray, 1985; Ghasem, 1999; Ho et al., 2012; McAuley, Macdonald, & McLellan, 1995; Shamiri, Hussain, Mjallic, & Mostoufid, 2013). Also noteworthy is that the maximum polyethylene production rates take place when they work in the unstable steady states which surely need a proper controller to make the steady states stable. McAuley (1993) studied the non-linear control of product properties in the industrial gas phase polyethylene reactors for instant polymer melt flow index (MFI) and density regulation. The performance of linear and non-linear temperature control schemes was studied for an open-loop and unstable gas-phase polyethylene FBR, with criteria such as the robustness , damping, speed, and the ability to keep the closed-loop steadiness in various operating conditions using the well-mixed model adopted by Lee and Sullivan (1988).

Despite the non-linear attribute of the chemical processes, most of them are still regulated by linear controllers aided by the plant models that are linearized. The Arrhenius behavior of the rate constants is a cause of non-linearity in chemical reactors. Similarly, constrained manipulated variables possibly will give saturation non-linearity. During recent decades, non-linear controller designs were suggested to control specific highly

non-linear systems where precise control was the important criterion. It is easy to design the input-output linearizing controllers, but they are restricted to minimum-phase systems since the zero dynamics of the process must be stable for the non-linear inversion.

4.3 Ethylene polymerization in fluidized–bed reactor process

A process schematic of an industrial gas-phase fluidized–bed polyethylene reactor is shown in Figure 4.1. The feed gas flow provides monomers, hydrogen and nitrogen for polymerization, agitates the bed to achieve fluidization through the distributor, and removes the heat of polymerization reaction. Polymerization occurs in the fluidized–bed under the presence of Ziegler–Natta catalyst, triethyl aluminum co-catalyst and reactants. The unreacted gas exits the top of the reactor and is then compressed and cooled before feeding the bottom of the fluidized–bed.

Figure 4.1 illustrates some of the possible control loops structures which are used to control different polymer and reactor properties such as temperature and MFI. As it can be seen from the MFI control loop, an advanced online rheometer installed on the reactor polymer outlet line can measure the MFI online and send the data to the controller which will manipulate the hydrogen concentration in the feed to reach a given set-point or deal with a disturbance. On the other hand, what happens within the temperature loop is that a sensor reads the temperature in the reactor and a transmitter sends the data to the controller. The controller then manipulates the cold water flow rate of a shell and tube heat exchanger which is on the way of the recycle stream. By increasing the cold water flow rate, the reactor would essentially cool down. The details on choosing these manipulative variables and their open loop is discussed in Section 4.7 and Section 4.8.

4.4 Reactor model

As described in the previous chapter, the improved two–phase model considers the presence of the particles in the bubbles and the excess gas in the emulsion phase and solid elutriation. This model proved to provide a more realistic explanation for the phenomena occurring in FBRs. Based on the advantages of the improved two–phase model over the other models, this control study uses this model.

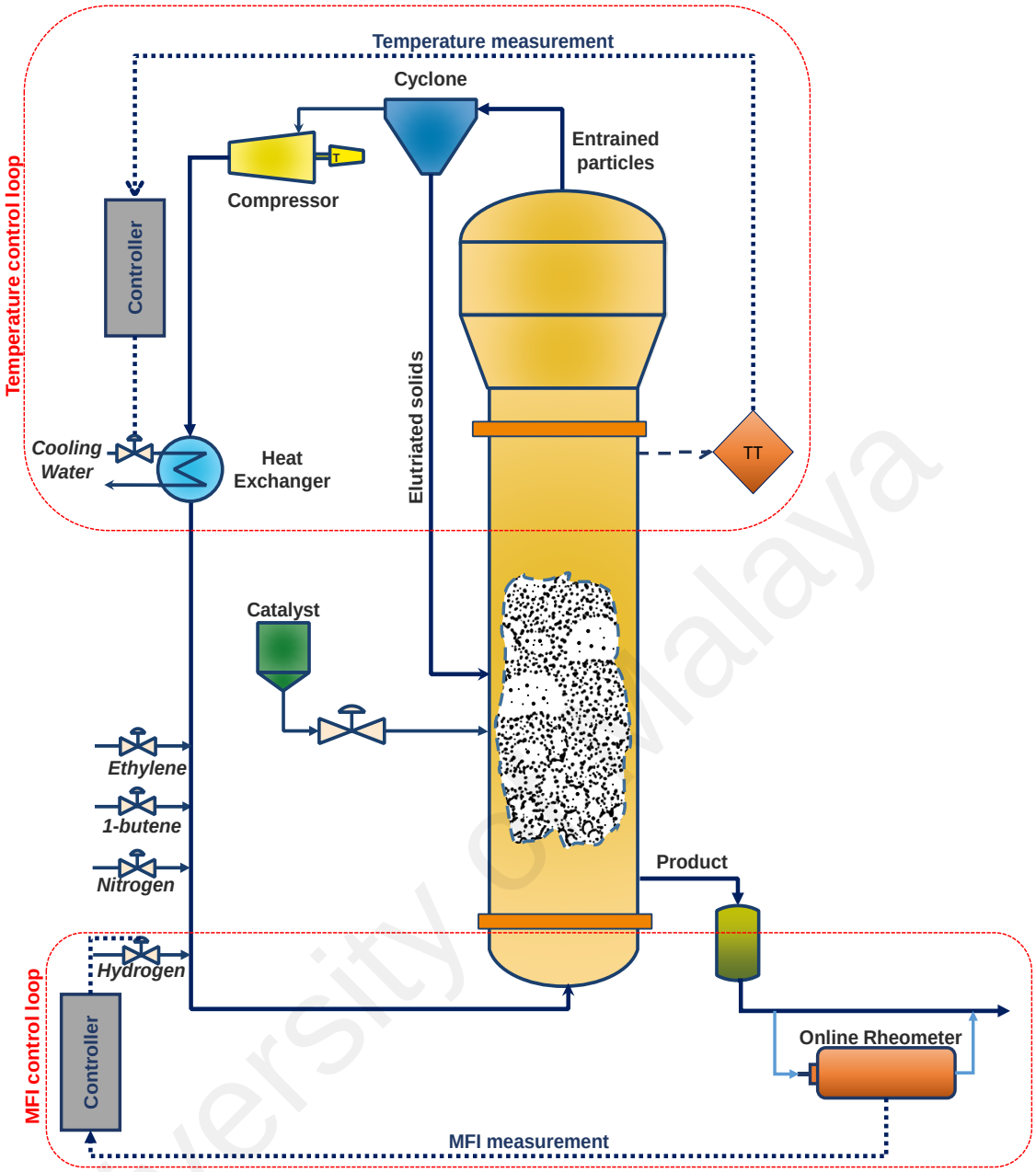

Figure 4.1: A typical fluidized–bed polymerization reactor with temperature and MFI control loop structures

4.5 Conventional PID Controller Design

Proportional–Integral–Derivative (PID) controller may be the most widely used controller in the industries for the past decades because of its simplicity and efficiency. The PID controller transfer function, $F(s)$, is:

$$F(s) = K_p(1 + \frac{1}{\tau_i s} + \tau_d s) \tag{4.1}$$

Where: K_p is the proportional gain of the Controller, $\frac{K_p}{\tau_i}$ is the integral gain of the

controller, and $K_p\tau_d$ is the differential gain of the controller. How to appropriately tune the gains of PID controller is always an attractive problem. The attempts to obtain better performance and robustness by improving tuning formulae lead to several achievements, such as Ziegler-Nichols formula. All of the tuning formulas need to know critical gain and critical period for tuning. If we don't have the prior knowledge of the system dynamics, the auto tuning method would be a solution. One of the main problems faced with PID controllers is that they are linear, and in particular symmetric. Thus, performance of PID controllers in non-linear systems is variable. There are many ways to tune the PID parameters. In this work, Ziegler-Nichols method is utilized.

4.5.1 Ziegler-Nichols tuning

Ziegler and Nichols, described several simple mathematical procedures for tuning PID controllers. These procedures are now accepted as standard in control systems practice. Both techniques make a prior assumptions on the system model, but do not require that these models be specifically known. Ziegler-Nichols formula for specifying the controllers are based on plant step responses. The details of the Ziegler-Nichols method is given by Ziegler and Nichols (1993)

4.6 Process control using Adaptive neuro-fuzzy inference system (ANFIS)

To start the design of the controller using the ANFIS scheme, first, a mathematical model of the system along with the controller mathematical model is required, which can be further used for simulation purposes. The model of the system was explained in detail in Chapter 3 and the model of the ANFIS controller is given in this section.

Fuzzy Logic theory uses incorporating engineering knowledge into the automatic control system by using the intuition and experience of the designer. In 1965, this strategy was first proposed by Zadeh (1965). Complicated systems control that are too hard to be analyzed by traditional mathematics. But fuzzy logic theory did not find wide popularity in various applications such as economics, management, medicine, or process control until the 1970's.

Mamdani (1974) introduced the first application of fuzzy set theory for controlling a small laboratory steam engine. After success of this theory many scientists were inspired

to attempt to control industrial processes such as automatic trains, chemical reactors, or nuclear reactors using fuzzy algorithms. Experiments showed that fuzzy controllers perform better at least the same as adaptive controllers. One of the advantages of this technique is requiring only a simple mathematical model to formulate the algorithm. It eases the digital implementation. There are also other fuzzy systems such as Sugeno or Takagi-Sugeno-Kang (TS) which differs with the Mamdani type only in output membership functions where they can only be either linear or constant Sugeno (1985).

However, the fuzzy logic approach is based on predefined rules (if-then) that lacks the ability to learn and adapt themselves to the new condition. Thus to overcome this drawback, Jang (1993) hybridized a FIS (fuzzy inference system) with ANN (Neuro Fuzzy) to form ANFIS.

The ANFIS methodology can be considered as an adaptive system in the form similar to ANN in which by training the system the parameters of the fuzzy membership functions (antecedent parameters) and the parameters of the fuzzy system output function (consequent parameters) are adapted.

ANFIS possesses the advantage of both FIS and ANN and it solved the drawbacks of both systems, where the complicated procedures of neural networks are bypassed by applying linguistic variables of FIS system, and the lack of FIS is solved by applying the neural inference system which create the ability to learn and adapt them-self to new condition. Therefore, this approach is capable to simulate complex nonlinear mappings using fuzzy system with ANN learning, and it is considered as a universal estimator capable for short, medium, and long-term forecasting.

ANFIS was developed as an adaptive system with a set of fuzzy rules (if-then) and tunable MF (membership function) parameters in the training phase. During the training phase of ANFIS, two different parameters should be optimized to provide the learning procedures:

1. antecedent parameters (the MF parameters)
2. consequent parameters (the fuzzy system output function)

As the consequent parameters are linear, to optimize these parameters the linear least-

squares method is applied and to optimize the antecedent parameters similar to neural networks the back-propagation algorithm in conjunction with an optimization method such as gradient descent is applied.

Generally, five different layers construct the ANFIS structure where each layer consists of node functions and the inputs of the nodes in the present layer are obtained from previous layers. The consecutive layers of ANFIS structure are as follows: layer 1 is fuzzification (if-part), layer 2 is production part, layer 3 is normalization part, layer 4 is defuzzification (then-part), and eventually layer 5 is total output generation part. Figure 4.2 shows the structure of an ANFIS with two independent variables (x and y) as input and one dependent variable f_{out} as an output.

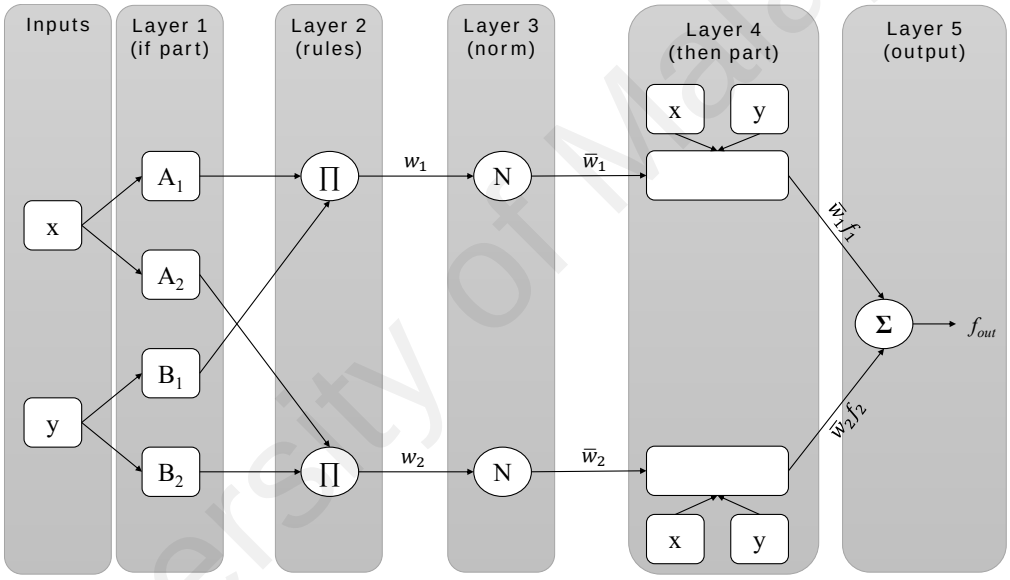

Figure 4.2: ANFIS structure for two inputs and one output

For fuzzy inference systems, difference in the consequence of the set of fuzzy rules (if-then) and defuzzification procedures lead to two different types of fuzzy inference systems known as Mamdani type FIS and Sugeno type FIS. In many respects, Mamdani type FIS is similar to Sugeno method. The fuzzifying the inputs data and executing the fuzzy operators are similar fuzzy inference process in both types. The main difference between Sugeno type FIS and Mamdani type FIS is the way the fuzzy inputs are converted to the crisp output. In Mamdani type FIS, for computing the crisp output the defuzzification technique of a fuzzy output is used while in Sugeno type FIS the weighted average method is used. As the consequents of the rules are not fuzzy in the Sugeno method, the

interpretability and expressive power of Mamdani output, are eliminated in this method. In comparison to Mamdani type FIS, Sugeno has faster processing time since instead of the time consuming defuzzification process the weighted average method is applied. Moreover, another difference between Sugeno and Mamdani type FIS is that Sugeno has no output membership functions whereas Mamdani FIS has output membership so, Sugeno method provides an output that is either linear (weighted) mathematical expression or a constant. Instead, Mamdani method provides an output that is a fuzzy set.

ANFIS architectures representing both the Mamdani and Sugeno methods. In comparison to Mamdani type FIS, Sugeno has more flexibility in system design as latter can be integrated with ANFIS tool to model the systems more precisely.

Considering ANFIS with Sugeno type FIS, so the rule base of ANFIS contains fuzzy IF-THEN rules of a first order Sugeno type FIS are stated as:

Rule 1: If x is A_1 and y is B_1 then z is $f_1(x, y; p_1, q_1, r_1) = xp_1 + yq_1 + r_1$

Rule 2: If x is A_2 and y is B_2 then z is $f_2(x, y; p_2, q_2, r_2) = xp_2 + yq_2 + r_2$

where $f_i(x, y; p_i, q_i, r_i)$ is a first order polynomial function which represents the outputs of the Sugeno type FIS, A_i and B_i are the fuzzy sets, and x and y are two different input and z is an output of ANFIS model.

In the ANFIS structure different layers consists of different node function. As shown in Figure 4.2, adaptive nodes which represent the adjustable parameter sets are denoted by squares whereas fixed nodes which represent the fixed parameter sets in the system are denoted by circles.

(a) ***Layer 1***

Every node in this layer is an adaptive node with a node function as follow:

$$Q_{1,i} = \mu_{A_i}(x) \qquad i = 1, 2 \tag{4.2}$$

$$Q_{1,i} = \mu_{B_i}(y) \qquad i = 3, 4 \tag{4.3}$$

Where x and y are the inputs to node i , A_i and B_i are linguistic labels, μ_{A_i} and μ_{B_i} are the membership functions for A_i and B_i fuzzy sets, respectively and $Q_{1,i}$ is the membership

grade of a fuzzy set and considered as the output of node i in the first layer which specifies the degree to the given input (x or y) satisfies the quantifies.

Typically in ANFIS, the MF (membership function) for a fuzzy set can be any parameterized membership function, such as generalized Bell shaped function ,Guassian , trapezoidal or triangular.

A generalized Bell shaped MF (bell MF) is specified as follows:

$$\mu_A(x; a, b, c) = \frac{1}{1 + \left[\frac{x - c}{a}\right]^{2b}} \tag{4.4}$$

A Guassian MF is specified as follows:

$$\mu_A(x;; c, \sigma) = e^{-0.5\left(\frac{x - c}{\sigma}\right)^2} \tag{4.5}$$

whileσ and c determined the width and center of Guassian MF, respectively.

A trapezoidal MF is specified as follows:

$$\mu_A(x;; a, b, c, d) = max\{min\left(\frac{x - a}{b - a}, 1, \frac{d - x}{d - c}\right\}, 0) \tag{4.6}$$

The parameters with $a \leq b \leq c \leq d$ specify the x coordinates of the four corners for the underlying trapezoidal MF.

A triangular MF is specified as folows: The parameters with $a \leq b \leq c$ specify the x coordinates of the three corners for the underlying triangular MF.

In this layer, the parameters a, b, c, d and σ are the antecedent parameters.

(b) ***Layer 2***

Every node in this layer is a fixed node whose output is the product of all the incoming signals. In this layer through multiplication of input signals the firing strength of each rule is determined.

$$Q_{2,i} = w_i = \mu_{A_i}(x)\,\mu_{B_i}(y) \qquad i = 1, 2 \tag{4.7}$$

where w_i is output signal which represents the firing strength of a rule.

(c) ***Layer 3***

Every node in this layer is a fixed node. In this layer, the firing strength provided in previous layer is normalized by computing the ratio of the i^{th} rule's firing strength to the sum of all rules' firing strengths.

$$Q_{3,i} = \overline{w}_i = \frac{w_i}{w_1 + w_2} \qquad i = 1, 2 \tag{4.8}$$

where $\overline{w}$ is output signal, which represents the normalized firing strength of a rule.

(d) ***Layer 4***

In this layer every node i is adaptive with a node function.

$$Q_{4,i} = \overline{w}_i f_i \qquad i = 1, 2 \tag{4.9}$$

where f_1 and f_2 are the fuzzy IF-THEN rules as follows:

Rule 1: If x is A_1 and y is B_1 then $z = f_1(x, y; p_1, q_1, r_1)$

Rule 2: If x is A_2 and y is B_2 then $z = f_2(x, y; p_2, q_2, r_2)$

where r_i, q_i and p_i are the parameter set, referred to as the linear consequent parameters.

(e) ***Layer 5***

This layer has only one fixed node that computes the overall output of ANFIS by summation of all incoming signals.

$$Q_{5,i} = f_{out} = \sum_i \overline{w}_i f_i = \frac{\sum_i w_i f_i}{\sum_i w_i} = overal\ output \qquad i = 1, 2 \tag{4.10}$$

The overall output is linear combination of the consequent parameters. Thus, the final output of ANFIS is expressed as

$$
\begin{aligned}
f_{out} &= \overline{w}_1 f_1 + \overline{w}_2 f_2 \\
&= \frac{w_1}{w_1 + w_2} f_1 + \frac{w_2}{w_1 + w_2} f_2 \\
&= (\overline{w}_1 x)\, p_1 + (\overline{w}_2 x)\, p_2 + (\overline{w}_1 y)\, q_1 + (\overline{w}_2 y)\, q_2 + (\overline{w}_1)\, r_1 + (\overline{w}_2)\, r_2
\end{aligned}
\tag{4.11}
$$

Eventually, ANFIS applies a hybrid learning algorithm for parameter tuning. It utilizes the back propagation algorithm and the least squared method for updating the input MF parameters (antecedent parameters) in layer 1, and training the consequent parameters, respectively.

The block diagram of the ANFIS controller is shown in Figure 4.3. Error and differential

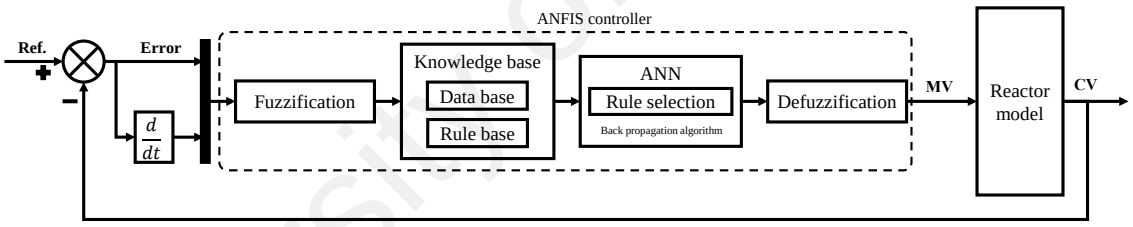

Figure 4.3: Block diagram of the ANFIS control scheme

Modeling and simulation of the control schemes was done using Simulink® suit. Figure 4.4 and Figure 4.5 show the type and values of membership functions for inputs of the designed MFI and temperature ANFIS controllers respectively.

Table 4.1 shows the specifications of the designed ANFIS controllers for controlling both MFI and temperature.

4.7 Control of polymer Melt Flow Index

As discussed in Section 3.4.1, MFI is one of the most important properties of the polymers. Melt flow rate is an indirect measure of molecular weight, with high melt flow rate corresponding to low molecular weight. At the same time, melt flow rate is a measure

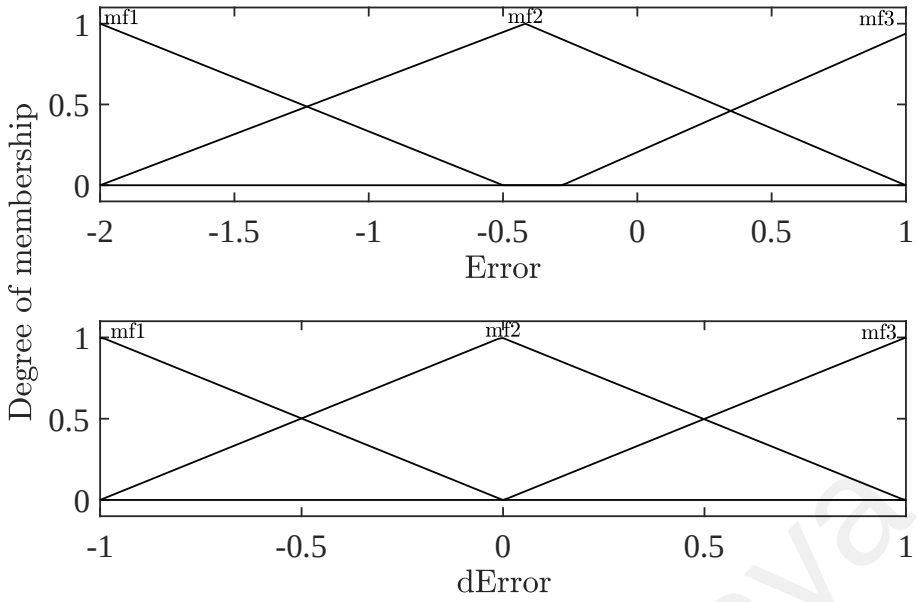

Figure 4.4: Input membership functions of the MFI ANFIS controller

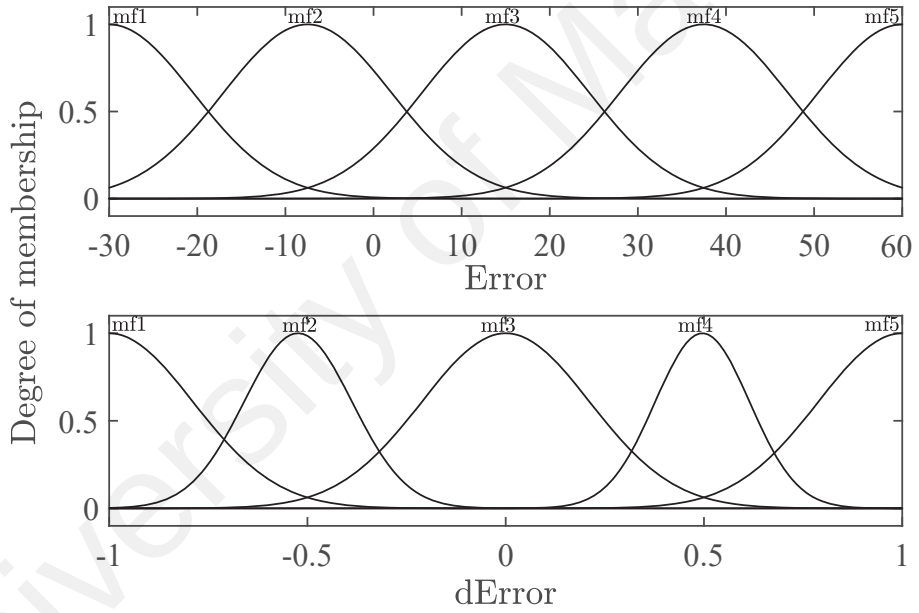

Figure 4.5: Input membership functions of the temperature ANFIS controller

of the ability of the material's melt to flow under pressure. Melt flow rate is inversely proportional to viscosity of the melt at the conditions of the test, though it should be borne in mind that the viscosity for any such material depends on the applied force. Ratios between the values of two melt flow rate for one material at different gravimetric weights are often used as a measure for the broadness of the molecular weight distribution.

Melt flow rate is commonly used for polyolefins where polyethylene is being measured at 190 °C and polypropylene at 230 °C. The plastics engineer should choose a material

Table 4.1: Specifications of the developed ANFIS structures for MFI and temperature control

Parameter	MFI ANFIS	Temperature ANFIS
Fuzzy structure	Sugeno	Sugeno
Membership function type	Triangular	Gaussian
Number of inputs	2	2
Number of outputs	1	1
Optimization method	Hybrid (least square and back propagation technique)	Hybrid (least square and back propagation technique)
Number of fuzzy rules	9	25

with a melt index high enough that the molten polymer can be easily formed into the article intended, but low enough that the mechanical strength of the final article will be sufficient for its use. Table 4.2 shows MFI ranges for different end usage high-density polyethylene grades.

Table 4.2: MFI ranges for different high density polyethylene grades (Shenoy & Saini, 1986)

MFI (190°C, 5kg)	Processing Method	Typical Applications
0.05-0.15	Compression molding extrusion	Profile, preformed blocks
0.1-1.3	Compression molding extrusion	Pipes, round bars
0.1-0.4	Blown film extrusion	Films
0.4-0.7	Extrusion blow molding	Fuel oil tanks
1.3-3	Extrusion blow molding	Hollow bodies (i.e. bottle)
3-13	Extrusion blow molding, Injection molding	Toys, household articles, Screw caps
13-25	Injection molding	can and bottle cases
25	Injection molding	Mass-produced articles for household uses, non deposit goods

Melt flow index (MFI) is basically defined as the weight of the polymer (g) extruded in 10 min through a capillary of specific diameter and length by pressure applied through a weight under prescribed temperature conditions. ASTM D1238 and ISO 1133 are the main

adopted standards to measure this property. These standards specify the details of the test conditions for each approach. ASTM D1238 gives the accuracy of the MFI value obtainable from a single measurement as carried out by different operators at different locations to be in the range of ±9 to ±15% depending upon the magnitude of the MFI (ASTM, 2003). Precise measurement of MFI calls for very strict control of all possible variables, and the test, though simple, must be performed with considerable care. Fortunately, recent technologies made it possible to measure MFI and viscosity of polymers continuously online while the test sample is not wasted and returns back to to the system. Pressure and temperature of these online MFI measuring instruments are controlled and recorded using a separate computer and the needed data can be transmitted to the controller (Figure 4.1).

Before any control study, open loop and step change dynamic responses of the system should be analyzed. Figure 4.6 shows the evolution of MFI over time. As it can be seen, it may take almost 2 hours for the system to stabilize and reach an almost constant MFI value that may essentially not be the designated values for that special polyethylene grade. As a result, to both minimize the stabilization time and control the MFI value at a fixed value, a control system is essential.

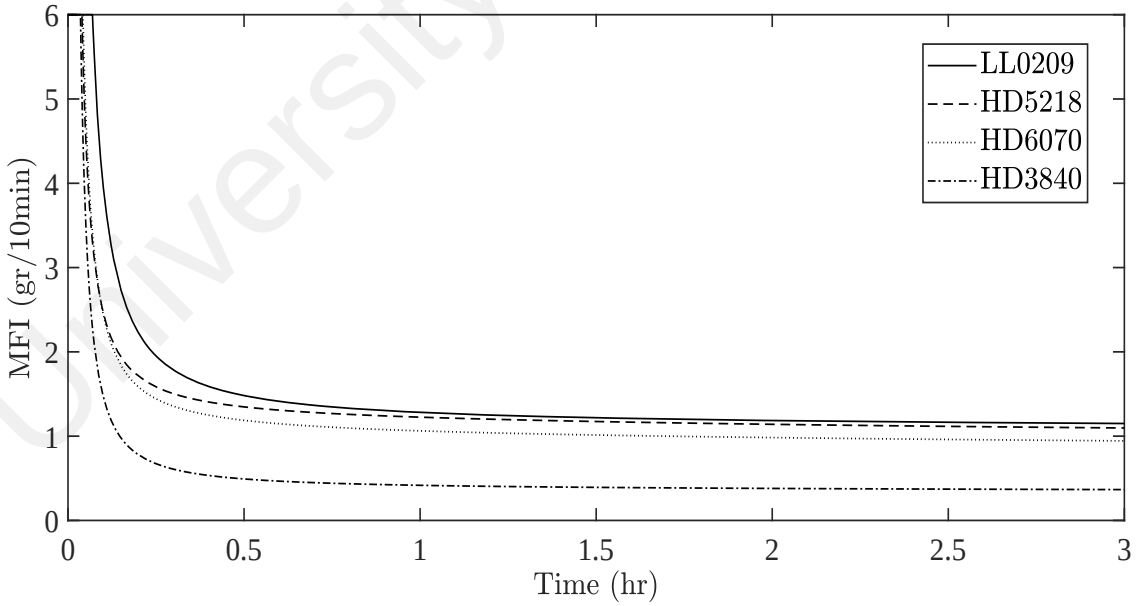

Figure 4.6: Evolution of Melt Flow Index (MFI) over time for different grades of polyethylene

In order to control the polymer MFI, an open loop sensitivity analysis showed that it is mostly dependent on the concentration of hydrogen in the inlet feed. Figure 4.7 shows this

nonlinear response to inlet hydrogen concentrations ranging from 2% to 18%. The initial concentration until 10^5 seconds was 10% while ethylene and 1-butene concentrations are kept constant at 40% and 17% respectively throughout the process. Inert gas (nitrogen) concentration varies so that the summation of all concentrations is at 100%. This nonlinear behaviour shows that conventional controllers will most likely be unable to control the MFI and an advanced controller is needed.

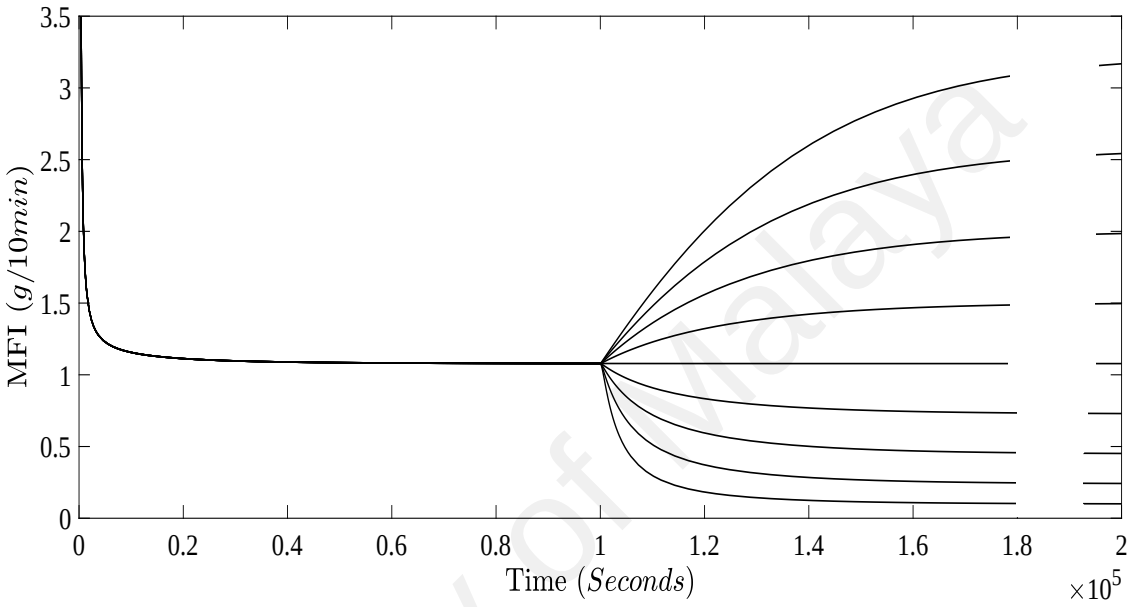

Figure 4.7: Open loop dynamic response of MFI for different inlet hydrogen concentrations

4.7.1 Set-point tracking

Figure 4.8 shows the MFI set point changes between 1 and 1.4 $g/10min$ tracked by PID and ANFIS controllers with 0 to 20 $percent$ saturation values respectively where P,I and D are K_p as the proportional gain of the Controller, $\frac{K_p}{\tau_i}$ as the integral gain of the controller, and $K_p\tau_d$ as the differential gain of the controller respectively. This figure illustrates that both controllers are capable of set-point tracking. Even though the PID controller reaches the set-point in every step change after a while, the ANFIS controller performance outperforms the PID controller as it has very small overshoots and has much less response times. For example, during the second step change from 1.4 to 1.3 at the seconds, it takes the PID controller around 3 hours to settle but it takes only 13 minutes for

the ANFIS controller to settle with a negligible post-transition undershoot of 0.015 in the MFI value.

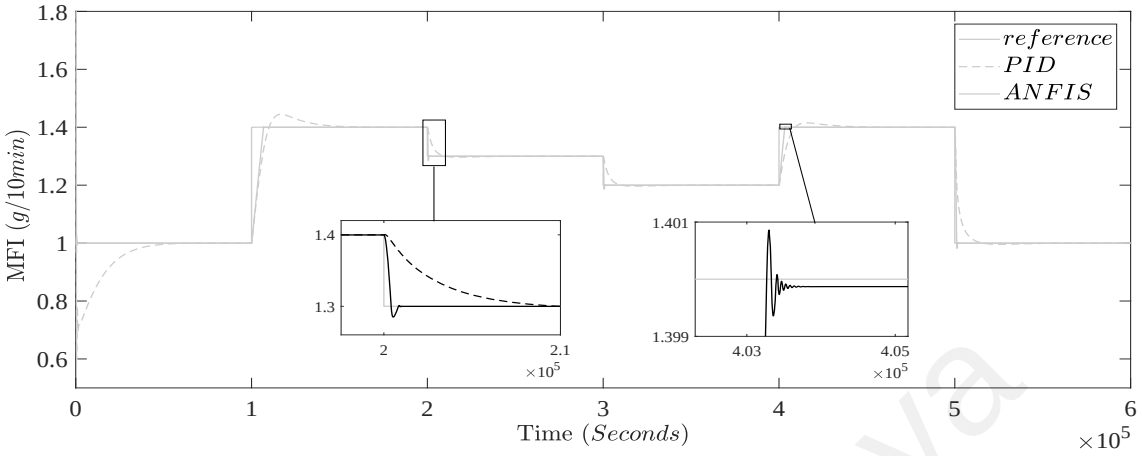

Figure 4.8: Comparison of MFI reference tracking for PID (P=0.6, I=0.0006, D=-50) and ANFIS controllers

The controller moves of ANFIS and PID controllers in MFI set point tracking are further shown in Figure 4.9. The controllers are constrained to a maximum 20% of hydrogen inlet concentration to make polymerization workable and realistic. To illustrate, it is found that the starting point of hydrogen concentration must be 9.6% to set the MFI at 1. However, after a step change to 1.4 , the controllers should set the inlet concentration to 11.5%. The controller moves of the ANFIS controller is fast and realistic. It fluctuates two times from minimum to the maximum of the manipulated variable and then some oscillations before reaching a steady state and this takes around 25 minutes for the ANFIS controller. On the other hand, PID controller jumps to the maximum and suddenly to the minimum of the manipulated variable before starting to rise slowly to reach the right value after a prolonged period of almost 8 hours. This shows that the ANFIS controller was much faster and robust in following the MFI setpoint, while the PID moves were more extreme and drastic in its controller moves.

4.7.2 Disturbance rejection

To verify that a controller can be employed in the industrial trials, it must be prepared to handle regulatory complications successfully as well. In the case of MFI, as Figure 4.10 shows, the concentration of ethylene has nonlinear and non-proportional effects on the MFI value such that increasing ethylene concentration in the feed leads to polymers with

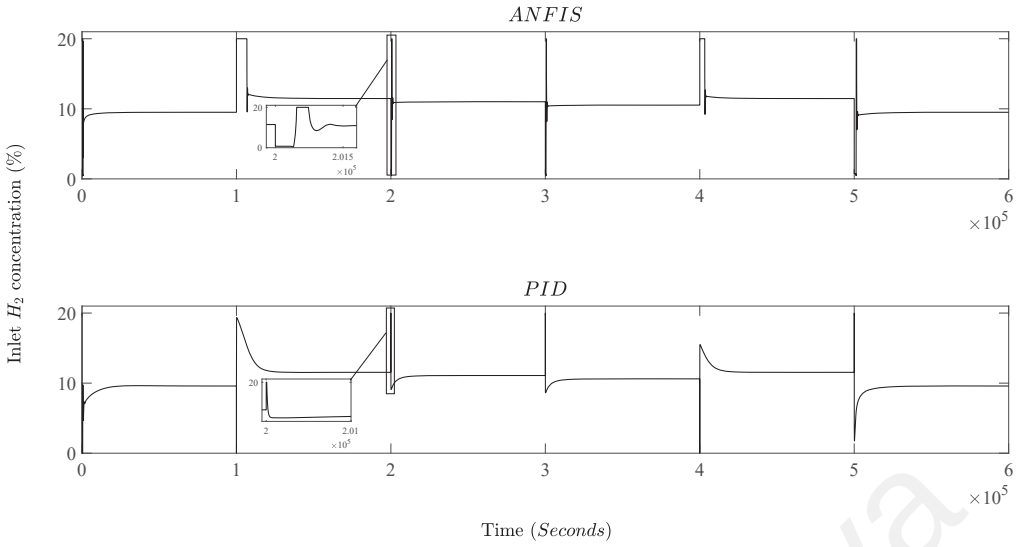

Figure 4.9: Controller moves in set point tracking of polymer MFI

higher density and lower MFI which may get above or below allowable specifications. As a result, variation in ethylene concentration was used as disturbance to test predictability and robustness of these controllers.

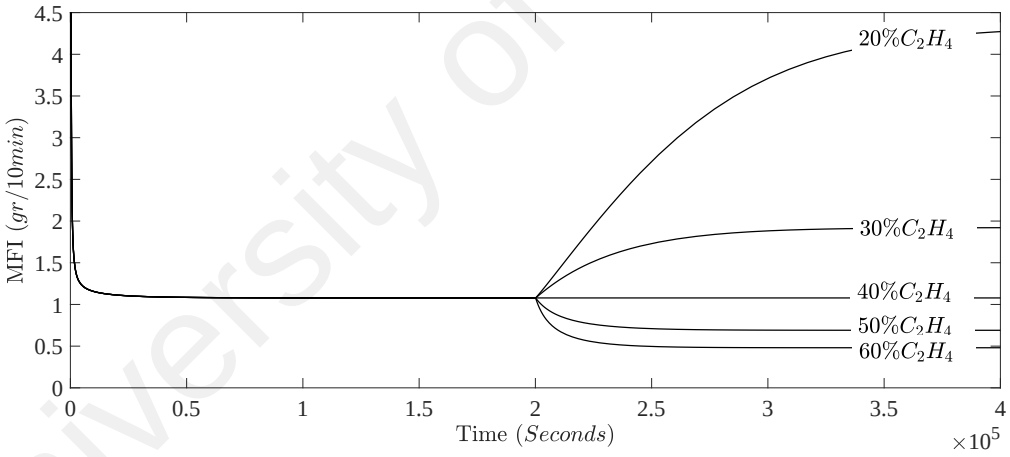

Figure 4.10: Effect of different inlet ethylene concentration step changes on the polymer MFI at 2×10^5 s**.**

Figure 4.11 displays the MFI response when it is controlled by ANFIS and PID controllers with a disturbance of 50% deduction in inlet ethylene concentration after 1×10^5 seconds. This figure shows clearly that the ANFIS controller is capable of disturbance rejection in a faster and more effective manner as compared to the PID controller.

As shown, since MFI has slow dynamics, ANFIS controller can completely omit the effect of the disturbance by rapidly changing the manipulated variable within just 8 minutes (Figure 4.12). However, although the disturbance makes little deviation from the set point

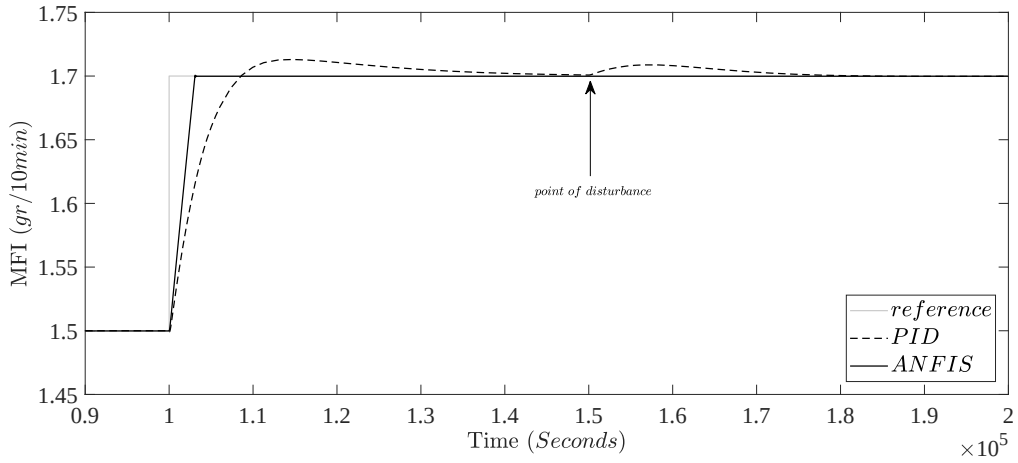

Figure 4.11: Performance comparison of the controllers in rejecting the effect of a 50% decrease in inlet ethylene concentration on the polymer MFI at 1.5×10^5 s

in case of the PID controller, it takes almost 19 hours for it to retract the system to the stable set-point. This is due to the less sensitiveness of the PID controller in this case with the very slow decrease it makes in the manipulated variable to compensate for the disturbance effect.

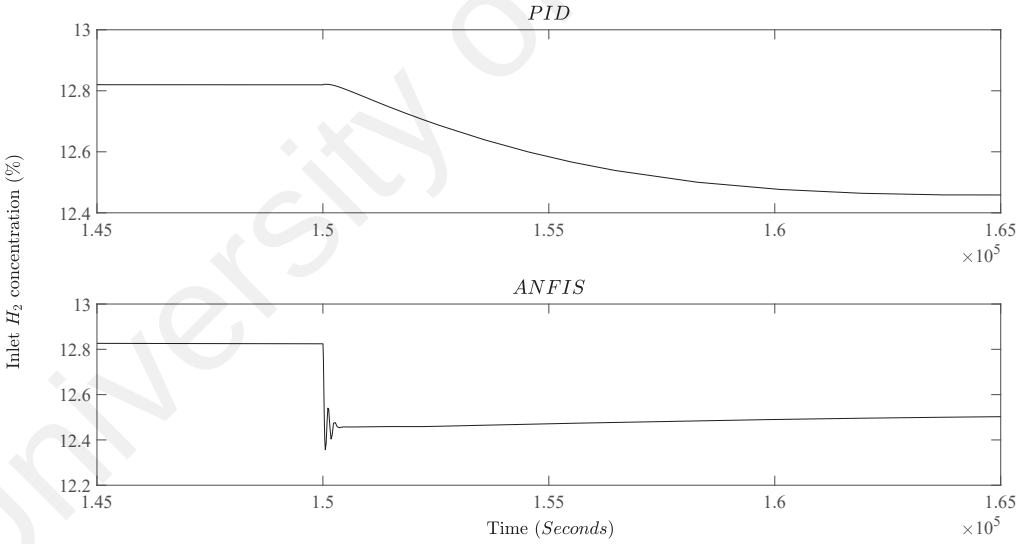

Figure 4.12: Controller moves in disturbance rejection for a 50% decrease in inlet ethylene concentration on the polymer MFI at 1.5×10^5 s

The measures of controlled system performance in terms of the integral of time absolute error (ITAE), the integral of absolute error (IAE), integral of squared error (ISE), and absolute percentage error (APE) for each MFI controller in both disturbance rejection and set-point tracking cases was also computed and is listed in Table 4.3. It is shown by the error values that the ANFIS controller showed improved performance compared to PID

since all the performance index values for the ANFIS controller is lower than the PID controller in both the disturbance rejection and set-point tracking studies.

Table 4.3: Performance indexes for MFI controllers

	Setpoint tracking		Disturbance rejection	
	PID	ANFIS	PID	ANFIS
ITAE	1.44×10^9	4.38×10^8	2.13×10^9	6.52×10^8
IAE	9826	2390	1.16×10^4	2886
ISE	1748	771.6	1911	870.4
APE	8687	1879	1.01×10^4	2302

4.8 Temperature control

Characteristically, the ethylene copolymerization reaction is very much exothermic. To keep the polyethylene production rates at the preferable values, it is important to make sure that the reactor's temperature is higher than reactants' dew point to prevent gas condensation within the reactor. Retaining the temperature below the polymer melting point is also necessary so that the particle melting, and agglomeration can be prevented, or the reactor will shut down. Consequently, an effective temperature control system must be implemented.

4.8.1 Heat exchanger model

As shown in Figure 4.1, the external gas cooler is a counter-current single-pass shell and tube heat exchanger with the recycle gas on the tube side and cooling water on the shell side. A linear first-order dynamic model obtained by imposing first order dynamics on the heat removal rate with a corresponding time constant, τ, to yield a linear dynamic model was considered for simulation of the heat removal system (Dadebo et al., 1997) given as:

$$\frac{dq}{dt} = \frac{q_{ss} - q}{\tau} \tag{4.12}$$

q is the dynamic heat removal rate and q_{ss} is the steady state heat removal rate, as:

$$q_{ss} = F_g C_{p_g}(T_e - T_{in}) \tag{4.13}$$

Where F_g is the gas flow rate, C_{p_g} is the gas heat capacity and T_e is the temperature of the gas entering the heat exchanger, which is also the reactor temperature. T_{in} is the outlet temperature of the gas from heat exchanger, which is also the temperature of the gas entering the reactor, given as:

$$T_{in} = \frac{T_{w_i}[1 - \exp(\gamma)] - T(1 - \eta)}{\eta - \exp(\gamma)} \tag{4.14}$$

where:

$$\gamma = A_{ex} U_{ex} \left[\frac{1}{F_g C_{p_g}} + \frac{1}{F_{cw} C_{p_w}} \right] \tag{4.15}$$

and

$$\eta = \frac{F_g C_{p_g}}{F_{cw} C_{p_w}} \tag{4.16}$$

Where T_{w_i} is the temperature of cooling water entering the heat exchanger, A_{ex} is the contact area and U_{ex} is the heat transfer coefficient. F_{cw} and C_{p_w} are the flow rate and heat capacity of the cooling water, respectively. Figure 4.13 shows these variables graphically.

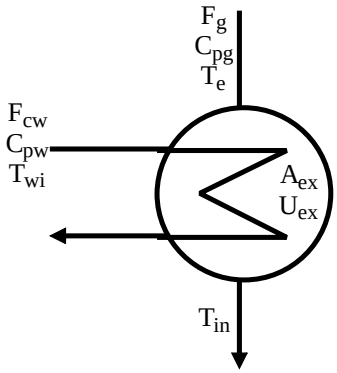

Figure 4.13: Heat exchanger model variables

In this study, cooling water flow rate in terms of its valve opening percentage to the recycle stream heat exchanger is used as the manipulated variable of the controller.

Figure 4.14 shows how the reactor temperature changes with incremental changes in valve opening for the cooling water flow rate. Exothermic reaction takes place in this reactor, therefore, reducing the cool water flow rate of the recycle stream heat exchanger leads to higher temperatures in the reactor.

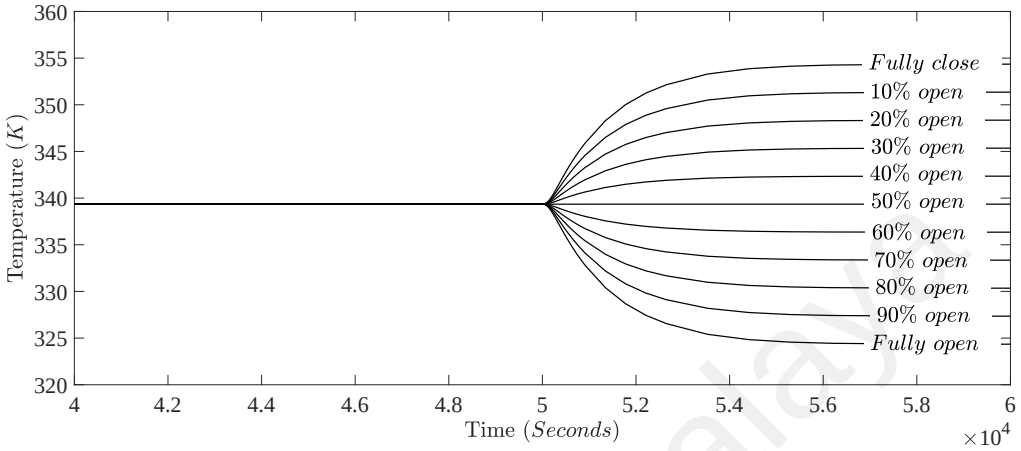

Figure 4.14: Open loop dynamic response of temperature to different opening percentages of the cool water valve

Figure 4.15 illustrates how fully closing and opening the cool water valve impacts the reactor temperature. As seen, unlike the case of MFI, here we have faster and responsive dynamics. While it took nearly 10 hours for the MFI to reach steady state after changing the manipulated variable from 10% to 20%, it takes the temperature only 2.5 hours to get to the steady value after altering the manipulated variable from 0% to 100% and vice versa. This shows the response dynamics are different in this case and an advanced controller design would be prefereable in this case.

4.8.2 Set-point tracking

Temperature control design also needs to be tested with step changes in set point and see how the controller follows it. Firstly, a conventional PID controller with 0 to 100 saturation values was tuned using the Ziegler–Nichols' closed loop method and tested in the servo scenario which is shown in Figure 4.16. As illustrated, rising, or falling time is short ($200 - 400 seconds$) and the controller eventually reaches and follows the setpoint. However, there is overshoots in both kinds of step changes where the duration and peak of it depends on the increase or decrease percentage in the setpoint. For increasing cases, it takes around 2.5 hours with a peak of almost $2K$ overshoot in temperature while decreasing

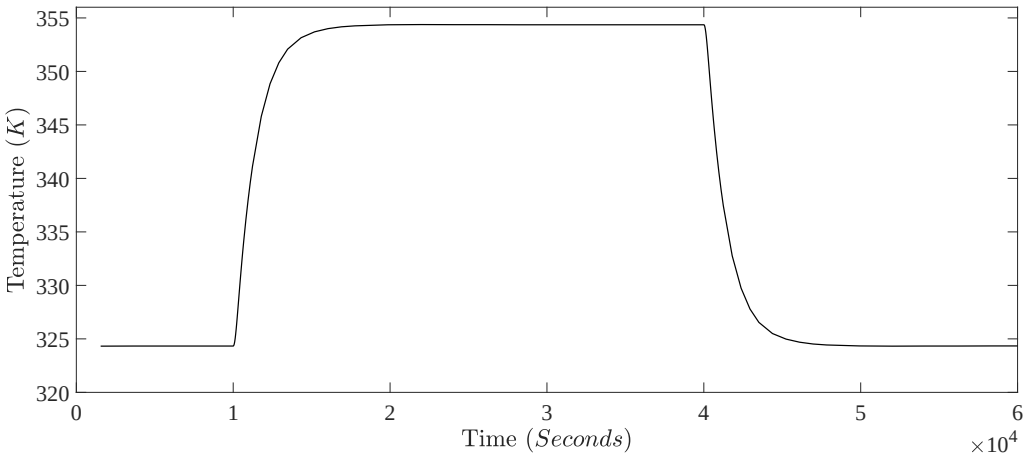

Figure 4.15: Open loop dynamic response of temperature to fully closing (1×10^4 *seconds*) **and fully opening** (4×10^4 *seconds*) **of the cool water valve**

the setpoint leads to some oscillation with around $\pm 1K$ overshoot and undershoots and with settling times of nearly half an hour.

The difference in temperature response to raising or lowering of the set points has a reason. In the case of a temperature increase the only thing that controller can do is to fully close the cool water valve and let temperature rise in the system because of the exothermic reaction. On the other hand, to decrease the temperature, the controller fully opens the valve. Since rising time for temperature increase is higher than falling time for temperature decrease, system gets cool faster than it gets hot in this system and with this specific heat exchanger capacity.

In this nonlinear system case, the only problem with the PID controller is the overshoots and undershoots. To alleviate this issue, we need to think of other advanced controllers which can control the process efficiently.

An ANFIS controller was designed and trained for controlling the temperature by manipulating the cool water valve and the result is presented in Figure 4.17. The ANFIS controller improves the performance of the PID controller but shows some oscillations around the setpoint. Depending on the amount of step change, these oscillations are within ±0.2 K of the setpoint with periods of around 5 minutes. This effect is because of the fast dynamics of the system and fuzzy rule changes of the ANFIS controller.

To mitigate the problems with both controllers, they can be used to control the temperature in a hybrid design. The Hybrid PID–ANFIS controller is combining two

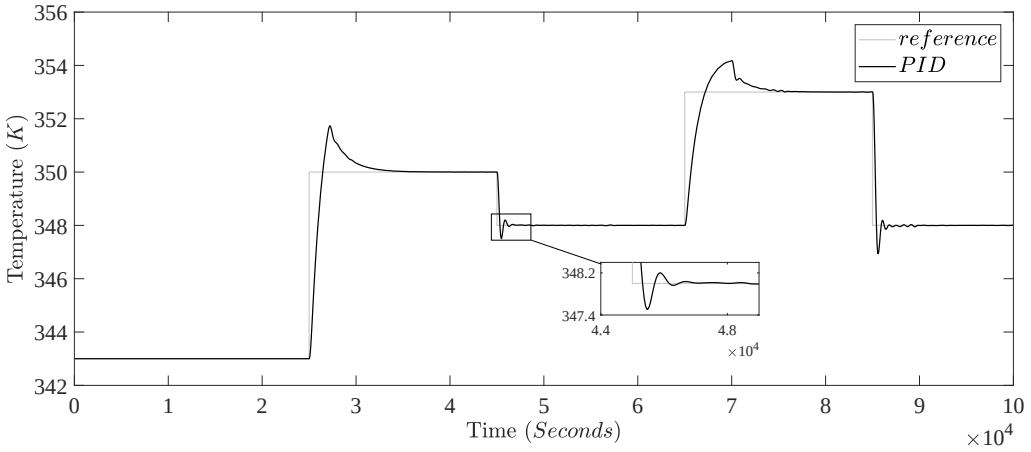

Figure 4.16: Temperature reference tracking using PID controller (P=-32.61, I=-0.018, D=47.32)

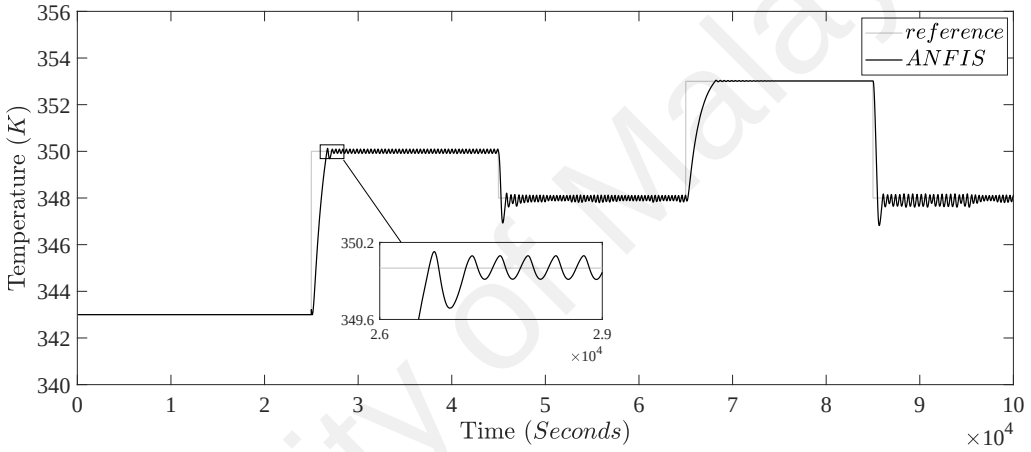

Figure 4.17: Temperature reference tracking using ANFIS controller

controller modes such as PID controller and ANFIS controller. There are two control structures of hybrid PID ANFIS controller are proposed, such as summing hybrid and selecting hybrid which is the one employed in this study. This structure, where the controller action is divided into two regions. The output of PID controller is the main control signal and the output of ANFIS controller is the recovery control signal which is switched based on the value of three variabels to determine the selecting hybrid controller which are the specified error threshold(ΔE_{error}), PID control signal (U_{PID}) and ANFIS control signal (U_{ANFIS}). The error threshold can be determined by trial and error. The block diagram and decision making flowchart of hybrid PID–ANFIS controller is shown

in Figure 4.18.

$$U_{hybrid} = \begin{cases} U_{PID}, & \text{for } Error < \Delta E_{error} \\ U_{ANFIS}, & \text{for } Error \geq \Delta E_{error} \end{cases} \tag{4.17}$$

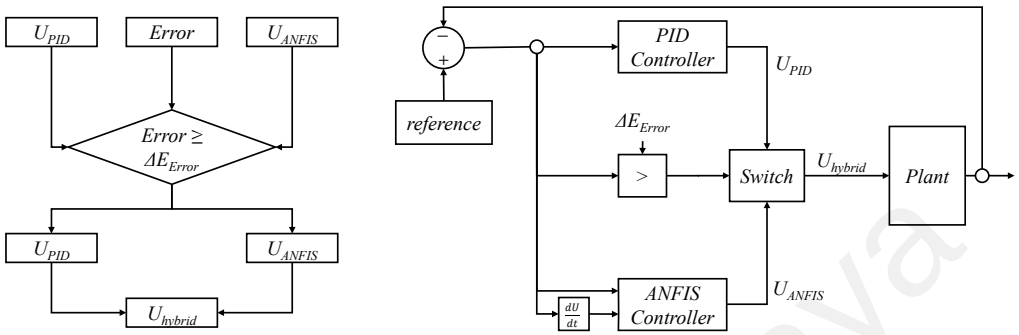

Figure 4.18: The flowchart and block diagram of summing hybrid PID–ANFIS controller

The result of this hybridization is illustrated in Figure 4.19. The main controller of this hybrid controller structure is the ANFIS controller and when the PID controller has passed its overshoot period, the controller switches to the PID to stick to the setpoint with no oscillations. This is made possible by setting a switching threshold of 0.2 degrees of error meaning the controller switches to the PID controller only after its error is less than this value.

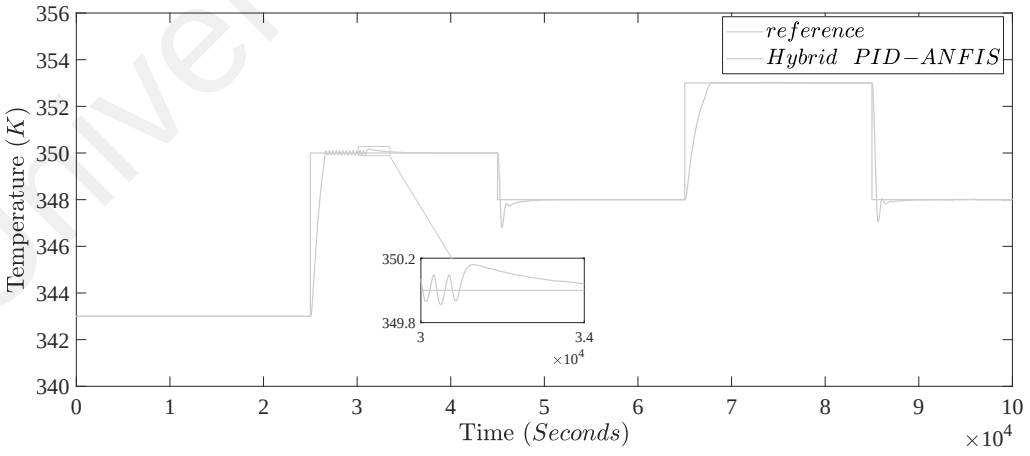

Figure 4.19: Temperature reference tracking using hybrid PID–ANFIS controller

Figure 4.20 shows the control moves for all three types of the temperature controllers. As can be seen, hybrid controller was again superior in performance since it greatly reduced

the oscillations. The cold-water valve opening and closing gradually takes place almost every 3 minutes within the oscillatory range which is acceptable for a control valve.

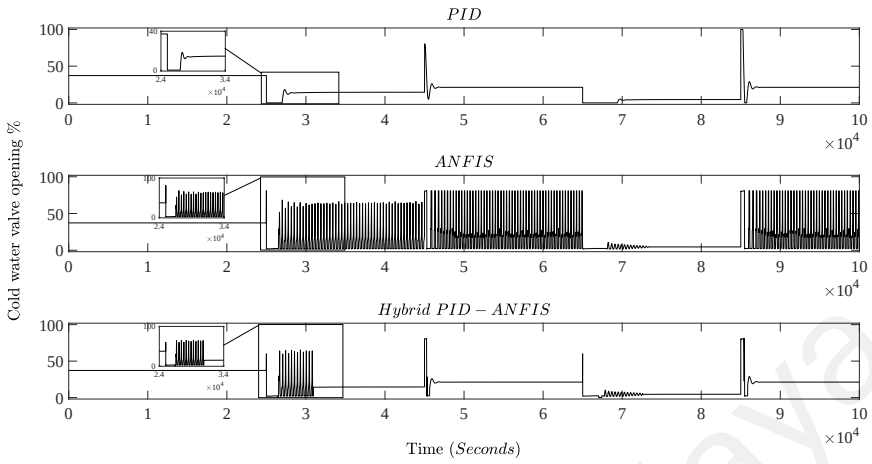

Figure 4.20: Controller moves in set point tracking of reactor temperature

4.8.3 Disturbance rejection

Several different step changes in the velocity of superficial gas was applied on the model to examine possible disturbances on the reactor temperature, as a key process parameter. The open-loop simulation result is shown in Figure 4.21. In this figure, after the reactor continues to work in steady state for a while, superficial gas velocity was altered with both additive and deductive increments which led to non-symmetrical responses. This figure suggests that superficial gas velocity has a significant effect on the reactor temperature. Furthermore, positive steps in the superficial gas velocity have less effect on the reactor temperature in comparison with equal negative steps. To put simply, the reactor temperature changes in a non-linear manner with the superficial gas velocity. With the demonstration of the nonlinear behavior, the conventional controllers lead to the process variables being poorly controlled. This justifies clearly the need to implement a more effective control system to control the superficial gas velocity effect on the process variable efficiently.

To examine the system response to superficial gas velocity disturbance, a high reduction of 50% in the process variable is introduced at 50000 seconds. The controller responses are given in Figure 4.22. Once again, PID was unable to mitigate the disturbance and

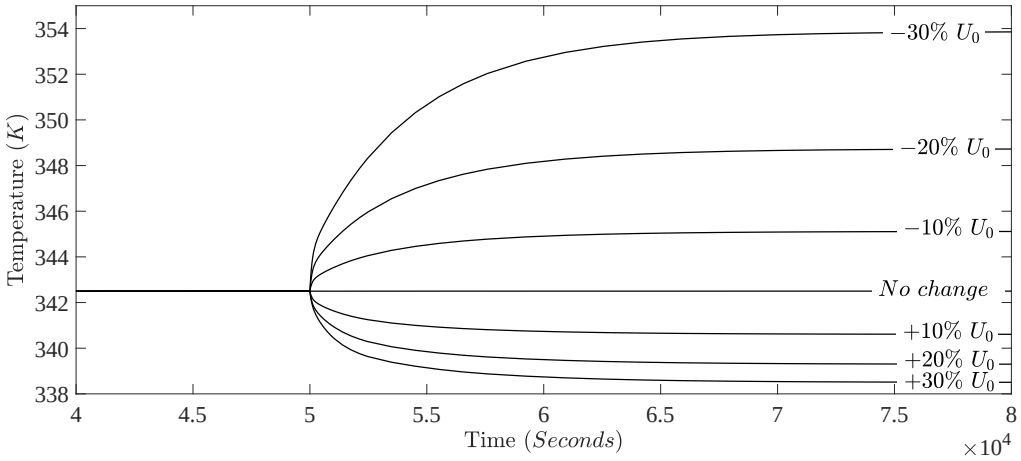

Figure 4.21: Effect of the superficial gas velocity step changes on the reactor temperature at 5×10^4 *s*

responded with an overshoot and a settling time of almost 3 hours. ANFIS controller starts to gradually diverge the oscillations from the set point with increase in the periods of oscillations. On the other hand, hybrid controller has successfully absorbed the effect of the disturbance and performed like a step change case where the ANFIS controller takes over right after the change and switches to the PID afterwards.

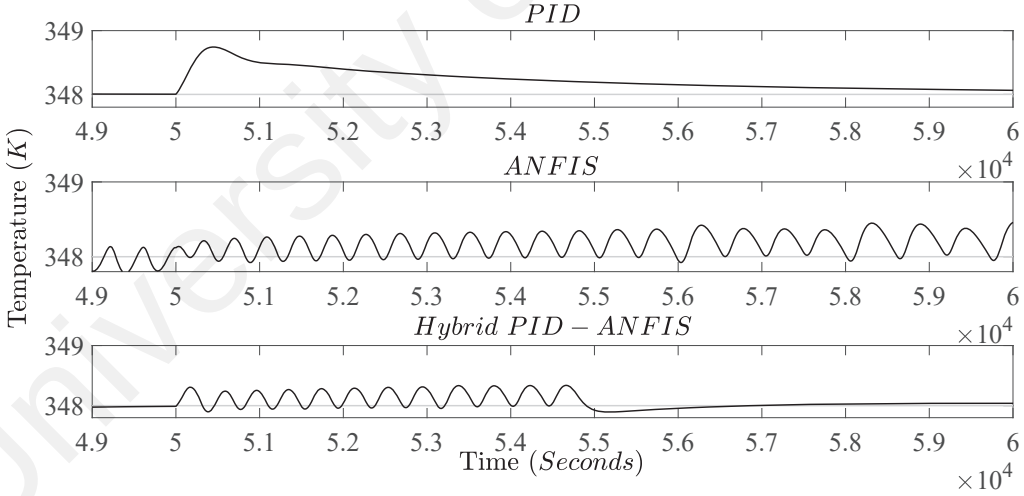

Figure 4.22: Performance comparison of the controllers in rejecting the effect of a 30% decrease in superficial gas velocity at 5×10^4 *s*.

Controller moves of temperature controllers are given in Figure 4.23. The same trend of control variable is seen here again. PID takes a lot of time to find the correct value, ANFIS starts to destabilize after the disturbance point and hybrid controller copes with the disturbance optimally and without getting affected.

Table 4.4 lists the calculated measures of the controlled system performance for different

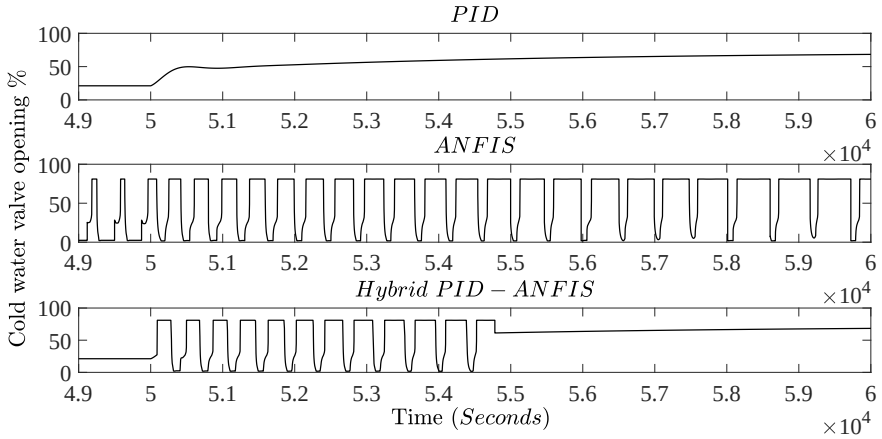

Figure 4.23: Controller moves in disturbance rejection for a 30% decrease in superficial gas velocity at 5×10^4 s.

temperature controller designs in both disturbance rejection and set-point tracking scenarios. The info shows the superiority of the hybrid controller in terms of performance compared to both PID and ANFIS alone since the ITAE, IAE, ISE and APE values for the hybrid controller prove to be the smallest in both disturbance rejection and set-point tracking studies.

Table 4.4: Performance indexes for temperature controllers

	Setpoint tracking			Disturbance rejection		
	PID	ANFIS	Hybrid	PID	ANFIS	Hybrid
ITAE	1.53×10^9	1.08×10^9	9.81×10^8	1.59×10^9	1.63×10^9	1.16×10^9
IAE	1.14×10^5	6.98×10^4	6.67×10^4	1.14×10^5	7.62×10^4	6.91×10^4
ISE	1.01×10^6	7.80×10^5	7.82×10^5	7.83×10^5	7.83×10^5	7.79×10^5
APE	3.31×10^2	2.03×10^2	1.93×10^2	3.34×10^1	2.21×10^2	2.01×10^2

4.9 Summary

The developed dynamic two–phase ethylene copolymerization model that was discussed in Chapter 3 was adopted to perform further control studies. Conventional controllers showed to exhibit unsatisfactory operations to control polymer MFI and reactor temperature by manipulating the hydrogen intake and cold water flow rate to the heat exchanger respectively in both set-point tracking and disturbance rejection scenarios. A right combination of AI-based controllers that can be used by industries were implemented

to address both the servo and regulatory control of the polymer MFI as a fundamental polymer property and reactor temperature as a very crucial process parameter. Based on the control performance indicators, results have shown that the ANFIS controller for MFI control and the hybrid PID–ANFIS controller for temperature control perform better with regard to the disturbance rejection and set point tracking in comparison with conventional methods. Results suggest that intelligent controllers are far easier to design and tune and their controlling capabilities are promising to be used in this highly nonlinear process and can benefit the industries by reducing the cost and waste and increasing the profits. Moreover, AI-based controllers can integrated well and easily within the industry 4.0 frameworks.

CHAPTER 5: CONCLUSION AND FUTURE WORKS

This study was aimed to develop modified two phase modeling for an ethylene polymerization fluidized–bed reactor and validate with the industrial data and also design and simulate an advanced process control system for the reactor. The main conclusions and observations for this project with recommendations for future works are as follows:

5.1 Conclusions

A comprehensive two–phase dynamic model to produce polyethylene in industrial catalytic gas phase fluidized–bed reactors was developed to describe the dynamics of the polyethylene production in FBRs. The hydrodynamics of the fluidized–bed reactor was based on the dynamic two–phase concept of fluidization. This hydrodynamic model was coupled with a two–site copolymerization (ethylene and 1-butene) kinetic model to provide a better understanding of the reactor performance. In this model, two types of active sites for the heterogeneous Ziegler–Natta catalyst were considered. In the improved two–phase model, polymerization reaction was considered to take place in both the bubble and emulsion phases to provide a more realistic understanding of the phenomena occurring in the bed. Besides, it was shown that the superficial gas velocity and reactant concentrations have a strong effect on the hydrodynamics and the reaction rate which results in a greater variation in the total production rate ratio.

The Polydispersity Index (PDI), Molecular Weight Distribution (MWD), production rate and reactor temperature results of the model were compared with actual plant data as well as the literature. To show the data agreement. A good agreement is observed between the model predictions and actual plant data which makes it a reliable simulation tool for further control studies. The validation outcome was that the model provides a tool to study the operational, hydrodynamics and kinetic parameters on reactor performance in addition to polymer properties, and can be used as a base for control studies.

Furthermore, the open loop simulation analysis revealed the strong dependency of the polyethylene fluidized–bed reactor behavior on the superficial gas velocity and feed concentrations and it was found that the process is highly sensitive and nonlinear, thus justifying the use of an advanced control algorithm for efficient control of the process

variables. Moreover, artificial intelligence based controllers have proven capabilities and are the focus of many research projects in academia and industry as they are an integral part to the industry 4.0 revolution. As a result, a right choice of advanced controllers based on artificial intelligence that can be used by industries were implemented to address both the servo and regulatory control of the polymer MFI as a fundamental polymer property and reactor temperature as a very crucial process parameter. Adaptive neuro-fuzzy inference system (ANFIS) which uses the advantage of both neural networks and fuzzy logic in one structure was chosen as the main type of controller. The hybrid PID–ANFIS controller was chosen as the second best option if the ANFIS was also unable to control the variable accurately.

The results showed that the set-point tracking of the conventional PID controller for controlling MFI had big settling time values and overshoots which are both drawbacks and should be avoided. On the other hand, the corresponding ANFIS controller was able to track changes in the MFI set-point smoothly and very fast. Similar behavior of the MFI controllers can be seen in disturbance rejection scenario as well. As for the temperature, PID or ANFIS controllers alone could not control properly. PID controller had unpleasant overshoots but did stable and stick to the set-point after a while. The ANFIS controller on the other hand had no huge overshoot and could stick to the set-point with small oscillations. In order to take advantage of the both controllers, a hybrid PID–ANFIS controller was designed to control the temperature. Similar trends was visible in the disturbance rejection study as well.

The advanced controllers were able not only to produce controller moves which were well within the specified input constraints for both profiles, but also the controller moves produced were non-aggressive and sufficiently smooth for practical implementations.

Performance indexes of ITAE, IAE, ISE and APE were used to quantify the performance of different controllers The values calculated for both variables in both set-point tracking and disturbance rejection scenarios showed that the performance of the advanced controllers were superior to the conventional PID controllers in these profiles.

To summarize, an improved fully dynamic two–phase ethylene and 1-butene copolymerization model with two–site kinetics was developed to predict the behavior of industrial

polyethylene production reactors and polymer properties. Particle elutriation was considered in order to take the losses of entrained catalyst and polymer particles from the fluidized–bed into account. Artificial Intelligence (AI) based controllers were applied on this system to control the parameters. An ANFIS controller for MFI and a hybrid ANFIS-PID controller for the reactor temperature were designed and proved to be capable of controlling these variables optimally. Applications in design, simulation, optimization and control studies are among the main future prospects of the developed strategy.

5.2 Future works

Based on the work done so far, the following recommendations for future work are suggested due to their importance in improving the modeling and process control of this polymerization reactor process.

- Considering condensed-mode cooling in the model to improve the prediction capabilities of the model and use the model to design more efficient cooling in the future.
- The kinetic mechanism can be fused with 3D CFD codes to make use of the recent powerful supercomputers to fully model the system.
- Different types of catalysts and co-catalyst can be tested to minimize operational expenses, increase plant safety and achieve optimum conditions to produce high quality production.
- Optimization studies can be done using the models to further improve the process and minimize waste and cost and maximize the production and profits.
- Model-based control can be used for this system in a way that the controller feedback helps to give a more precise and robust model.
- Other control strategies can be applied to the system such as advanced MIMO structures in which all the variables of the system are controlled using just one main controller.
- On-line optimization is a promising method and can be applied to the model linked to the pilot plant.

REFERENCES

Abonyi, J., Madar, J., & Szeifert, F. (2002). Combining First Principles Models and Neural Networks for Generic Model Control. In R. Roy, M. Köppen, S. Ovaska, T. Furuhashi, & F. Hoffmann (Eds.), *Soft computing and industry* (pp. 111–122). Springer London.

Abrahamsen, A. R., & Geldart, D. (1980). Behaviour of gas-fluidized beds of fine powders part II. voidage of the dense phase in bubbling beds. *Powder Technology*, *26*(1), 47–55.

Akbari, V., Borhani, T. N. G., Godini, H. R., & Hamid, M. K. A. (2014). Model-based analysis of the impact of the distributor on the hydrodynamic performance of industrial polydisperse gas phase fluidized bed polymerization reactors. *Powder Technology*, *267*, 398–411.

Akbari, V., Borhani, T. N. G., Shamiri, A., Aramesh, R., Hussain, M. A., & Hamid, M. K. A. (2015). 2D CFD-PBM simulation of hydrodynamic and particle growth in an industrial gas phase fluidized bed polymerization reactor. *Chemical Engineering Research and Design*, *104*, 53–67.

Akbari, V., Nejad Ghaffar Borhani, T., Aramesh, R., Hamid, M. K. A., Shamiri, A., & Hussain, M. A. (2015). Evaluation of hydrodynamic behavior of the perforated gas distributor of industrial gas phase polymerization reactor using CFD-PBM coupled model. *Computers & Chemical Engineering*, *82*, 344–361.

Akbari, V., Nejad Ghaffar Borhani, T., Shamiri, A., & Kamaruddin Abd. Hamid, M. (2015). A CFD–PBM coupled model of hydrodynamics and mixing/segregation in an industrial gas-phase polymerization reactor. *Chemical Engineering Research and Design*, *96*, 103–120.

Alb, A. M., & Reed, W. F. (2008). Recent Advances in Automatic Continuous Online Monitoring of Polymerization Reactions (ACOMP). *Macromolecular Symposia*, *271*(1), 15–25.

Alb, A. M., & Reed, W. F. (2010). Fundamental Measurements in Online Polymerization Reaction Monitoring and Control with a Focus on ACOMP. *Macromolecular Reaction Engineering*, *4*(8), 470–485.

Alexandridis, A. P., Siettos, C. I., Sarimveis, H. K., Boudouvis, A. G., & Bafas, G. V.

(2002). Modelling of nonlinear process dynamics using Kohonen's neural networks, fuzzy systems and Chebyshev series. *Computers & Chemical Engineering*, *26*(4), 479–486.

Ali, E., Al-Humaizi, K., & Ajbar, A. (2003). Multivariable Control of a Simulated Industrial Gas-Phase Polyethylene Reactor. *Industrial & Engineering Chemistry Research*, *42*(11), 2349–2364.

Ali, E. M., & Abasaeed, A. E. (1998). Optimization and Control of Industrial Gas-Phase Ethylene Polymerization Reactors. *Industrial & Engineering Chemistry Research*, *37*, 3414–3423.

Ali, E. M., & Abasaeed, A. E. (1999). Improved Regulatory Control of Industrial Gas-Phase Ethylene Polymerization Reactors. *Industrial and Engineering Chemistry Research*, *38*, 2383–2390.

Ali, E. M., & Ali, M. A.-h. (2010). Broadening the polyethylene molecular weight distribution by controlling the hydrogen concentration and catalyst feed rates. *ISA transactions*, *49*(1), 177–87.

Ali, M. A., Betlem, B., Weickert, G., & Roffel, B. (2007). Non-linear model based control of a propylene polymerization reactor. *Chemical Engineering and Processing: Process Intensification*, *46*(6), 554–564.

Alizadeh, A., Chmelař, J., Sharif, F., Ebrahimi, M., Kosek, J., & McKenna, T. F. L. (2017). Modeling Condensed Mode Operation for Ethylene Polymerization: Part I. Thermodynamics of Sorption. *Industrial & Engineering Chemistry Research*, *56*(5), 1168–1185.

Alizadeh, A., Namkajorn, M., Somsook, E., & McKenna, T. F. L. (2015). Condensed Mode Cooling for Ethylene Polymerization: Part II. The Effect of Different Condensable Comonomers and Hydrogen on Polymerization Rate. *Macromolecular Chemistry and Physics*, *216*(9), 985–995.

Alizadeh, M., Mostoufi, N., Pourmahdian, S., & Sotudeh-Gharebagh, R. (2004). Modeling of fluidized bed reactor of ethylene polymerization. *Chemical Engineering Journal*, *97*(1), 27–35.

Anwar, M., Azlan, M., & Mjalli, F. S. (2011). Control of polystyrene batch reactors using neural network based model predictive control (NNMPC): An experimental

investigation. *Control Engineering Practice*, *19*(5), 454–467.

Aoyagi, M., & Kunii, D. (1974). Importance of dispersed solids in bubbles for exothermic reactions in fluidized beds. *Chemical Engineering Communications*, *1*(4), 191–197.

Ashrafi, O., Nazari-pouya, H., & Mostoufi, N. (2008). Particle Size Distribution in Gas-phase Polyethylene Reactors. *Advanced Powder Technology*, *19*(4), 321–334.

ASTM. (2003). *Test method for melt flow rates of thermoplastics by extrusion plastometer. (d1238).* ASTM International.

Bequette, B. W. (1991). Nonlinear control of chemical processes: a review. *Industrial & Engineering Chemistry Research*, *30*(7), 1391–1413.

Biswas, P., & Samanta, A. N. (2013). Backstepping control of polymerization reactor. In *2013 9th asian control conference (ascc)* (pp. 1–5). IEEE.

Bolsoni, A., Lima, E. L., & Pinto, J. C. (2000). Advanced control of propylene polimerizations in slurry reactors. *Brazilian Journal of Chemical Engineering*, *17*(4-7), 565–574.

Braun, D., Cherdron, H., & Ritter, H. (2013). *Polymer Synthesis: Theory and Practice: Fundamentals, Methods, Experiments*. Springer Science & Business Media.

Brempt, W. V., Backx, T., Ludlage, J., Overschee, P. V., & Moor, B. D. (2001). A high performance model predictive controller : application on a polyethylene gas phase reactor. *Control Engineering Practice*, *9*, 829–835.

Campello, R. J. G. B., Von Zuben, F. J., Amaral, W. C., Meleiro, L. A. C., & Maciel Filho, R. (2003). Hierarchical fuzzy models within the framework of orthonormal basis functions and their application to bioprocess control. *Chemical Engineering Science*, *58*(18), 4259–4270.

Carlos E., G., David M., P., & Manfred, M. (1989). Model Predictive Control : Theory and Practice a Survey. *Automatica*, *25*(3), 335–338.

Causa, J., Karer, G., Núñez, A., Sáez, D., Škrjanc, I., & Zupančič, B. (2008). Hybrid fuzzy predictive control based on genetic algorithms for the temperature control of

a batch reactor. *Computers & Chemical Engineering*, *32*(12), 3254–3263.

Cerrada, M., Aguilar, J., Colina, E., & Titli, A. (2005). Dynamical membership functions: an approach for adaptive fuzzy modelling. *Fuzzy Sets and Systems*, *152*(3), 513–533.

Chatzidoukas, C., Perkins, J. D., Pistikopoulos, E. N., & Kiparissides, C. (2003). Optimal grade transition and selection of closed-loop controllers in a gas-phase olefin polymerization fluidized bed reactor. *Chemical Engineering Science*, *58*(16), 3643–3658.

Che, Y., Tian, Z., Liu, Z., Zhang, R., Gao, Y., Zou, E., ... Liu, B. (2015a). A CFD-PBM model considering ethylene polymerization for the flow behaviors and particle size distribution of polyethylene in a pilot-plant fluidized bed reactor. *Powder Technology*, *286*, 107–123.

Che, Y., Tian, Z., Liu, Z., Zhang, R., Gao, Y., Zou, E., ... Liu, B. (2015b). CFD prediction of scale-up effect on the hydrodynamic behaviors of a pilot-plant fluidized bed reactor and preliminary exploration of its application for non-pelletizing polyethylene process. *Powder Technology*, *278*, 94–110.

Che, Y., Tian, Z., Liu, Z., Zhang, R., Gao, Y., Zou, E., ... Liu, B. (2016). An Insight into the Temperature Field and Particle Flow Patterns in a Fluidized Bed Reactor for Nonpelletizing Polyethylene Process Using a 3D CFD-PBM Model. *Industrial & Engineering Chemistry Research*, *55*(30), 8258–8270.

Choi, K.-Y., & Ray, W. H. (1985). The dynamic behaviour of fluidized bed reactors for solid catalysed gas phase olefin polymerization. *Chemical Engineering Science*, *40*(12), 2261–2279.

Choi, K. Y., & Ray, W. H. (1988). The dynamic behavior of continuous stirred-bed reactors for the solid catalyzed gas phase polymerization of propylene. *Chemical Engineering Science*, *43*(10), 2587–2604.

Cui, H., Mostoufi, N., & Chaouki, J. (2000). Characterization of dynamic gas–solid distribution in fluidized beds. *Chemical Engineering Journal*, *79*(2), 133–143.

da Costa Sousa, J. M., & Kaymak, U. (2001). Model predictive control using fuzzy decision functions. *IEEE Transactions on Systems, Man, and Cybernetics, Part B (Cybernetics)*, *31*(1), 54–65.

Dadebo, S. A., Bell, M. L., McLellan, P. J., & McAuley, K. B. (1997). Temperature control of industrial gas phase polyethylene reactors. *Journal of Process Control*, *7*(2), 83–95.

de Carvalho, A. B., Gloor, P. E., & Hamielec, A. E. (1989). A kinetic mathematical model for heterogeneous Ziegler-Natta copolymerization. *Polymer*, *30*(2), 280–296.

Dompazis, G., Kanellopoulos, V., Touloupides, V., & Kiparissides, C. (2008). Development of a multi-scale, multi-phase, multi-zone dynamic model for the prediction of particle segregation in catalytic olefin polymerization FBRs. *Chemical Engineering Science*, *63*(19), 4735–4753.

Dougherty, D., & Cooper, D. (2003). A practical multiple model adaptive strategy for multivariable model predictive control. *Control Engineering Practice*, *11*(6), 649–664.

Fernandes, F. A. N., & Ferrareso Lona, L. M. (2001). Fluidized-bed reactor modeling for polyethylene production. *Journal of Applied Polymer Science*, *81*(2), 321–332.

Fernandes, F. A. N., & Lona, L. M. F. (2001). Heterogeneous modeling for fluidized-bed polymerization reactor. *Chemical Engineering Science*, *56*(3), 963–969.

Fernandes, F. A. N., & Lona Batista, L. M. F. (1999). Fluidized-bed reactor and physicalchemical properties modeling for polyethylene production. *Computers and Chemical Engineering*, *23*(SUPPL. 1), 803–806.

Floyd, S., Choi, K. Y., Taylor, T. W., & Ray, W. H. (1986). Polymerization of olefins through heterogeneous catalysis. III. polymer particle modelling with an analysis of intraparticle heat and mass transfer effects. *Journal of Applied Polymer Science*, *32*(1), 2935–2960.

Ghasem, N. M. (1999). Effect of Polymer Particle Size and Inlet Gas Temperature on Industrial Fluidized Bed Polyethylene Reactors. *Chemical Engineering & Technology*, *22*(9), 777.

Ghasem, N. M. (2000). Dynamic Behavior of Industrial Gas Phase Fluidized Bed Polyethylene Reactors under PI Control. *Chemical Engineering & Technology*, *23*(2), 133–140.

Ghasem, N. M. (2006). Design of a Fuzzy Logic Controller for Regulating the Temperature in Industrial Polyethylene Fluidized Bed Reactor. *Chemical Engineering Research and Design*, *84*(2), 97–106.

Gilbertson, M. A., & Yates, J. G. (1996). The motion of particles near a bubble in a gas-fluidized bed. *Journal of Fluid Mechanics*, *323*, 377–385.

Guiamba, I. R. F., & Mulholland, M. (2004). Adaptive Linear Dynamic Matrix Control applied to an integrating process. *Computers & Chemical Engineering*, *28*(12), 2621–2633.

Habbi, H., Zelmat, M., & Ould Bouamama, B. (2003). A dynamic fuzzy model for a drum-boiler-turbine system. *Automatica*, *39*(7), 1213–1219.

Harmon Ray, W., & Villa, C. M. (2000). Nonlinear dynamics found in polymerization processes — a review. *Chemical Engineering Science*, *55*(2), 275–290.

Harshe, Y. M., Utikar, R. P., & Ranade, V. V. (2004). A computational model for predicting particle size distribution and performance of fluidized bed polypropylene reactor. *Chemical Engineering Science*, *59*(22), 5145–5156.

Hassimi, A., Mostoufi, N., & Sotudeh-Gharebagh, R. (2009). Unsteady-State Modeling of the Fluidized Bed Polyethylene Reactor. *Iranian Journal of Chemical Engineering*, *6*(1), 23–39.

Hatzantonis, H., Yiannoulakis, H., Yiagopoulos, A., & Kiparissides, C. (2000). Recent developments in modeling gas-phase catalyzed olefin polymerization fluidized-bed reactors: The effect of bubble size variation on the reactor's performance. *Chemical Engineering Science*, *55*(16), 3237–3259.

Hillegardt, K., & Werther, J. (1986). Local bubble gas hold-up and expansion of gas/solid fluidized beds. *German chemical engineering*, *9*(4), 215–221.

Ho, Y. K., Shamiri, A., Mjalli, F. S., & Hussain, M. A. (2012). Control of industrial gas phase propylene polymerization in fluidized bed reactors. *Journal of Process Control*, *22*(6), 947–958.

Hutchinson, R. A., Chen, C. M., & Ray, W. H. (1992). Polymerization of olefins through heterogeneous catalysis X: Modeling of particle growth and morphology. *Journal*

of Applied Polymer Science, *44*(8), 1389–1414.

Ibrehem, A. S., Hussain, M. A., & Ghasem, N. M. (2008). Mathematical Model and Advanced Control for Gas-phase Olefin Polymerization in Fluidized-bed Catalytic Reactors. *Chinese Journal of Chemical Engineering*, *16*(1), 84–89.

Ibrehem, A. S., Hussain, M. A., & Ghasem, N. M. (2009). Modified mathematical model for gas phase olefin polymerization in fluidized-bed catalytic reactor. *Chemical Engineering Journal*, *149*(1-3), 353–362.

Immanuel, C. D., Cordeiro, C. F., Sundaram, S. S., Meadows, E. S., Crowley, T. J., & Doyle, F. J. (2002). Modeling of particle size distribution in emulsion co-polymerization: comparison with experimental data and parametric sensitivity studies. *Computers & Chemical Engineering*, *26*(7-8), 1133–1152.

Jafari, R., Sotudeh-Gharebagh, R., & Mostoufi, N. (2004). Modular simulation of fluidized bed reactors. *Chemical engineering & technology*, *27*(2), 123–129.

Jang, J.-S. R. (1993). ANFIS: adaptive-network-based fuzzy inference system. *IEEE Transactions on Systems, Man, and Cybernetics*, *23*(3), 665–685.

Jiang, Y., McAuley, K. B., & Hsu, J. C. C. (1997). Nonequilibrium modeling of condensed mode cooling of polyethylene reactors. *AIChE Journal*, *43*(1), 13–24.

Kammona, O., Chatzi, E. G., & Kiparissides, C. (1999). Recent Developments in Hardware Sensors For the On-Line Monitoring of Polymerization Reactions. *Journal of Macromolecular Science, Part C: Polymer Reviews*, *39*(1), 57–134.

Karer, G., Mušič, G., Škrjanc, I., & Zupančič, B. (2007). Hybrid fuzzy model-based predictive control of temperature in a batch reactor. *Computers & Chemical Engineering*, *31*(12), 1552–1564.

Kato, K., & Wen, C. Y. (1969). Bubble assemblage model for fluidized bed catalytic reactors. *Chemical Engineering Science*, *24*(8), 1351–1369.

Khan, M. J. H., Hussain, M., Mansourpour, Z., Mostoufi, N., Ghasem, N. M., & Abdullah, E. C. (2014). CFD simulation of fluidized bed reactors for polyolefin production – A review. *Journal of Industrial and Engineering Chemistry*.

Khang, D. Y., & Lee, H. H. (1997). Particle size distribution in fluidized beds for catalytic polymerization. *Chemical Engineering Science*, *52*(3), 421–431.

Khare, N. P., Lucas, B., Seavey, K. C., Liu, Y. A., Sirohi, A., Ramanathan, S., . . . Chen, C.-C. (2004). Steady-State and Dynamic Modeling of Gas-Phase Polypropylene Processes Using Stirred-Bed Reactors. *Industrial & Engineering Chemistry Research*, *43*(4), 884–900.

Kiashemshaki, A., Mostoufi, N., & Sotudeh-Gharebagh, R. (2006). Two-phase modeling of a gas phase polyethylene fluidized bed reactor. *Chemical Engineering Science*, *61*(12), 3997–4006.

Kiashemshaki, A., Mostoufi, N., Sotudeh-Gharebagh, R., & Pourmahdian, S. (2004). Reactor Modeling of Gas-Phase Polymerization of Ethylene. *Chemical Engineering & Technology*, *27*(11), 1227–1232.

Kiparissides, C. (1996). Polymerization reactor modeling: A review of recent developments and future directions. *Chemical Engineering Science*, *51*(10), 1637–1659.

Kissin, Y. V. (1985). Kinetics of olefin polymerization with heterogeneous Ziegler-Natta catalysts. In *Isospecific polymerization of olefins* (pp. 1–93). Springer Science + Business Media.

Kunii, D., & Levenspiel, O. (1991). *Fluidization Engineering*. Butterworth-Heinemann.

Lee, P. L., & Sullivan, G. R. (1988). Generic model control (GMC). *Computers & Chemical Engineering*, *12*(6), 573–580.

Lucas, A., Arnaldos, J., Casal, J., & Puigjaner, L. (1986). Improved equation for the calculation of minimum fluidization velocity. *Industrial & Engineering Chemistry Process Design and Development*, *25*(2), 426–429.

Luo, Z.-H., Su, P.-L., Shi, D.-P., & Zheng, Z.-W. (2009). Steady-state and dynamic modeling of commercial bulk polypropylene process of Hypol technology. *Chemical Engineering Journal*, *149*(1-3), 370–382.

Mahecha-Botero, A., Grace, J. R., Elnashaie, S. S. E. H., & Lim, C. J. (2009). Advances in modeling of fluidized-bed catalytic reactors: a comprehensive review. *Chemical Engineering Communications*, *196*(11), 1375–1405.

Makkawi, Y. T., & Wright, P. C. (2002). Fluidization regimes in a conventional fluidized bed characterized by means of electrical capacitance tomography. *Chemical Engineering Science*, *57*(13), 2411–2437.

Mamdani, E. (1974). Application of fuzzy algorithms for control of simple dynamic plant. *Proceedings of the Institution of Electrical Engineers*, *121*(12), 1585.

McAuley, K. B. (1993). *Modelling, estimation and control of product properties in a gas-phase polyethylene reactor* (Unpublished doctoral dissertation). McMaster University.

McAuley, K. B., Macdonald, D. A., & McLellan, P. J. (1995). Effects of operating conditions on stability of gas-phase polyethylene reactors. *AIChE Journal*, *41*(4), 868–879.

Mcauley, K. B., & Macgregor, F. (1993). Nonlinear Product Gas-Phase Property Control in Industrial Polyethylene Reactors. *AIChE Journal*, *39*(5).

McAuley, K. B., & MacGregor, J. F. (1992). Optimal grade transitions in a gas phase polyethylene reactor. *AIChE Journal*, *38*(10), 1564–1576.

McAuley, K. B., MacGregor, J. F., & Hamielec, A. E. (1990). A kinetic model for industrial gas-phase ethylene copolymerization. *AIChE Journal*, *36*(6), 837–850.

McAuley, K. B., Talbot, J. P., & Harris, T. J. (1994). A comparison of two-phase and well-mixed models for fluidized-bed polyethylene reactors. *Chemical Engineering Science*, *49*(13), 2035–2045.

McKenna, T. F., & Soares, J. B. P. (2001). Single particle modelling for olefin polymerization on supported catalysts: A review and proposals for future developments. *Chemical Engineering Science*, *56*(13), 3931–3949.

Mendonça, L. F., Sousa, J. M., & Sá da Costa, J. M. G. (2004). Optimization problems in multivariable fuzzy predictive control. *International Journal of Approximate Reasoning*, *36*(3), 199–221.

Mirzaei, A., Kiashemshaki, A., & Emami, M. (2007). Fluidized Bed Polyethylene Reactor Modeling in Condensed Mode Operation. *Macromolecular Symposia*, *259*(1), 135–144.

Mollov, S., van den Boom, T., Cuesta, F., Ollero, A., & Babuska, R. (2002). Robust stability constraints for fuzzy model predictive control. *IEEE Transactions on Fuzzy Systems*, *10*(1), 50–64.

Mostoufi, N., Cui, H., & Chaouki, J. (2001). A comparison of two-and single-phase models for fluidized-bed reactors. *Industrial & engineering chemistry research*, *40*(23), 5526–5532.

Namkajorn, M., Alizadeh, A., Somsook, E., & McKenna, T. F. L. (2014). Condensed-Mode Cooling for Ethylene Polymerization: The Influence of Inert Condensing Agent on the Polymerization Rate. *Macromolecular Chemistry and Physics*, *215*(9), 873–878.

Nascimento Lima, N. M., Manenti, F., Filho, R. M., Embiruçu, M., & Wolf Maciel, M. R. (2009). Fuzzy model-based predictive hybrid control of polymerization processes. *Industrial & Engineering Chemistry Research*, *48*(18), 8542–8550.

Noor, R. a. M., Ahmad, Z., Don, M. M., & Uzir, M. H. (2010). Modelling and control of different types of polymerization processes using neural networks technique: A review. *The Canadian Journal of Chemical Engineering*, *88*(6), 1065–1084.

Özkan, G., Özen, S., Erdoğan, S., Hapoğlu, H., & Alpbaz, M. (2001). Nonlinear control of polymerization reactor. *Computers & chemical engineering*, *25*(4), 757–763.

Pan, H., Liang, X.-F., Zhu, L.-T., & Luo, Z.-H. (2017). Importance Analysis of Liquid Vaporization Modeling Scheme in CFD Modeling of Gas-Liquid-Solid Polyethylene FBR. *Industrial & Engineering Chemistry Research*, *56*.

Park, M.-J., & Rhee, H.-K. (2003). Property evaluation and control in a semibatch MMA/MA solution copolymerization reactor. *Chemical Engineering Science*, *58*(3), 603–611.

Philippsen, C. G., Vilela, A. C. F., & Zen, L. D. (2015). Fluidized bed modeling applied to the analysis of processes: review and state of the art. *Journal of Materials Research and Technology*, *4*(2), 208–216.

Qin, S. J., & Badgwell, T. A. (2003). A survey of industrial model predictive control technology. *Control Engineering Practice*, *11*(7), 733–764.

Ramaswamy, S., Cutright, T. J., & Qammar, H. K. (2005). Control of a continuous bioreactor using model predictive control. *Process Biochemistry*, *40*(8), 2763–2770.

Ray, W. H. (1991). Modelling of addition polymerization processes -free radical, ionic, group transfer, and ziegler-natta kinetics. *Canadian Journal of Chemical Engineering*, *69*(3), 626–629.

Reed, W. (2004). Feature Article: Automatic Continuous Online Monitoring of Polymerization Reactions (ACOMP). *Polymer News*, *29*(9), 271–279.

Rhodes, M. (2008). *Introduction to Particle Technology*. John Wiley & Sons Ltd.

Roubos, J. A., Mollov, S., Babuška, R., & Verbruggen, H. B. (1999). Fuzzy model-based predictive control using Takagi–Sugeno models. *International Journal of Approximate Reasoning*, *22*(1-2), 3–30.

Salau, N. P. G., Neumann, G. A., Trierweiler, J. O., & Secchi, A. R. (2008). Dynamic Behavior and Control in an Industrial Fluidized-Bed Polymerization Reactor. *Industrial & Engineering Chemistry Research*, *47*(16), 6058–6069.

Santos, L. O., Afonso, P. A. F. N. A., Castro, J. A. A. M., Oliveira, N. M. C., & Biegler, L. T. (2001). On-line implementation of nonlinear MPC: an experimental case study. *Control Engineering Practice*, *9*(8), 847–857.

Sarimveis, H., & Bafas, G. (2003). Fuzzy model predictive control of non-linear processes using genetic algorithms. *Fuzzy Sets and Systems*, *139*(1), 59–80.

Sarvaramini, A., Mostoufi, N., & Sotudeh-Gharebagh, R. (2008). Influence of hydrodynamic models on dynamic response of the fluidized bed polyethylene reactor. *International Journal of Chemical Reactor Engineering*, *6*(1).

Sato, C., Ohtani, T., & Nishitani, H. (2000). Modeling, simulation and nonlinear control of a gas-phase polymerization process. *Computers & Chemical Engineering*, *24*(2-7), 945–951.

Schneiderbauer, S., Haider, M. F., Hauzenberger, F., & Pirker, S. (2016). A Lagrangian-Eulerian hybrid model for the simulation of industrial-scale gas-solid cyclones. *Powder Technology*, *304*, 229–240.

Schneiderbauer, S., Puttinger, S., Pirker, S., Aguayo, P., & Kanellopoulos, V. (2015). CFD modeling and simulation of industrial scale olefin polymerization fluidized bed reactors. *Chemical Engineering Journal*, *264*, 99–112.

Schnelle, P. D., & Rollins, D. L. (1997). Industrial model predictive control technology as applied to continuous polymerization processes. *ISA Transactions*, *36*(4), 281–292.

Seborg, D., Edgar, T., Mellichamp, D., & Doyle, F. (2016). *Process dynamics and control, 4th edition*. Wiley.

Sederman, A. J., Gladden, L. F., & Mantle, M. D. (2007). Application of magnetic resonance imaging techniques to particulate systems. *Advanced Powder Technology*, *18*(1), 23–38.

Seki, H., Ogawa, M., Ooyama, S., Akamatsu, K., Ohshima, M., & Yang, W. (2001). Industrial application of a nonlinear model predictive control to polymerization reactors. *Control Engineering Practice*, *9*(8), 819–828.

Shamiri, A., Chakrabarti, M., Jahan, S., Hussain, M. A., Kaminsky, W., Aravind, P., & Yehye, W. (2014). The Influence of Ziegler-Natta and Metallocene Catalysts on Polyolefin Structure, Properties, and Processing Ability. *Materials*, *7*(7), 5069–5108.

Shamiri, A., Hussain, M. A., Mjalli, F. S., & Mostoufi, N. (2010). Kinetic modeling of propylene homopolymerization in a gas-phase fluidized-bed reactor. *Chemical Engineering Journal*, *161*(1), 240–249.

Shamiri, A., Hussain, M. A., Mjalli, F. S., & Mostoufi, N. (2012). Improved single phase modeling of propylene polymerization in a fluidized bed reactor. *Computers & chemical engineering*, *36*, 35–47.

Shamiri, A., Hussain, M. A., Mjalli, F. S., Shafeeyan, M. S., & Mostoufi, N. (2014). Experimental and Modeling Analysis of Propylene Polymerization in a Pilot-Scale Fluidized Bed Reactor. *Industrial & Engineering Chemistry Research*, *53*(21), 8694–8705.

Shamiri, A., Hussain, M. A., Mjallic, F. S., & Mostoufid, N. (2013). Comparative simulation study of gas-phase propylene polymerization in fluidized bed reactors using aspen polymers and two phase models. *Chemical Industry and Chemical Engineering Quarterly*, *19*(1), 13–24.

Shamiri, A., Hussain, M. A., Sabri Mjalli, F., Mostoufi, N., & Saleh Shafeeyan, M. (2011). Dynamic modeling of gas phase propylene homopolymerization in fluidized bed reactors. *Chemical Engineering Science*, *66*(6), 1189–1199.

Shamiri, A., Hussain, M. A., sabri Mjalli, F., Mostoufi, N., & Hajimolana, S. (2013). Dynamics and Predictive Control of Gas Phase Propylene Polymerization in Fluidized Bed Reactors. *Chinese Journal of Chemical Engineering*, *21*(9), 1015–1029.

Shamiri, A., Wei, S., Fauzi, M., Hussain, M. A., & Mostoufi, N. (2015). Modified two-phase model with hybrid control for gas phase propylene copolymerization in fluidized bed reactors. *Chemical Engineering Journal*, *264*, 706–719.

Shenoy, a. V., & Saini, D. R. (1986). Melt flow index: More than just a quality control rheological parameter. Part I. *Advances in Polymer Technology*, *6*(1), 1–58.

Signal, P. D., & Lee, P. L. (1992). Generic model adaptive control. *Chemical Engineering Communications*, *115*(1), 35–52.

Soares, J. B. P. (2001). Mathematical modelling of the microstructure of polyolefins made by coordination polymerization: a review. *Chemical Engineering Science*, *56*(13), 4131–4153.

Soares, J. B. P., & McKenna, T. F. L. (2012). *Polyolefin Reaction Engineering*. Weinheim, Germany: Wiley-VCH Verlag GmbH & Co. KGaA.

Sugeno, M. (1985). *Industrial applications of fuzzy control*. North-Holland.

Tamadondar, M. R., Azizpour, H., Zarghami, R., Mostoufi, N., & Chaouki, J. (2012). Using particle trajectory for determining the fluidization regime in gas–solid fluidized beds. *Advanced Powder Technology*, *23*(3), 349–351.

The Freedonia Group. (2014). *World Polyethylene; Industry Study with Forecasts for 2018 & 2023* (Tech. Rep.). Cleveland: The Freedonia Group.

Vahidi, O., Shahrokhi, M., & Mirzaei, A. (2008). Control of a fluidized bed polyethylene reactor. *Iranian Journal of Chemistry and Chemical Engineering*, *27*(3), 87–101.

Xie, T., McAuley, K. B., Hsu, J. C. C., & Bacon, D. W. (1994). Gas Phase Ethylene Polymerization: Production Processes, Polymer Properties, and Reactor Modeling. *Industrial & Engineering Chemistry Research*, *33*(3), 449–479.

Yan, W.-C., Luo, Z.-H., Lu, Y.-H., & Chen, X.-D. (2012). A CFD-PBM-PMLM integrated model for the gas-solid flow fields in fluidized bed polymerization reactors. *AIChE Journal*, *58*(6), 1717–1732.

Yang, Y. R., Yang, J. Q., Chen, W., & Rong, S. X. (2002). Instability Analysis of the Fluidized Bed for Ethylene Polymerization with Condensed Mode Operation. *Industrial & Engineering Chemistry Research*, *41*(10), 2579–2584.

Zacca, J. J., Debling, J. A., & Ray, W. H. (1996). Reactor residence time distribution effects on the multistage polymerization of olefins—I. Basic principles and illustrative examples, polypropylene. *Chemical Engineering Science*, *51*(21), 4859–4886.

Zadeh, L. (1965). Fuzzy sets. *Information and Control*, *8*(3), 338–353.

Zheng, Z.-W., Shi, D.-P., Su, P.-L., Luo, Z.-H., & Li, X.-J. (2011). Steady-State and Dynamic Modeling of the Basell Multireactor Olefin Polymerization Process. *Industrial & Engineering Chemistry Research*, *50*(1), 322–331.

Zhou, Y.-f., Wang, J.-d., Yang, Y.-r., & Wu, W.-q. (2013). Modeling of the Temperature Profile in an Ethylene Polymerization Fluidized-Bed Reactor in Condensed-Mode Operation. *Industrial & Engineering Chemistry Research*, *52*(12), 4455–4464.

Ziegler, J. G., & Nichols, N. B. (1993). Optimum settings for automatic controllers. *Journal of Dynamic Systems, Measurement, and Control*, *115*(2B), 220.

LIST OF PUBLICATIONS AND PAPERS PRESENTED

Journal Articles

Abbasi, M. R., Shamiri, A., & Hussain, M. A. (2016). Dynamic modeling and Molecular Weight Distribution of ethylene copolymerization in an industrial gas-phase Fluidized-Bed Reactor. *Advanced Powder Technology*, *27*(4), 1526–1538. doi: 10.1016/j.apt.2016.05.014

Abbasi, M. R., Shamiri, A., & Hussain, M. A. (2018). A review on modeling and control of olefin polymerization in fluidized-bed reactors. *Reviews in Chemical Engineering*. doi: 10.1515/revce-2017-0040

Abbasi, M. R., Shamiri, A., Hussain, M. A., & Aghay Kaboli, S. H. (2018). Dynamic process modeling and hybrid intelligent control of ethylene copolymerization in Gas-phase catalytic fluidized-bed reactors. *Journal of Chemical Technology and Biotechnology (under review)*.

Conference Proceedings

Abbasi, M. R., Shamiri, A., & Hussain, M. A. (2016). Improved dynamic model for ethylene co-polymerization in industrial gas phase fluidized bed reactors. In *International conference on chemical engineering*. Phoenix, USA. doi: 10.4172/2157-7048.C1.003

Abbasi, M. R., Shamiri, A., & Hussain, M. A. (2017). Improved dynamic model and process control for ethylene co-polymerization in industrial gas-phase fluidized-bed reactors. In *10th world congress of chemical engineering*. Barcelona , Spain.

Abbasi, M. R., Shamiri, A., Hussain, M. A., & Aghay Kaboli, S. H. (2018). Hybrid intelligent control of ethylene copolymerization in gas-phase catalytic fluidized-bed reactors. In *25th regional symposium on chemical engineering*. Manila,Philippines.

APPENDIX A: MATLAB® CODES FOR THE MODELING OF ETHYLENE COPOLYMERIZATION IN THE FLUIDIZED-BED REACTOR

```
function dx=reza_LL0209(t,p,Input);
global CM_e CM_b C_cocat ro CMT_e CMT_b Fin1_e Fin2_e Fin1_b Fin2_b
    epsilon_mf CN22_e
global epsilon_e epsilon_b Delta C_cocat_e C_cocat_b CH2_e CH2_b H Dt
    U0 U_mf
global kp11 kp12 kp21 kp22 VR Vp_e Vp_b mw R_e1 R_e2 R_b1 R_b2 Rv_e
    Rv_b Ncat1_e Ncat2_e
global khT kp1T kp2T kpTT kfsT kiT kfm1T kfm2T CN11_e CN11_b VR_b VR_e
     kf N0ini1_e N0ini2_e
global kpT1 kpT2 kfhT kfrT kfmT1 kfmT2 kfmTT ki1 ki2 kh1 kh2 khr kfm11
     kfm12 kfm21 ...
          kfm22 cm CM
global Delta Dt gi At U0 kfh1 kfh2 kfr1 kfr2 kfs1 kfs2 kds kdI ka
    CNH1_e CNH2_e CN12_e...
          CN21_e Rv_e Rv_b
global CNH1_b CNH2_b CN12_b CN21_b CN22_b N0ini1_b N0ini2_b Ncat1_b
    Ncat2_b VR1 ...
          ttt R1_e R2_e RH_e R1_b R2_b RH_b
global epsilon_e epsilon_b Delta C_cocat_e C_cocat_b H Dt U0 Rv_e Rv_b
global Delta Dt gi At U0 K_be V_b V_e Rp_e Rp_b
global epsilon_e epsilon_b Delta CM CH2 CN2 H Dt U_e A_e U_b A_b
global R1_e R1_b RH_e RH_b Rv_e Rv_b n R1_e R2_e RH_e R1_b R2_b RH_b
    CH2 CM Im
global Delta Dt gi At U0 Tin Tref Vpe Vpb Hr_m Cp_pol cm mx
global a11 a12 a13 b11 b12 c11 c12 c13 e11 e12 e13
global d11 d12 d13 f11 f12 a21 a22 a23 b21 b22 c21 c22 c23 d21 d22 d23
     e21 e22 e23 f21 f22

Tin= Input(1);
%Tin=input(' Inlet Temperature (Centigerad):  ');
%Tin=44;
%Tin=Tin+273.15;
%T=input(' Reactor Temperature (Centigerad): ');
U0= Input(2);
Cat_in= Input(3); %mole/day
PC2=Input(4);
PC4=Input(5);
PH2=Input(6);
%Press=input('presure(bara):');
Press=Input(7);
%dp=input(' Average Particle Size(microns): ')*1e-6;
dp=Input(8);
%CH2= Input(3);
%CM(1)= Input(4)
%CM(2)= Input(5)
```

```
T=72;
ro=920; %Density of Polyethylene (kg/m^3)
ro_s=920; %solid density(kg/m3) for hydrodynamic calculation
miu_g=1.14e-4; %gas viscosity(pa.s) for hydrodynamic calculation
fi=1; %shape factor of particles for hydrodynamic calculation
H=14.5; %Bed Height(m)
Dt=4.8; %diameter of reactor(m) for hydrodynamic calculation
At=(pi*Dt^2)/4;
VR=At*H;
%U0=input(' Superficial Gas Velocity(m/s): ');
%U0=.57;

%PC2=input(' PC2(bar): ');
%PC2=8;
%PC4C2=input(' PC4/PC2(ratio): ');
%PC4=.25;
%PH2C3=input(' PH2/PC2(ratio): ');
%PH2=.225;
PN2=Press-PC2*(1+PH2+PC4);
yC2H4=(PC2)/Press;
yC4H8=(PC4)*(yC2H4);
yH2=(PH2)*(yC2H4);
yN2=1-(yC2H4+yH2+yC4H8);
mwC4H8=56;
mwC2H4=28;
mwH2=2;
mwN2=28;
mwTi=47.9;
%Average molecular weight of inlet gas
mw_avg=yC2H4*mwC2H4+yC4H8*mwC4H8+yH2*mwH2+yN2*mwN2;
R=0.08311665; %m3.bar/kmol.k
T=T+273; %reaction temperature(k)
Z=.90; %Z factor
%o_g0=(Press*mw_avg)/(Z*Tin*R); %Inlet Gas Density(kg/m^3);
%ro_g=ro_g0*Tin/T %Gas Density @ T(kg/m^3);
ro_g=23.45;
Cg=Press/(T*Z*.08314); %total inlet gas(gmol/lit) or (kmol/m3)
CM(1)=yC2H4*Cg; %Ethylene Concentration(mol/lit)
CM(2)=yC4H8*Cg; %1-Butene Concentration(mol/lit)
CH2=yH2*Cg; %Hydrogen Concentration(mol/lit)
CN2=yN2*Cg; %Nitrogen Concentration(mol/lit)
%CH2=.082;
%CM1=1.267%yC3H6*Cg; %Ethylene Concentration(mol/lit)
%CM2=.8%yC2H4*Cg; %1-Butene Concentration(mol/lit)
%CM1=.3767;
%CM2=.1649;
%CM1_0=CM1;
%CM2_0=CM2;
%CH2_0=CH2;
CMT=CM(1)+CM(2);
```

```
f1=CM(1)/CMT; %Fraction of Monomer Type 1 in Total Monomer
f2=CM(2)/CMT; %Fraction of Monomer Type 2 in Total Monomer
gi=9.81; %Garavity Accelaration(m/s^2)
Ar=(ro_g*(ro_s-ro_g)*gi*dp^3)/miu_g^2; %Arashmides Number
Re_mf=sqrt((29.5)^2+.0357*Ar)-29.5 ; %Lucas
%Re_mf=sqrt((27.2)^2+.0408*Ar)-27.2 ; %Grace
%Re_mf=sqrt((25.3)^2+.0651*Ar)-27.2 ; %Babu
%Re_mf=sqrt((33.7)^2+.0408*Ar)-27.2 ; %Wen & Yu
%Re_mf=sqrt((25.7)^2+.0365*Ar)-27.2 ; %Richardson
epsilon_mf=.45;%.586*fi^(-.72)*Ar^(-.029)*(ro_g/ro_s)^.021; %Bed
    Voidage at Minimum Fluidization
U_mf=Re_mf*miu_g/(dp*ro_g);
Vg=U0*At; %Total Inlet Gas(m^3/s)
Ng=Vg*3600; %Total Inlet Gas(m^3/hr)
%Cat_in=549.888; %mole/day ;%input(' Catalyst_Concentration(mol/day):
    ');
%Al_ratio=input(' Al/Ti: ');
Al_ratio=1.05;
Cat_in=Cat_in/24; %mol/hr
%Fin=Cat_in/Ng; %mol/lit
Fin=Cat_in/Ng; %mol/lit
C_cocat=Fin*Al_ratio; %Input Concentration of CoCatalyst(mol/lit)
%Assume That the Distribution Ratio Between Two Type of Sites is 3:2
Fin1=.6*Fin;
Fin2=.4*Fin;
%Hydrodynamic Relationships
epsilon_b=1-.146*exp(-(U0-U_mf)/4.439);
epsilon_e=epsilon_mf+.2-.059*exp(-(U0-U_mf)/.429);
Delta=.534-.534*exp(-(U0-U_mf)/.413);
CM_e(1)=CM(1);
CM_e(2)=CM(2);
CMT_e=CM_e(1)+CM_e(2);
CM_b(1)=CM(1);
CM_b(2)=CM(2);
CMT_b=CM_b(1)+CM_b(2);
CH2_e=CH2;
CH2_b=CH2;
%Fin1_e=Fin1;
%Fin2_e=Fin2;
%Fin1_b=Fin1;
%Fin2_b=Fin2;
%C_cocat_e=C_cocat;
%C_cocat_b=C_cocat;
Fin1_e=Fin1;%.88*Fin1;
Fin2_e=Fin2;%.88*Fin2;
Fin1_b=Fin1;%.12*Fin1;
Fin2_b=Fin2;%.12*Fin2;
C_cocat_e=C_cocat;%.88*C_cocat;
C_cocat_b=C_cocat;%.12*C_cocat;
Ea1=9000; %activation energy(cal/mol)
```

```
Ea2=8000; %activation energy(cal/mol)
Rg=1.987; %general gases constant(cal/mol.k)
Tref1=353.15; %refrence temperature(k)
Tref=353.15;
%% pseudokinetic rate constant calculation step
%% Formation rate constant(s^-1)
kf(1)=1;%mcualy
kf(2)=1;%mcualy
%% Initiation rate constant(L/mol.s)
ki1(1)=1; %9.8;%khare
ki1(2)=1; %9.8;%khare
ki2(1)=0.14; %14.6;%khare
ki2(2)=0.14; %14.6;%khare
kh1(1)=1;%mcualy
kh1(2)=1;%mcualy
kh2(1)=.1;%mcualy
kh2(2)=.1;%mcualy
khr(1)=20;%mcualy
khr(2)=20;%mcualy
%% Transfer rate constant(L/mol.s)
beta1=1.3;
beta2=1.8;
kfm110(1)=0.0021; %0.006;%.0021;%*beta1;khare
kfm110(2)=0.0021; %0.006;%.0021;%*beta2;khare
kfm120(1)=0.006; %0.0021;%.006;%*beta1; khare
kfm120(2)=0.11; %0.0021;%.11;%*beta2; khare
kfm210(1)=0.0021; %0.006;%.0021;%*beta1; khare
kfm210(2)=0.001; %0.006;%.001;%*beta2;khare
kfm220(1)=0.006; %.0021;%.006;%*beta1;khare
kfm220(2)=0.11; %.0021;%.11;%*beta2;khare
kfh10(1)=.088*beta1; %khare
kfh10(2)=.37*beta2; %khare
kfh20(1)=.088*beta1; %khare
kfh20(2)=.37*beta2; %khare
kfr10(1)=.024;%*beta1;%mcualy
kfr10(2)=.12;%*beta2;%mcualy
kfr20(1)=.048;%*beta1;%mcualy
kfr20(2)=.24;%*beta2;%mcualy
kfs10(1)=.0001;%*beta1;%mcualy
kfs10(2)=.0001;%*beta2; %mcualy
kfs20(1)=.0001;%*beta1; %mcualy
kfs20(2)=.0001;%*beta2;%mcualy
%% Deactivation rate constant
kds(1)=.0001;%mcualy
kds(2)=.0001; %mcualy
kdI(1)=2000;
kdI(2)=2000;
Im=0;
%Impurity Deactivation(s^-1)
ka(1)=.0003;
```

```
ka(2)=.0003;
%% Propagation rate constant(L/mol.s)
alpha=1;
kp110(1)=85*alpha; %khare
kp110(2)=85*alpha; %khare
kp120(1)=2*alpha; %khare
kp120(2)=15*alpha; %khare
kp210(1)=64*alpha; %khare
kp210(2)=64*alpha; %khare
kp220(1)=1.5*alpha; %khare
kp220(2)=6.2*alpha; %khare
%% input propagation rate constant(L/mol.s) for various Temperature
kp11(1)=kp110(1)*exp(-Ea1*((1/T)-(1/Tref1))/Rg);
kp11(2)=kp110(2)*exp(-Ea1*((1/T)-(1/Tref1))/Rg);
kp12(1)=kp120(1)*exp(-Ea1*((1/T)-(1/Tref1))/Rg);  % propgation rate
    constant for
kp12(2)=kp120(2)*exp(-Ea1*((1/T)-(1/Tref1))/Rg); % a site of type j(1
    or 2)
kp21(1)=kp210(1)*exp(-Ea1*((1/T)-(1/Tref1))/Rg); % with terminal
    monomer 1 or
kp21(2)=kp210(2)*exp(-Ea1*((1/T)-(1/Tref1))/Rg); % 2(Ethylene or
    Butene) reacting
kp22(1)=kp220(1)*exp(-Ea1*((1/T)-(1/Tref1))/Rg); % withmonomer 1 or 2
kp22(2)=kp220(2)*exp(-Ea1*((1/T)-(1/Tref1))/Rg); % (Ethylene or Butene)

%% input transfer rate constant(L/mol.s) for various Temperature
kfm11(1)=kfm110(1)*exp(-Ea2*((1/T)-(1/Tref1))/Rg);
kfm11(2)=kfm110(2)*exp(-Ea2*((1/T)-(1/Tref1))/Rg);
kfm12(1)=kfm120(1)*exp(-Ea2*((1/T)-(1/Tref1))/Rg);
kfm12(2)=kfm120(2)*exp(-Ea2*((1/T)-(1/Tref1))/Rg);
kfm21(1)=kfm210(1)*exp(-Ea2*((1/T)-(1/Tref1))/Rg);
kfm21(2)=kfm210(2)*exp(-Ea2*((1/T)-(1/Tref1))/Rg);
kfm22(1)=kfm220(1)*exp(-Ea2*((1/T)-(1/Tref1))/Rg);
kfm22(2)=kfm220(2)*exp(-Ea2*((1/T)-(1/Tref1))/Rg);
kfh1(1)=kfh10(1)*exp(-Ea2*((1/T)-(1/Tref1))/Rg);
kfh1(2)=kfh10(2)*exp(-Ea2*((1/T)-(1/Tref1))/Rg);
kfh2(1)=kfh20(1)*exp(-Ea2*((1/T)-(1/Tref1))/Rg);
kfh2(2)=kfh20(2)*exp(-Ea2*((1/T)-(1/Tref1))/Rg);
kfr1(1)=kfr10(1)*exp(-Ea2*((1/T)-(1/Tref1))/Rg);
kfr1(2)=kfr10(2)*exp(-Ea2*((1/T)-(1/Tref1))/Rg);
kfr2(1)=kfr20(1)*exp(-Ea2*((1/T)-(1/Tref1))/Rg);
kfr2(2)=kfr20(2)*exp(-Ea2*((1/T)-(1/Tref1))/Rg);
kfs1(1)=kfs10(1)*exp(-Ea2*((1/T)-(1/Tref1))/Rg);
kfs1(2)=kfs10(2)*exp(-Ea2*((1/T)-(1/Tref1))/Rg);
kfs2(1)=kfs20(1)*exp(-Ea2*((1/T)-(1/Tref1))/Rg);
kfs2(2)=kfs20(2)*exp(-Ea2*((1/T)-(1/Tref1))/Rg);
% %% input propagation rate constant(L/mol.s) for various Temperature
% kp11(1)=kp110(1);%*exp(-Ea1*((1/T)-(1/Tref1))/Rg);
% kp11(2)=kp110(2);%*exp(-Ea1*((1/T)-(1/Tref1))/Rg);
% kp12(1)=kp120(1);%*exp(-Ea1*((1/T)-(1/Tref1))/Rg);  % propgation
```

```
    rate constant for
% kp12(2)=kp120(2);%*exp(-Ea1*((1/T)-(1/Tref1))/Rg); % a site of type
    j(1 or 2)
% kp21(1)=kp210(1);%*exp(-Ea1*((1/T)-(1/Tref1))/Rg); % with terminal
    monomer 1 or
% kp21(2)=kp210(2);%*exp(-Ea1*((1/T)-(1/Tref1))/Rg); % 2(Ethylene or
    Butene) reacting
% kp22(1)=kp220(1);%*exp(-Ea1*((1/T)-(1/Tref1))/Rg); % withmonomer 1
    or 2
% kp22(2)=kp220(2);%*exp(-Ea1*((1/T)-(1/Tref1))/Rg); % (Ethylene or
    Butene)
% %% input transfer rate constant(L/mol.s) for various Temperature
% kfm11(1)=kfm110(1);%*exp(-Ea2*((1/T)-(1/Tref1))/Rg);
% kfm11(2)=kfm110(2);%*exp(-Ea2*((1/T)-(1/Tref1))/Rg);
% kfm12(1)=kfm120(1);%*exp(-Ea2*((1/T)-(1/Tref1))/Rg);
% kfm12(2)=kfm120(2);%*exp(-Ea2*((1/T)-(1/Tref1))/Rg);
% kfm21(1)=kfm210(1);%*exp(-Ea2*((1/T)-(1/Tref1))/Rg);
% kfm21(2)=kfm210(2);%*exp(-Ea2*((1/T)-(1/Tref1))/Rg);
% kfm22(1)=kfm220(1);%*exp(-Ea2*((1/T)-(1/Tref1))/Rg);
% kfm22(2)=kfm220(2);%*exp(-Ea2*((1/T)-(1/Tref1))/Rg);
% kfh1(1)=kfh10(1);%*exp(-Ea2*((1/T)-(1/Tref1))/Rg);
% kfh1(2)=kfh10(2);%*exp(-Ea2*((1/T)-(1/Tref1))/Rg);
% kfh2(1)=kfh20(1);%*exp(-Ea2*((1/T)-(1/Tref1))/Rg);
% kfh2(2)=kfh20(2);%*exp(-Ea2*((1/T)-(1/Tref1))/Rg);
% kfr1(1)=kfr10(1);%*exp(-Ea2*((1/T)-(1/Tref1))/Rg);
% kfr1(2)=kfr10(2);%*exp(-Ea2*((1/T)-(1/Tref1))/Rg);
% kfr2(1)=kfr20(1);%*exp(-Ea2*((1/T)-(1/Tref1))/Rg);
% kfr2(2)=kfr20(2);%*exp(-Ea2*((1/T)-(1/Tref1))/Rg);
% kfs1(1)=kfs10(1);%*exp(-Ea2*((1/T)-(1/Tref1))/Rg);
% kfs1(2)=kfs10(2);%*exp(-Ea2*((1/T)-(1/Tref1))/Rg);
% kfs2(1)=kfs20(1);%*exp(-Ea2*((1/T)-(1/Tref1))/Rg);
% kfs2(2)=kfs20(2);%*exp(-Ea2*((1/T)-(1/Tref1))/Rg);
%% Reactivity Ratio of Ethylene & 1-Butene
r1(1)=kp11(1)/kp12(1);
r2(1)=kp22(1)/kp21(1);
r1(2)=kp11(2)/kp12(2);
r2(2)=kp22(2)/kp21(2);
%% pseudokinetic rate constant
for j=1:2
    khT(j)=f1*kh1(j)+f2*kh2(j);
    kp1T(j)=f1*kp11(j)+f2*kp12(j);
    kp2T(j)=f1*kp21(j)+f2*kp22(j);
     %fraction of active sites of type j
 %having terminal monomer 1 or 2(Ethylene or Butene)
    say(j)=f1*kp21(j)+f2*kp12(j);
    fi1(j)=f1*kp21(j)/say(j);
    fi2(j)=f2*kp12(j)/say(j);
    kpT1(j)=fi1(j)*kp11(1)+fi2(j)*kp21(j);
    kpT2(j)=fi1(j)*kp12(1)+fi2(j)*kp22(j);
    kpTT(j)=f1*kpT1(j)+f2*kpT2(j);
```

```
    kfhT(j)=fi1(j)*kfh1(j)+fi2(j)*kfh2(j);
    kfrT(j)=fi1(j)*kfr1(j)+fi2(j)*kfr2(j);
    kfsT(j)=fi1(j)*kfs1(j)+fi2(j)*kfs2(j);
    kiT(j)=f1*ki1(j)+f2*ki2(j);
    kfm1T(j)=f1*kfm11(j)+f2*kfm12(j);
    kfm2T(j)=f1*kfm21(j)+f2*kfm22(j);
    kfmT1(j)=fi1(j)*kfm11(j)+fi2(j)*kfm21(j);
    kfmT2(j)=fi1(j)*kfm12(j)+fi2(j)*kfm22(j);
    kfmTT(j)=f1*kfmT1(j)+f2*kfmT2(j);
end
%% Mass Transfer Calculation
d_bo=.0085; %for Geldart B
d_b=d_bo*((1+27*(U0-U_mf))^(1/3))*(1+6.84*H/2)^.5; %Correlation by
    Hilligardt & Werther
%dp_z=dp*((miu_g^(-2))*ro_g*(ro-ro_g)*gi)^(1/3);
%uT=(18*(dp_z)^(-2)+(2.335-1.744*1)*(dp_z)^(-0.5))^(-1);
%U_T=uT*((miu_g*(ro_g^-2))*(ro-ro_g)*gi)^(1/3);
%d_b=2*(U_T^2)/gi;
%d_bzero=fzero('findzero',.08);
%d_b=d_bzero;
D_AB=4e-7; %Gas Diffusion Coefficient (m2/s)
U_b=((1-Delta)/(1-2*Delta))*(-Delta*U0/(1-Delta)+.711*(gi*d_b)^.5); %
    Bubble Velocity
U_e=(U0-Delta*U_b)/(1-Delta); %Emulsion Velocity
u_br=.711*(gi*d_b)^.5;
K_bc=4.5*(U_e/d_b)+5.85*((((D_AB)^.5)*gi^.25)/d_b^1.25);
K_ce=6.77*(D_AB*epsilon_e*u_br/d_b^3)^.5;
K_be=(1/K_bc+1/K_ce)^-1; %Bubble to Emulsion Gas Interchange
    Coefficient (1/s)
hatta=(D_AB*kp11(1)*(CN11_e+CN11_b))^.5/K_be;
J=hatta*U0/U_mf;
%% Heat Transfer Calculation
ro_pol=920; %kg/m3
Hr_m=3835.11; %kj/kg
Hr=Hr_m*30.26; %kj/mol
%Hr=118042.3552; %j/mol
Cp_gg=1.77939; %kj/kg.k
Cp_pol=4.01933; %kj/kg.k
kg=3.18e-5; %kj/m.s.k
H_bc=4.5*(U_e*100*ro_g/1000*Cp_gg/4.184/(d_b*100))+5.85*...
(kg*10/4.184*ro_g/1000*Cp_gg/4.184)^.5*(gi*100)^.25/(d_b*100)^1.25; %
    kj/s.k.m3
H_ce=6.77*(ro_g/1000*Cp_gg/4.184*kg*10/4.184)^.5...
*(epsilon_e*u_br*100/(d_b*100)^3)^.5; %kj/s.k.m3
H_be=(1/H_bc+1/H_ce)^(-1)*4184; %kj/s.k.m3
%Number of CSTR=4
n=1;
A_e=At*(1-Delta); %m2
A_b=At*Delta;
dp_z=dp*(((miu_g^(-2))*ro_g*(ro_pol-ro_g)*gi)^(1/3));
```

```
uT=(18*((dp_z)^(-2))+(2.335-1.744*1)*((dp_z)^(-0.5)))^(-1);
U_T=uT*(((miu_g*(ro_g^-2))*(ro_pol-ro_g)*gi)^(1/3));
K=23.7*ro_g*U0*exp(-5.4*U_T/U0);
W_e=A_e*H*(1-epsilon_e)*ro_pol;
W_b=A_b*H*(1-epsilon_b)*ro_pol;
Vi=VR/n; %m3
V_e=Vi*(1-Delta); %m3
V_b=Vi*Delta; %m3
V_CSTR=VR*epsilon_e; %m3
V_PLUG=VR*epsilon_b; %m3
%Energy Balance
Cp_C4H8=149.83; %kj/kmol.k
Cp_C2H4=51.63; %kj/kmol.k
Cp_H2=28.636; %kj/kmol.k
Cp_N2=30.139; %kj/kmol.k
%Cp_ave=Cp_C2H4*CM1_0+Cp_C4H8*CM2_0+Cp_H2*CH2_0+Cp_N2*CN2;
mw(1)=28;
mw(2)=56;
%Hydrodynamic Calculation
VR1=((pi*Dt^2))/4*H*1000; %lit
%epsilon_b=1-.146*exp((U0-U_mf)/4.439);
%epsilon_e=epsilon_mf+.2-.059*exp(-(U0-U_mf)/.429);
%Delta=.534*[1-exp(-(U0-U_mf)/.413)];
Vp_e=(1-epsilon_e)*VR1*(1-Delta);
VR_e=VR1*(1-Delta);
%Rate Calculation
R_e(1)=CM_e(1)*p(1).*kpT1(1)+CM_e(1)*p(2).*kpT1(2);
R_e(2)=CM_e(2)*p(1).*kpT2(1)+CM_e(2)*p(2).*kpT2(2);
Rv_e=(mw(1)*R_e(1)+mw(2)*R_e(2))/ro;
%Catalyst Active Sites Concentration
Ncat1_e=Fin1_e/(kf(1)+Rv_e/Vp_e);
Ncat2_e=Fin2_e/(kf(2)+Rv_e/Vp_e);
N0ini1_e=(kf(1)*Ncat1_e)/(kiT(1)*CMT_e+kds(1)+kdI(1)*Im+Rv_e/Vp_e);
N0ini2_e=(kf(2)*Ncat2_e)/(kiT(2)*CMT_e+kds(2)+kdI(2)*Im+Rv_e/Vp_e);
CNH1_e=p(1)*(kfhT(1)*CH2_e+kfsT(1))/(khT(1)...
*CMT_e+kds(1)+khr(1)*C_cocat_e+kdI(1)*Im+Rv_e/Vp_e);
CNH2_e=p(2)*(kfhT(2)*CH2_e+kfsT(2))/(khT(2)...
*CMT_e+kds(2)+khr(2)*C_cocat_e+kdI(2)*Im+Rv_e/Vp_e);
CN11_e=(ki1(1)*N0ini1_e*CM_e(1)+CNH1_e*(kh1(1)...
    *CM_e(1)+khr(1)*C_cocat_e)+p(1)*(kfmT1(1)*CM_e(1)+...
    kfrT(1)*C_cocat_e))/(kp1T(1)*CMT_e...
    +kfm1T(1)*CMT_e+kfh1(1)*CH2_e+kfr1(1)...
        *C_cocat_e+kfs1(1)+kds(1)+kdI(1)*Im+Rv_e/Vp_e);
CN12_e=(ki1(2)*N0ini2_e*CM_e(1)+CNH2_e*(kh1(2)...
    *CM_e(1)+khr(2)*C_cocat_e)+p(2)*(kfmT1(2)*...
    CM_e(1)+kfrT(2)*C_cocat_e))/(kp1T(2)*CMT_e...
    +kfm1T(2)*CMT_e+kfh1(2)*CH2_e+kfr1(2)*...
        C_cocat_e+kfs1(2)+kds(2)+kdI(2)*Im+Rv_e/Vp_e);
CN21_e=(ki2(1)*N0ini1_e*CM_e(2)+CNH1_e*kh2(1)...
        *CM_e(2)+p(1)*kfmT2(1)*CM_e(2))/(kp2T(1)*...
```

```
        CMT_e+kfm2T(1)*CMT_e+kfh2(1)*CH2_e+kfr2(1)*...
        C_cocat_e+kfs2(1)+kds(1)+kdI(1)*Im+Rv_e/Vp_e);
CN22_e=(ki2(2)*N0ini2_e*CM_e(2)+CNH2_e*kh2(2)*...
        CM_e(2)+p(2)*kfmT2(2)*CM_e(2))/(kp2T(2)*CMT_e+...
        kfm2T(2)*CMT_e+kfh2(2)*CH2_e+kfr2(2)*C_cocat_e+...
        kfs2(2)+kds(2)+kdI(2)*Im+Rv_e/Vp_e);
%Moment Equations
Var_e1=CMT_e*(kiT(1)*N0ini1_e+khT(1)*CNH1_e)+khr(1)*CNH1_e*C_cocat_e...
    -p(1)*(kfhT(1)*CH2_e+kfsT(1)+kds(1)+kdI(1)*Im+Rv_e/Vp_e);
Var_e2=CMT_e*(kiT(2)*N0ini2_e+khT(2)*CNH2_e)+khr(2)*CNH2_e*C_cocat_e...
    -p(2)*(kfhT(2)*CH2_e+kfsT(2)+kds(2)+kdI(2)*Im+Rv_e/Vp_e);
Var_e3=CMT_e*(kiT(1)*N0ini1_e+khT(1)*CNH1_e)+khr(1)*CNH1_e*C_cocat_e...
    +CMT_e*kpTT(1)*p(1)+(p(1)-p(3))*(kfmTT(1)*CMT_e+kfrT(1)*C_cocat_e)
        ...
    -p(3)*(kfhT(1)*CH2_e+kfsT(1)+kds(1)+kdI(1)*Im+Rv_e/Vp_e);
Var_e4=CMT_e*(kiT(2)*N0ini2_e+khT(2)*CNH2_e)+khr(2)*CNH2_e*C_cocat_e...
    +CMT_e*kpTT(2)*p(2)+(p(2)-p(4))*(kfmTT(2)*CMT_e+kfrT(2)*C_cocat_e)
        ...
    -p(4)*(kfhT(2)*CH2_e+kfsT(2)+kds(2)+kdI(2)*Im+Rv_e/Vp_e);
Var_e5=CMT_e*(kiT(1)*N0ini1_e+khT(1)*CNH1_e)+khr(1)*CNH1_e*C_cocat_e...
    +CMT_e*kpTT(1)*(2*p(3)-p(1))+(p(1)-p(5))*(kfmTT(1)*CMT_e...
    +kfrT(1)*C_cocat_e)-p(5)*(kfhT(1)*CH2_e+kfsT(1)+kds(1)+kdI(1)*Im+
        Rv_e/Vp_e);
Var_e6=CMT_e*(kiT(2)*N0ini2_e+khT(2)*CNH2_e)+khr(2)*CNH2_e*C_cocat_e...
    +CMT_e*kpTT(2)*(2*p(4)-p(2))+(p(2)-p(6))*(kfmTT(2)*CMT_e...
    +kfrT(2)*C_cocat_e)-p(6)*(kfhT(2)*CH2_e+kfsT(2)+kds(2)+kdI(2)*Im+
        Rv_e/Vp_e);
Var_e7=(p(1)-(CN11_e+CN21_e))*(kfmTT(1)*CMT_e+kfrT(1)*C_cocat_e...
    +kfhT(1)*CH2_e+kfsT(1)+kds(1)+kdI(1)*Im)-p(7)*Rv_e/Vp_e;
Var_e8=(p(2)-(CN12_e+CN22_e))*(kfmTT(2)*CMT_e+kfrT(2)*C_cocat_e...
    +kfhT(2)*CH2_e+kfsT(2)+kds(2)+kdI(2)*Im)-p(8)*Rv_e/Vp_e;
Var_e9=(p(3)-(CN11_e+CN21_e))*(kfmTT(1)*CMT_e+kfrT(1)*C_cocat_e...
    +kfhT(1)*CH2_e+kfsT(1)+kds(1)+kdI(1)*Im)-p(9)*Rv_e/Vp_e;
Var_e10=(p(4)-(CN12_e+CN22_e))*(kfmTT(2)*CMT_e+kfrT(2)*C_cocat_e...
    +kfhT(2)*CH2_e+kfsT(2)+kds(2)+kdI(2)*Im)-p(10)*Rv_e/Vp_e;
Var_e11=(p(5)-(CN11_e+CN21_e))*(kfmTT(1)*CMT_e+kfrT(1)*C_cocat_e...
    +kfhT(1)*CH2_e+kfsT(1)+kds(1)+kdI(1)*Im)-p(11)*Rv_e/Vp_e;
Var_e12=(p(6)-(CN12_e+CN22_e))*(kfmTT(2)*CMT_e+kfrT(2)*C_cocat_e...
    +kfhT(2)*CH2_e+kfsT(2)+kds(2)+kdI(2)*Im)-p(12)*Rv_e/Vp_e;
Var_e13=R_e(1)-p(13)*Rv_e/Vp_e;
Var_e14=R_e(2)-p(14)*Rv_e/Vp_e;
%Hydrodynamic Calculation
VR1=((pi*Dt^2))/4*H*1000; %lit
%epsilon_b=1-.146*exp((U0-U_mf)/4.439);
```

```
%epsilon_e=epsilon_mf+.2-.059*exp(-(U0-U_mf)/.429);
%Delta=.534*[1-exp(-(U0-U_mf)/.413)];
Vp_b=(1-epsilon_b)*VR1*(Delta);
VR_b=VR1*Delta;
%Rate Calculation
R_b(1)=CM_b(1)*p(15).*kpT1(1)+CM_b(1)*p(16).*kpT1(2);
R_b(2)=CM_b(2)*p(15).*kpT2(1)+CM_b(2)*p(16).*kpT2(2);
Rv_b=(mw(1)*R_b(1)+mw(2)*R_b(2))/ro;
%Catalyst Active Sites Concentration
Ncat1_b=Fin1_b/(kf(1)+Rv_b/Vp_b);
Ncat2_b=Fin2_b/(kf(2)+Rv_b/Vp_b);
N0ini1_b=(kf(1)*Ncat1_b)/(kiT(1)*CMT_b+kds(1)+kdI(1)*Im+Rv_b/Vp_b);
N0ini2_b=(kf(2)*Ncat2_b)/(kiT(2)*CMT_b+kds(2)+kdI(2)*Im+Rv_b/Vp_b);
CNH1_b=p(15)*(kfhT(1)*CH2_b+kfsT(1))/(khT(1)*CMT_b+...
       kds(1)+khr(1)*C_cocat_b+kdI(1)*Im+Rv_b/Vp_b);
CNH2_b=p(16)*(kfhT(2)*CH2_b+kfsT(2))/(khT(2)*CMT_b+...
       kds(2)+khr(2)*C_cocat_b+kdI(2)*Im+Rv_b/Vp_b);
CN11_b=(ki1(1)*N0ini1_b*CM_b(1)+CNH1_b*(kh1(1)*CM_b(1)+khr(1)*
    C_cocat_b)...
    +p(15)*(kfmT1(1)*CM_b(1)+kfrT(1)*C_cocat_b))/(kp1T(1)*CMT_b...
    +kfm1T(1)*CMT_b+kfh1(1)*CH2_b+kfr1(1)*C_cocat_b+kds(1)+kdI(1)*Im+
       Rv_b/Vp_b);
CN12_b=(ki1(2)*N0ini2_b*CM_b(1)+CNH2_b*(kh1(2)*CM_b(1)+khr(2)*
    C_cocat_b)...
    +p(16)*(kfmT1(2)*CM_b(1)+kfrT(2)*C_cocat_b))/(kp1T(2)*CMT_b...
    +kfm1T(2)*CMT_b+kfh1(2)*CH2_b+kfr1(2)*C_cocat_b+kds(2)+kdI(2)*Im+
       Rv_b/Vp_b);
CN21_b=(ki2(1)*N0ini1_b*CM_b(2)+CNH1_b*kh2(1)*CM_b(2)+p(15)*...
       kfmT2(1)*CM_b(2))/(kp2T(1)*CMT_b+kfm2T(1)*CMT_b+kfh2(1)*...
       CH2_b+kfr2(1)*C_cocat_b+kfs2(1)+kds(1)+kdI(1)*Im+Rv_b/Vp_b);
CN22_b=(ki2(2)*N0ini2_b*CM_b(2)+CNH2_b*kh2(2)*CM_b(2)+p(16)*...
       kfmT2(2)*CM_b(2))/(kp2T(2)*CMT_b+kfm2T(2)*CMT_b+kfh2(2)*...
       CH2_b+kfr2(2)*C_cocat_b+kfs2(2)+kds(2)+kdI(2)*Im+Rv_b/Vp_b);
%Moment Equations
Var_b1=CMT_b*(kiT(1)*N0ini1_b+khT(1)*CNH1_b)+khr(1)*CNH1_b*C_cocat_b...

    -p(15)*(kfhT(1)*CH2_b+kfsT(1)+kds(1)+kdI(1)*Im+Rv_b/Vp_b);
Var_b2=CMT_b*(kiT(2)*N0ini2_b+khT(2)*CNH2_b)+khr(2)*CNH2_b*C_cocat_b...

    -p(16)*(kfhT(2)*CH2_b+kfsT(2)+kds(2)+kdI(2)*Im+Rv_b/Vp_b);
Var_b3=CMT_b*(kiT(1)*N0ini1_b+khT(1)*CNH1_b)+khr(1)*CNH1_b*C_cocat_b...

    +CMT_b*kpTT(1)*p(15)+(p(15)-p(17))*(kfmTT(1)*CMT_b+kfrT(1)*
       C_cocat_b)...
    -p(17)*(kfhT(1)*CH2_b+kfsT(1)+kds(1)+kdI(1)*Im+Rv_b/Vp_b);
Var_b4=CMT_b*(kiT(2)*N0ini2_b+khT(2)*CNH2_b)+khr(2)*CNH2_b*C_cocat_b...

    +CMT_b*kpTT(2)*p(16)+(p(16)-p(18))*(kfmTT(2)*CMT_b+kfrT(2)*
       C_cocat_b)...
    -p(18)*(kfhT(2)*CH2_b+kfsT(2)+kds(2)+kdI(2)*Im+Rv_b/Vp_b);
```

```
Var_b5=CMT_b*(kiT(1)*N0ini1_b+khT(1)*CNH1_b)+khr(1)*CNH1_b*C_cocat_b...
    +CMT_b*kpTT(1)*(2*p(17)-p(15))+(p(15)-p(19))*(kfmTT(1)*CMT_b...
    +kfrT(1)*C_cocat_b)-p(19)*(kfhT(1)*CH2_b+kfsT(1)+kds(1)+kdI(1)*Im+
       Rv_b/Vp_b);
Var_b6=CMT_b*(kiT(2)*N0ini2_b+khT(2)*CNH2_b)+khr(2)*CNH2_b*C_cocat_b...
    +CMT_b*kpTT(2)*(2*p(18)-p(16))+(p(16)-p(20))*(kfmTT(2)*CMT_b...
    +kfrT(2)*C_cocat_b)-p(20)*(kfhT(2)*CH2_b+kfsT(2)+kdI(2)*Im+kds(2)+
       Rv_b/Vp_b);
Var_b7=(p(15)-(CN11_b+CN21_b))*(kfmTT(1)*CMT_b+kfrT(1)*C_cocat_b...
    +kfhT(1)*CH2_b+kfsT(1)+kds(1)+kdI(1)*Im)-p(21)*Rv_b/Vp_b;
Var_b8=(p(16)-(CN12_b+CN22_b))*(kfmTT(2)*CMT_b+kfrT(2)*C_cocat_b...
    +kfhT(2)*CH2_b+kfsT(2)+kds(2)+kdI(2)*Im)-p(22)*Rv_b/Vp_b;
Var_b9=(p(17)-(CN11_b+CN21_b))*(kfmTT(1)*CMT_b+kfrT(1)*C_cocat_b...
    +kfhT(1)*CH2_b+kfsT(1)+kds(1)+kdI(1)*Im)-p(23)*Rv_b/Vp_b;
Var_b10=(p(18)-(CN12_b+CN22_b))*(kfmTT(2)*CMT_b+kfrT(2)*C_cocat_b...
    +kfhT(2)*CH2_b+kfsT(2)+kds(2)+kdI(2)*Im)-p(24)*Rv_b/Vp_b;
Var_b11=(p(19)-(CN11_b+CN21_b))*(kfmTT(1)*CMT_b+kfrT(1)*C_cocat_b...
    +kfhT(1)*CH2_b+kfsT(1)+kds(1)+kdI(1)*Im)-p(25)*Rv_b/Vp_b;
Var_b12=(p(20)-(CN12_b+CN22_b))*(kfmTT(2)*CMT_b+kfrT(2)*C_cocat_b...
    +kfhT(2)*CH2_b+kfsT(2)+kds(2)+kdI(2)*Im)-p(26)*Rv_b/Vp_b;
Var_b13=R_b(1)-p(27)*Rv_b/Vp_b;
Var_b14=R_b(2)-p(28)*Rv_b/Vp_b;
%Monomers and Hydrogen Rate Calculations in Emulsion Phase
s1_e1=p(7,:)+p(8,:)+p(1,:)+p(2,:);
s2_e1=p(9,:)+p(10,:)+p(3,:)+p(4,:);
s3_e1=p(11,:)+p(12,:)+p(5,:)+p(6,:);
R11_e1=p(1,:).*kpT1(1)*CM(1); %mol/s
R12_e1=p(2,:).*kpT1(2)*CM(1); %mol/s
R1_e=R11_e1(1,:)+R12_e1(1,:); %mol/s
R21_e1=p(1,:).*kpT2(1)*CM(2); %mol/s
R22_e1=p(2,:).*kpT2(2)*CM(2); %mol/s
R2_e=R21_e1(1,:)+R22_e1(1,:); %mol/s
RH1_e1=p(1,:).*kfhT(1)*CH2; %mol/s
RH2_e1=p(2,:).*kfhT(2)*CH2; %mol/s
RH_e=RH1_e1(1,:)+RH2_e1(1,:); %mol/s
N_e131=p(13,:);
N_e141=p(14,:);
%Monomers and Hydrogen Rate Calculations in Bubble phase
s1_b1=p(21,:)+p(22,:)+p(15,:)+p(16,:);
s2_b1=p(23,:)+p(24,:)+p(17,:)+p(18,:);
s3_b1=p(25,:)+p(26,:)+p(19,:)+p(20,:);
R11_b1=p(15,:).*kpT1(1)*CM(1); %mol/s
R12_b1=p(16,:).*kpT1(2)*CM(1); %mol/s
R1_b=R11_b1(1,:)+R12_b1(1,:); %mol/s
R21_b1=p(15,:).*kpT2(1)*CM(2); %mol/s
R22_b1=p(16,:).*kpT2(2)*CM(2); %mol/s
R2_b=R21_b1(1,:)+R22_b1(1,:); %mol/s
RH1_b1=p(15,:).*kfhT(1)*CH2; %mol/s
```

```
RH2_b1=p(16,:).*kfhT(2)*CH2; %mol/s
RH_b=RH1_b1(1,:)+RH2_b1(1,:); %mol/s
N_b131=p(27,:);
N_b141=p(28,:);
R_e1=R1_e+R2_e+RH_e; %mol/s
Rp_e1=mwC2H4*R1_e+mwC4H8*R2_e+mwH2*RH_e; %g/s
Rpp_e1=Rp_e1*3.6e-3; %ton/hr
R_b1=R1_b+R2_b+RH_b; %mol/s
Rp_b1=mwC2H4*R1_b+mwC4H8*R2_b+mwH2*RH_b; %g/s
Rpp_b1=Rp_b1*3.6e-3; %ton/hr
%Production Rates of Polymer in Emulsion Phase
%R1_e=R1_e1;
%R2_e=R2_e1;
%RH_e=RH_e1;
R_e=R1_e+R2_e+RH_e; %mol/s
Rv_e=((mwC2H4*R1_e+mwC4H8*R2_e+mwH2*RH_e)/ro)/1000; %m3/s
Rp_e=mwC2H4*R1_e+mwC4H8*R2_e+mwH2*RH_e; %g/s
Rpp_e=Rp_e*3.6e-3; %Polymer Production (ton/hr)
%Production Rates of Polymer in Bubble phase
%R1_b=R1_b1;
%R2_b=R2_b1;
%RH_b=RH_b1;
R_b=R1_b+R2_b+RH_b; %mol/s
Rv_b=((mwC2H4*R1_b+mwC4H8*R2_b+mwH2*RH_b)/ro)/1000;
Rp_b=mwC2H4*R1_b+mwC4H8*R2_b+mwH2*RH_b;%g/s
Rpp_b=Rp_b*3.6e-3; %Polymer Production (ton/hr)
Vp_b=((1-epsilon_b)*VR1*(Delta));
Vp_e=(1-epsilon_e)*VR1*(1-Delta);
VR_b=VR1*Delta;
varmass1=(CM(1)*U_e*A_e-p(29)*U_e*A_e-(Rv_e(end)*epsilon_e*..
       p(29))+K_be*V_e*(Delta/(1-Delta))*(p(30)-p(29))-((1-epsilon_e)
          *...
       R1_e/1000))-(V_e*epsilon_e*K*A_e*(p(29))/W_e)./(V_e*epsilon_e);
varmass2=(CM(1)*U_b*A_b-p(30)*U_b*A_b-(Rv_b(end)*epsilon_b*...
      p(30))-K_be*V_b*(p(30)-p(29))-((1-epsilon_b)*R1_b/1000))-...
      (V_b*epsilon_b*K*A_b*(p(30))/W_b)./(V_b*epsilon_b);
varmass3=(CM(2)*U_e*A_e-p(31)*U_e*A_e-(Rv_e(end)*epsilon_e*...
      p(31))+K_be*V_e*(Delta/(1-Delta))*(p(32)-p(31))-((1-epsilon_e)
          *...
      R2_e/1000))-(V_e*epsilon_e*K*A_e*(p(31))/W_e)./(V_e*epsilon_e);
varmass4=(CM(2)*U_b*A_b-p(32)*U_b*A_b-(Rv_b(end)*epsilon_b*...
       p(32))-K_be*V_b*(p(32)-p(31))-((1-epsilon_b)*R2_b/1000))-...
       (V_b*epsilon_b*K*A_b*(p(32))/W_b)./(V_b*epsilon_b);
varmass5=(CH2*U_e*A_e-p(33)*U_e*A_e-(Rv_e(end)*epsilon_e*...
       p(33))+K_be*V_e*(Delta/(1-Delta))*(p(34)-p(33))-((1-epsilon_e)
          *...
       RH_e/1000))-(V_e*epsilon_e*K*A_e*(p(33))/W_e)./(V_e*epsilon_e);
varmass6=(CH2*U_b*A_b-p(34)*U_b*A_b-(Rv_b(end)*epsilon_b*p(34))-...
       K_be*V_b*(p(34)-p(33))-((1-epsilon_b)*RH_b/1000))-(V_b*
          epsilon_b*...
```

```
542         K*A_b*(p(34))/W_b)./(V_b*epsilon_b);
543 %a11=U_e*A_e*(Cp_C2H4*CM_e(1)+Cp_C4H8*CM_e(2)+Cp_H2*CH2_e+Cp_N2*CN2)
    ;%*1000; %j/s
544 %a21=U_b*A_b*(Cp_C2H4*CM_b(1)+Cp_C4H8*CM_b(2)+Cp_H2*CH2_b+Cp_N2*CN2)
    ;%*1000;
545 %b11=U_e*A_e*(Cp_C2H4*CM_e2(1)+Cp_C4H8*CM_e2(2)+Cp_H2*CH2_e2+Cp_N2*CN2)
    ;%*1000;
546 %b21=U_b*A_b*(Cp_C2H4*CM_b2(1)+Cp_C4H8*CM_b2(2)+Cp_H2*CH2_b2+Cp_N2*CN2)
    ;%*1000;
547 %a11=U_e*A_e*(CM_e(1)+CM_e(2)+CH2_e+CN2)*Cp_gg*30.26;
548 %a21=U_b*A_b*(CM_b(1)+CM_b(2)+CH2_b+CN2)*Cp_gg*30.26;
549 %b11=U_e*A_e*(CM_e2(1)+CM_e2(2)+CH2_e2+CN2)*Cp_gg*30.26;
550 %b21=U_b*A_b*(CM_b2(1)+CM_b2(2)+CH2_b2+CN2)*Cp_gg*30.26;
551 a11=U_e*A_e*(CM(1)*63+CM(2)*51.63+CH2*28.636+CN2*30.139);
552 %Reza a21 is inlet gas into the first bubble cell
553 %a21=U_b*A_b*(CM_b(1)+CM_b(2)+CH2_b+CN2)*Cp_gg*30.26;
554 a21=U_b*A_b*(CM(1)*63+CM(2)*51.63+CH2*28.636+CN2*30.139);
555 %Reza b11 is outlet gas from the first emulsion cell
556 %b11=U_e*A_e*(CM_e2(1)+CM_e2(2)+CH2_e2+CN2)*Cp_gg*30.26;
557 %b11=U_e*A_e*(CM_e2(1)+CH2_e2+CN2)*Cp_gg*36.58;
558 b11=U_e*A_e*(p(29)*63+p(31)*51.63+p(33)*28.636+CN2*30.139);
559 %Reza b21 is outlet gas from the first bubble cell
560 %b21=U_b*A_b*(CM_b2(1)+CM_b2(2)+CH2_b2+CN2)*Cp_gg*30.26;
561 %b21=U_b*A_b*(CM_b2(1)+CH2_b2+CN2)*Cp_gg*36.58;
562 b21=U_b*A_b*(p(30)*63+p(32)*51.63+p(34)*28.636+CN2*30.139);
563 %Energy Balance step 1
564 %Reza described in thesis
565 %a11*(Tin-Tref)-b11*(T_e1-Tref)+c11-d11*(T_e1-T_b1)+e11*(T_e2-Tref)-
    f11*(T_e1-Tref)=0
566 %Reza for emulsion phase
567 %c11=Rp_e1(end)*Hr_m/1000;
568 c11=Hr_m/1000;
569 d11=H_be*V_e;
570 e11=0;
571 f11=(Rp_e(end))*Cp_pol/1000;
572 %a21*(Tin-Tref)-b21*(T_b1-Tref)+c21+d21*(T_e1-T_b1)+e21*(T_b2-Tref)-
    f21*(T_b1-Tref)=0
573 %Reza for bubble phase
574 %c21=Rp_b1(end)*Hr_m/1000;
575 c21=Hr_m/1000;
576 d21=H_be*V_b;
577 e21=0;
578 f21=(Rp_b(end))*Cp_pol/1000;
579 %R1=R1_e+R1_b;
580 %R2=R2_e+R2_b;
581 %RH=RH_e+RH_b;
582 %Production Rates of Polymer
583 %Rv=Rv_e+Rv_b; %ton/hr
584 Rpp=Rpp_e+Rpp_b;
585 %temp
```

```
%Vp_b=((1-epsilon_b)*VR1*(Delta));
%Vp_e=(1-epsilon_e)*VR1*(1-Delta);
% Cp_C2H4=51.63; %kj/kmol.k
% Cp_C4H8=149.83;
% Cp_H2=28.636; %kj/kmol.k
% Cp_N2=30.139; %kj/kmol.k
%Vp_b=((1-epsilon_b)*VR1*(Delta));
%Vp_e=(1-epsilon_e)*VR1*(1-Delta);
%A1=a11*(Tin-Tref);
%B1=b11*(tdo(1)-Tref);
%C1=((Rv_e(end))*(tdo(1)-Tref)*((epsilon_e*(((cm(end,1)*51.63+...
        %cm(end,3)*149.83+cm(end,5)*28.636+CN2*30.139))))+((1-epsilon_e
            )*ro*Cp_pol)));
%D1=(V_e.*epsilon_e.*(tdo(1)-Tref)*(mx(n,1)*51.63+mx(n,3)*149.83+mx(n
    ,5)*28.636));
%E1=(c11.*Rp_e1(n));
%F1=(d11.*(tdo(1)-tdo(2)));
%G1=(V_e.*((epsilon_e.*(((cm(end,1)*51.63+cm(end,3)*149.83+cm(end,5)
    *...
        %28.636+CN2*30.139))))+((1-epsilon_e)*ro*(Cp_pol))));
%A2=a21*(Tin-Tref);
%B2=b21*(tdo(2)-Tref);
%C2=((Rv_b(end))*(tdo(2)-Tref)*((epsilon_b*(((cm(end,2)*51.63+....
        %cm(end,4)*149.83+cm(end,6)*28.636+CN2*30.139))))+((1-epsilon_b
            )*ro*Cp_pol)))
%D2=(V_b.*epsilon_b.*(tdo(2)-Tref)*(mx(n,2)*51.63+mx(n,4)*149.83+mx(n
    ,6)*28.636))
%E2=(c21.*Rp_b1(n))
%F2=(d21.*(tdo(1)-tdo(2)))
%G2=(V_b.*((epsilon_b.*(((cm(end,2)*51.63+cm(end,4)*149.83+...
        %cm(end,6)*28.636+CN2*30.139))))+((1-epsilon_b)*ro*(Cp_pol))))
A1=epsilon_e*(a11*(Tin)-a11*(Tref));
B1=epsilon_e*(b11*(p(35))-b11*(Tref));
%C1=f11*tdo(1)-f11*1.0001*tdo(1);
C1=((Rv_e(end))*(p(35))*((epsilon_e*(((p(29)*63+p(31)*51.63+p(33)*...
    28.636+CN2*30.139))))+((1-epsilon_e)*ro*Cp_pol)))...
-((Rv_e(end))*(Tref)*((epsilon_e*(((p(29)*63+p(31)*51.63+...
        p(33)*28.636+CN2*30.139))))+((1-epsilon_e)*ro*Cp_pol)));
D1=(V_e.*epsilon_e.*(p(35))*(p(29,end)*63+p(31)*51.63+...
        p(33)*28.636))-(V_e.*epsilon_e.*(1.0001*p(35))*(p(29)*63+p(31)
            *51.63+p(33)*28.636));
E1=(1-epsilon_e)*(c11.*Rp_e(end));
F1=(Delta/(1-Delta))*(d11.*(p(35))-d11.*(p(36)));
H1=(((K*A_e*V_e/W_e))*(p(35))*((epsilon_e*(((p(29)*63+p(31)*...
        51.63+p(33)*28.636+CN2*30.139))))+((1-epsilon_e)*ro*Cp_pol)))...

-(((K*A_e*V_e/W_e))*(Tref)*((epsilon_e*(((p(29)*63+p(31)*51.63+...
        p(33)*28.636+CN2*30.139))))+((1-epsilon_e)*ro*Cp_pol)));
G1=(V_e.*((epsilon_e.*(((p(29)*63+p(31)*51.63+p(33)*28.636+...
        CN2*30.139))))+((1-epsilon_e)*ro*(Cp_pol))));
```

```
A2=epsilon_b*(a21*(Tin)-a21*Tref);
B2=epsilon_b*(b21*p(36)-b21*Tref);
%C2=f21*tdo(2)-f21*1.0001*tdo(2);
C2=((Rv_b(end))*(p(36))*((epsilon_b*(((p(30)*63+p(32)*51.63+...
       p(34)*28.636+CN2*30.139))))+((1-epsilon_b)*ro*Cp_pol)))...
 -((Rv_b(end))*(Tref)*((epsilon_b*(((p(30)*63+p(32)*51.63+...
       p(34)*28.636+CN2*30.139))))+((1-epsilon_b)*ro*Cp_pol)));
D2=(V_b.*epsilon_b.*(p(36))*(p(30)*63+p(32)*51.63+p(34)*28.636))-...
       (V_b.*epsilon_b.*(1.0001*p(36))*(p(30)*63+p(32)*51.63+p(34)
          *28.636));
E2=(1-epsilon_b)*(c21.*Rp_b(end));
F2=d21.*p(35)-d21*p(36);
H2=((K*A_b*V_b/W_b)*(p(36))*((epsilon_b*(((p(30)*63+p(32)*...
       51.63+p(34)*28.636+CN2*30.139))))+((1-epsilon_b)*ro*Cp_pol)))...

 -((K*A_b*V_b/W_b)*(Tref)*((epsilon_b*(((p(30)*63+p(32)*...
       51.63+p(34)*28.636+CN2*30.139))))+((1-epsilon_b)*ro*Cp_pol)));
G2=(V_b.*((epsilon_b.*(((p(30)*63+p(32)*51.63+p(34)*28.636+...
       CN2*30.139))))+((1-epsilon_b)*ro*(Cp_pol))));
% WHEN WE DELETE THE D1 AND D2 AND PUT THE Tref Instead of
% 1.0001*tdo(1,2)EVERYTHING BECOME SOLVE OR IF WE PUT Tref instead of
% 1.0001*tdo(1,2)except for D1 and D2 everything become solve as well.
var1=((A1-B1-C1-D1+E1-F1-H1)./G1);
var2=((A2-B2-C2-D2+E2+F2-H2)./G2);
to1=(kfmTT(1)*CMT+kfhT(1)*CH2+kfrT(1)*C_cocat+kfsT(1))/(kpTT(1)*CMT);
to2=(kfmTT(2)*CMT+kfhT(2)*CH2+kfrT(2)*C_cocat+kfsT(2))/(kpTT(2)*CMT);
dx=[Var_e1;Var_e2;Var_e3;Var_e4;Var_e5;Var_e6;Var_e7;Var_e8;Var_e9;...
       Var_e10;Var_e11;Var_e12;Var_e13;Var_e14;Var_b1;Var_b2;Var_b3;...

       Var_b4;Var_b5;Var_b6;Var_b7;Var_b8;Var_b9;Var_b10;Var_b11;...
       Var_b12;Var_b13;Var_b14;varmass1;varmass2;varmass3;...
       varmass4;varmass5;varmass6;var1;var2];
```

The codes of S-function to link the model to Simulink for control studies.

```
function [sys,x0,str,ts]= reza_sfcn_LL0209(t,x,u,flag,N0_e1,N0_e2,...
       N0_e3,N0_e4,N0_e5,N0_e6,N0_e7,N0_e8,N0_e9,N0_e10,N0_e11,N0_e12
          ,...
       N0_e13,N0_e14,N0_b1,N0_b2,N0_b3,N0_b4,N0_b5,N0_b6,N0_b7,N0_b8
          ,...
       N0_b9,N0_b10,N0_b11,N0_b12,N0_b13,N0_b14,c1_e,c1_b,c2_e,c2_b,...

       c3_e,c3_b,tdo_e,tdo_b)
%global shf pg pc dp m g uo D h DAB kg H2 Qc
%global rg met1 mbu pn po pin hw cps Qo nit
switch flag
case 0 % initialize
str=[] ;
ts = [0 0] ;
```

```
%initial condition of model ASM3:dx=[dXFCATdt;dXPEdt;dXCEdt;...
       %dXTEdt;dXU0dt;dXU1dt;dXU2dt;dXV0dt;dXV1dt;dXV2dt;dXMW1dt;...
       %dXPRODdt;dXCENdt;dXTENdt]';
%x0(1)=.002;
%x0(2)=3.17;
%x0(3)=0.04236;
%x0(4)=443.3; %zero LIVE moment
%x0(5)=5.622e7;% First LIVE moment
%x0(6)=5.378e6;%second LIVE moment
%x0(7)=2.143e8;%zero dead moment
%x0(8)=6.533e10;%first dead moment
%x0(9)=6.249e9;%secod dead moment
%x0(10)=2.49e11;
%x0(11)=3.574e6;%molecular weight
%x0(12)=4.958;
%x0(13)=0.0272;
%x0(14)=400.2;s = simsizes ;
s.NumContStates = 36;% NUMBER OF EQUATIONS (STATES)
s.NumDiscStates = 0 ;
s.NumOutputs = 36 ;
s.NumInputs = 8 ;%IN ASM3MODEL:[uo Qc Tref Tcat eth but hyd]
s.DirFeedthrough = 0 ;
s.NumSampleTimes = 1 ;
sys = simsizes(s) ;
x0=[N0_e1,N0_e2,N0_e3,N0_e4,N0_e5,N0_e6,N0_e7,N0_e8,N0_e9,...
       N0_e10,N0_e11,N0_e12,N0_e13,N0_e14,N0_b1,N0_b2,N0_b3,...
       N0_b4,N0_b5,N0_b6,N0_b7,N0_b8,N0_b9,N0_b10,N0_b11,N0_b12,...
       N0_b13,N0_b14,c1_e,c1_b,c2_e,c2_b,c3_e,c3_b,tdo_e,tdo_b];
% x0=[a_1,a_2,a_3,a_4,a_5,a_6,a_7,a_8,a_9,a_10,N0_e1, N0_e2,...
       %N0_e3, N0_e4, N0_e5, N0_e6, N0_e7, N0_e8, N0_e9, N0_e10, ...
       %N0_e11, N0_e12, N0_e13,N0_e14,c1,c2,c3,tdo];
case 1 % derivatives
    Input=u;
sys = reza_LL0209(t,x,Input) ;
case 3 % output
sys = x;
case {2 4 9} % 2:discrete
% 4:calcTimeHit
% 9:termination
sys =[];
otherwise
error(['unhandled flag =',num2str(flag)]) ;
end
```

APPENDIX B: SIMULINK® MODELS OF MODELING AND CONTROL OF ETHYLENE COPOLYMERIZATION IN THE FLUIDIZED-BED REACTOR

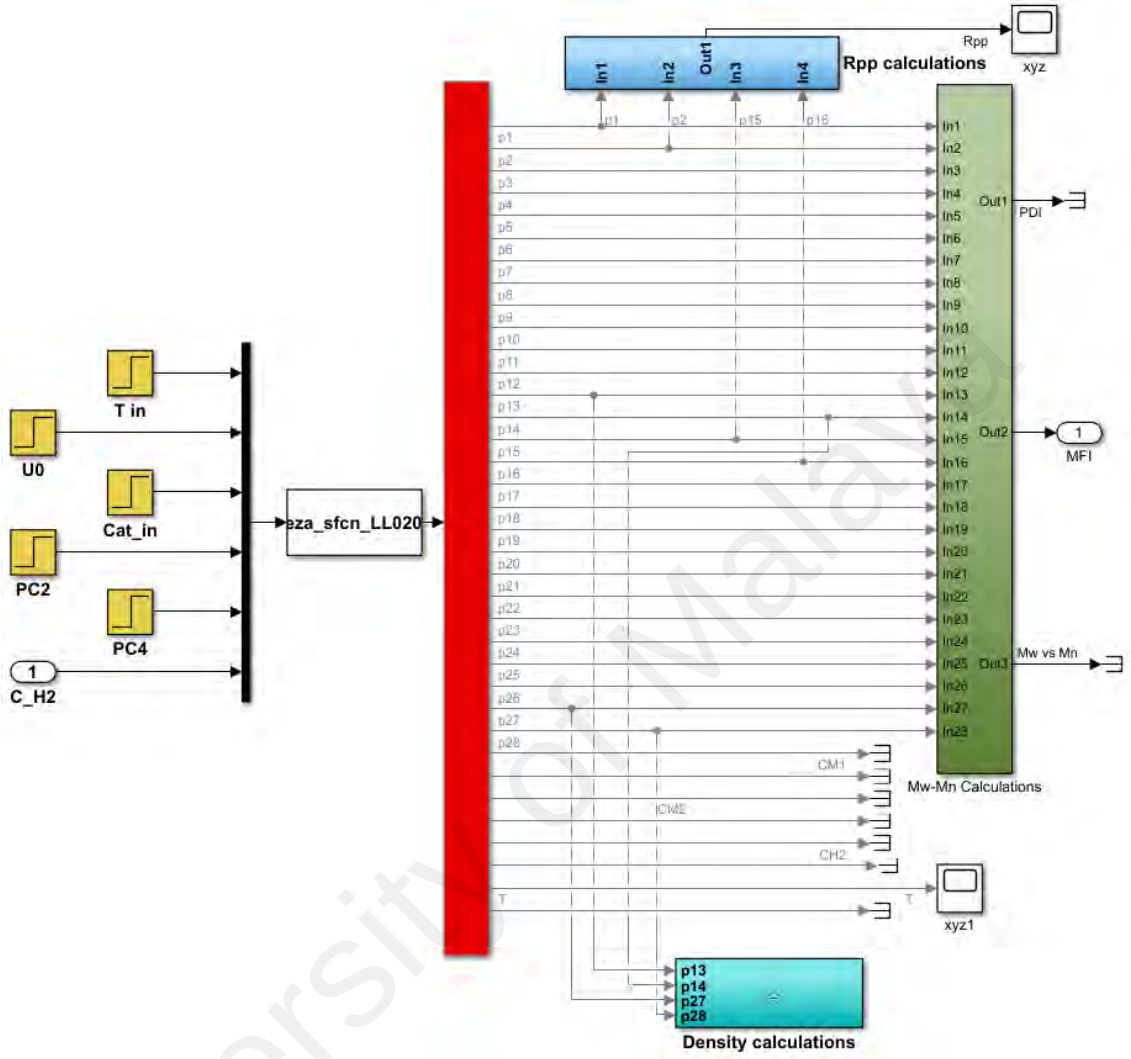

Figure B.1: Simulink® model of the FBR reactor with included subsystems

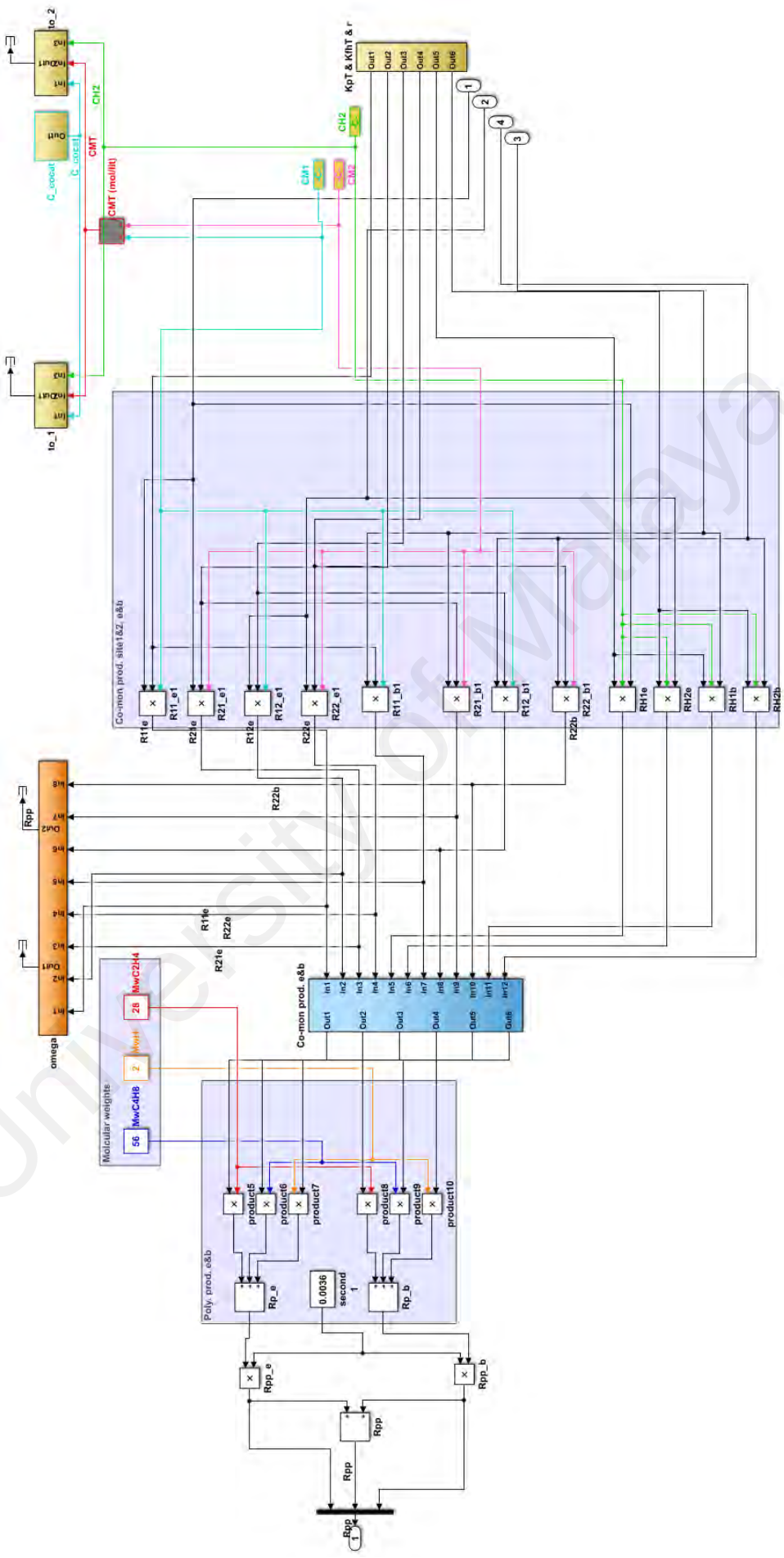

Figure B.2: Simulink® subsystem for production rate calculations

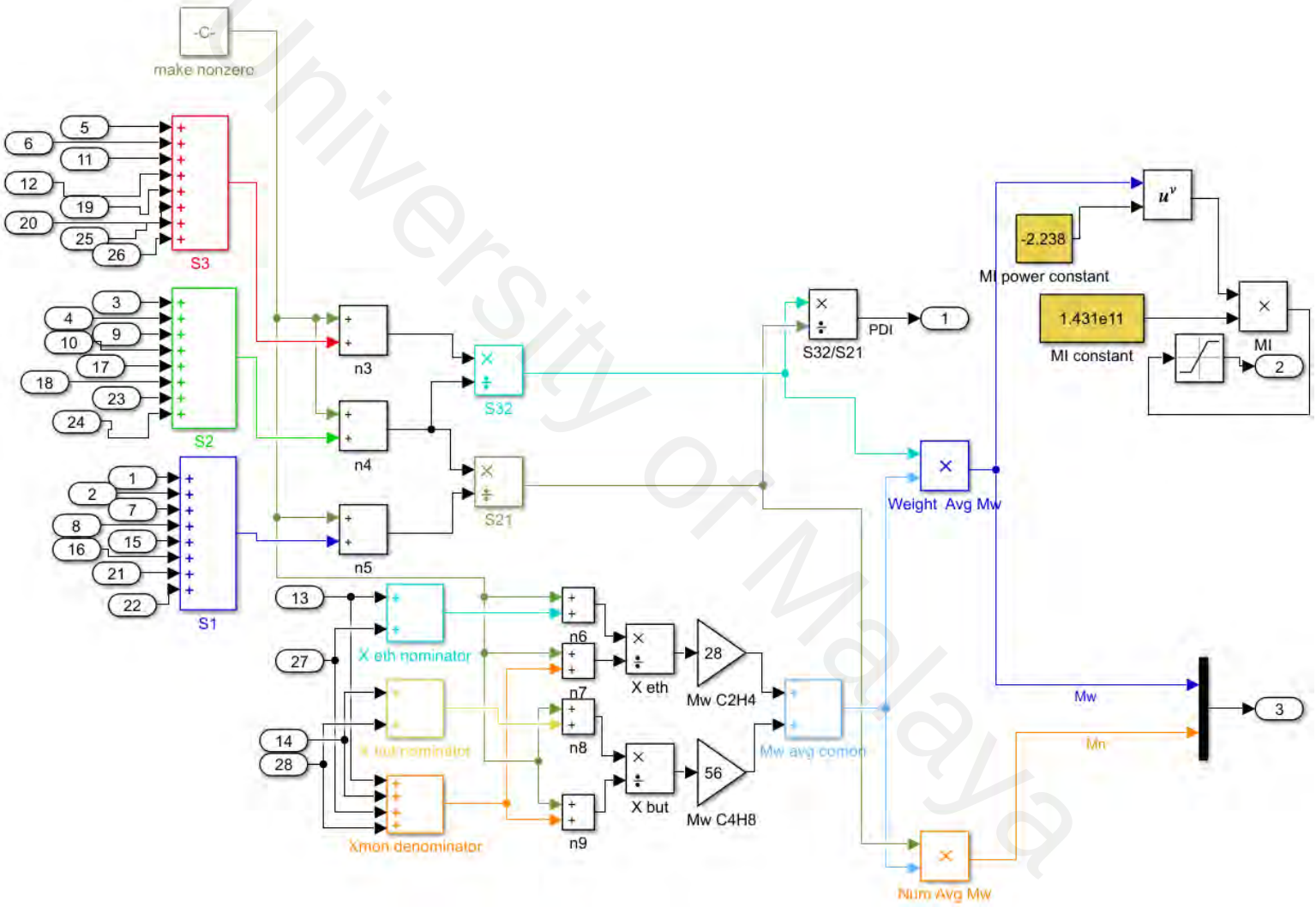

Figure B.3: Simulink® subsystem for molecular weight calculations

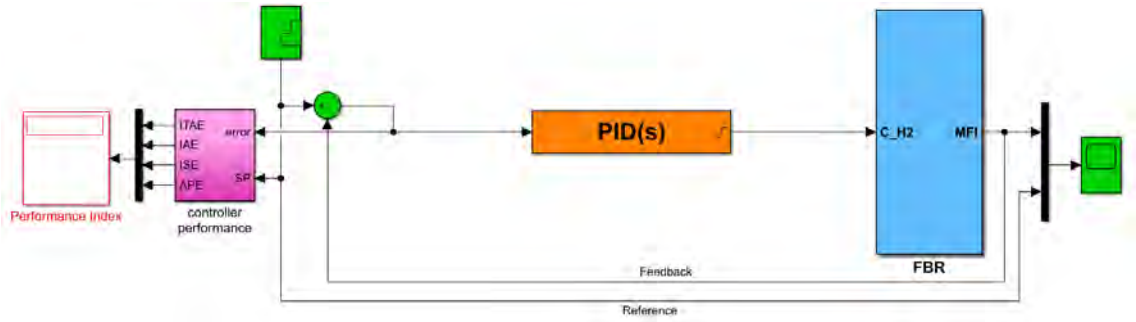

Figure B.4: Simulink® model to control MFI by using PID controller

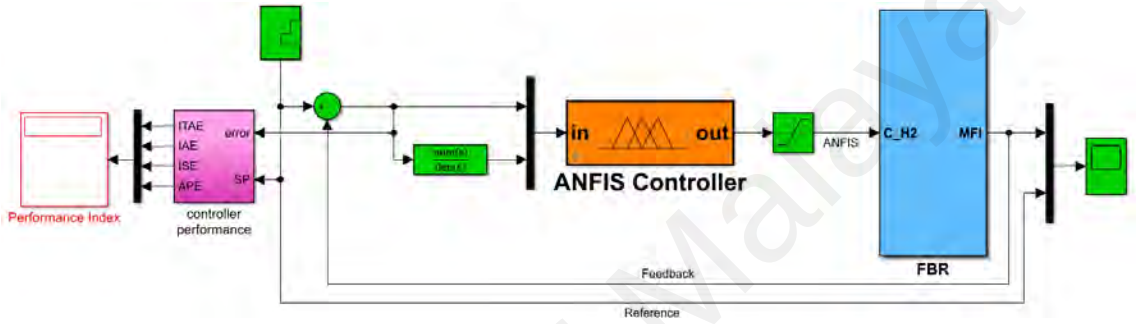

Figure B.5: Simulink® model for MFI setpoint tracking by using ANFIS controller

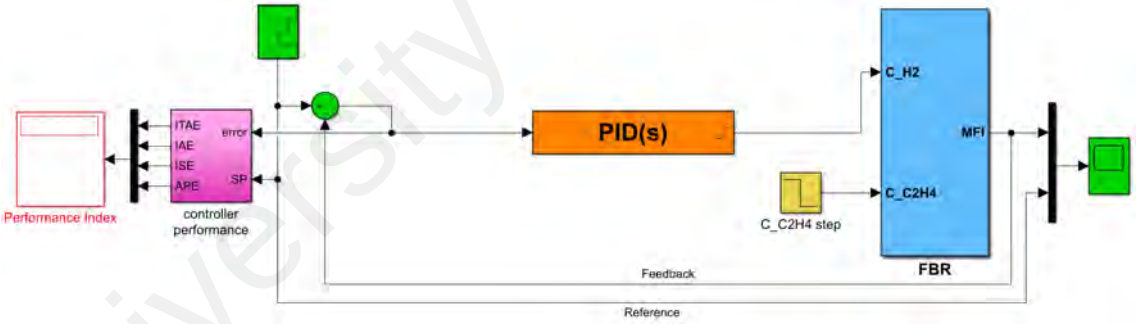

Figure B.6: Simulink® model for MFI disturbance rejection by using PID controller

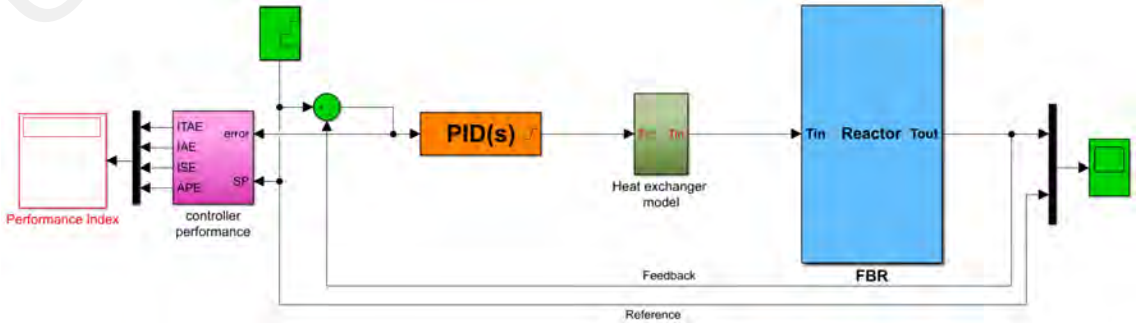

Figure B.7: Simulink® model for temperature setpoint tracking by using PID controller

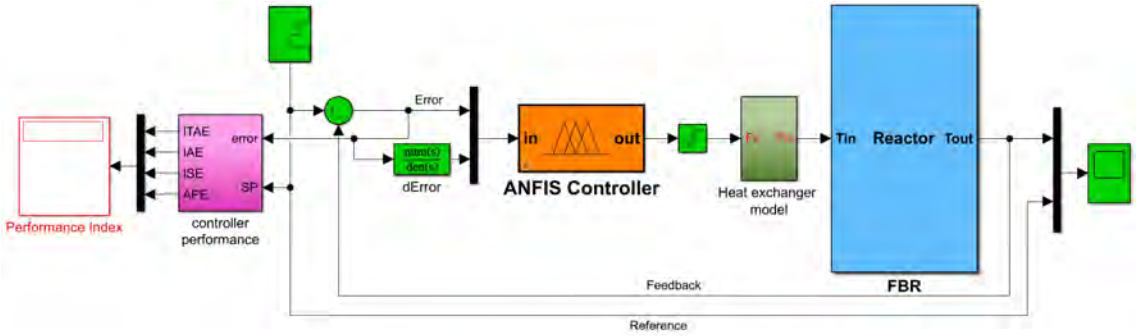

Figure B.8: Simulink® model for temperature setpoint tracking by using ANFIS controller

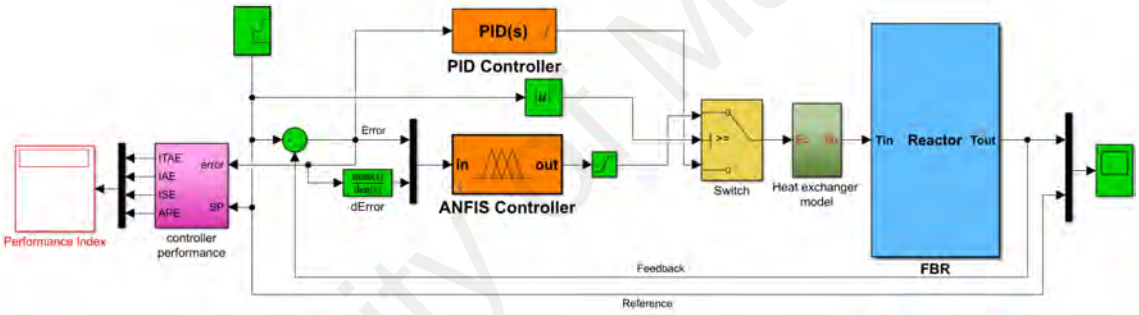

Figure B.9: Simulink® model for temperature setpoint tracking by using hybrid PID–ANFIS controller

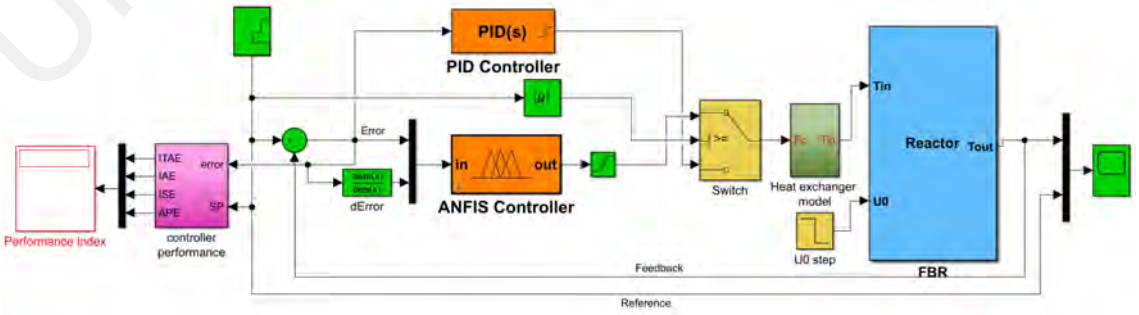

Figure B.10: Simulink® model for temperature disturbance rejection by using hybrid PID–ANFIS controller